ESC-TR-92-135

Technical Report
786
Revision 1

Ground Clutter Measurements for Surface-Sited Radar

J.B. Billingsley

1 February 1993
(Originally Issued 10 November 1987)

Lincoln Laboratory
MASSACHUSETTS INSTITUTE OF TECHNOLOGY
LEXINGTON, MASSACHUSETTS

Prepared for the Department of the Air Force and the Defense Advanced Research Projects Agency
under Air Force Contract F19628-90-C-0002.

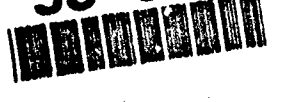

This report is based on studies performed at Lincoln Laboratory, a center for research operated by Massachusetts Institute of Technology. The work was sponsored by the Department of the Air Force and the Defense Advanced Projects Agency under Air Force Contract F19628-90-C-0002.

The ESC Public Affairs Office has reviewed this report, and it is releasable to the National Technical Information Service, where it will be available to the general public, including foreign nationals.

This technical report has been reviewed and is approved for publication.

FOR THE COMMANDER

Gary Tutungian
Administrative Contracting Officer
Directorate of Contracted Support Management

MASSACHUSETTS INSTITUTE OF TECHNOLOGY
LINCOLN LABORATORY

GROUND CLUTTER MEASUREMENTS FOR SURFACE-SITED RADAR

J.B. BILLINGSLEY
Group 105

TECHNICAL REPORT 786
Revision 1

1 FEBRUARY 1993

(Originally Issued 10 November 1987)

LEXINGTON MASSACHUSETTS

ABSTRACT

A large volume of radar ground clutter measurement data was collected from many sites widely distributed over the North American continent. At each site backscatter was recorded from all the terrain within the field of view, typically to ranges extending to 25 or 50 km. As a result, in most of these measurements the angle of illumination of the earth's surface was usually very low, typically within a degree or so of grazing incidence, with much intermittent shadowing of low regions. This report examines the nature of low-angle radar ground clutter as it has come to be understood through analysis of this extensive new base of measurements. Depression angle, that is, the angle below the horizontal at which the backscattering terrain point is observed at the radar antenna, is shown to be the principal parametric influence on clutter amplitude statistics, even for the very low angles and small (i.e., typically fractional) variations in angle that occur in surface-sited radar. This principal role of depression angle is the result of its effect on shadowing in a sea of patchy visibility and discrete or localized scattering sources. Following this understanding, a general predictive model for ground clutter spatial amplitude statistics is developed based on very precise computation of depression angle but on only relatively gross specification of terrain type. The important radar parameters entering the model are radar frequency as it affects mean strength of clutter amplitude distributions and radar spatial resolution as it affects spread in these distributions.

ACKNOWLEDGMENTS

The results of this report are due to dedicated efforts by many people in measuring, reducing, and analyzing our ground clutter data. The five-frequency measurement equipment was fabricated and operated by the General Electric Company. Many of our measurements were made in Canada within a joint program in which support was provided by the Canadian Department of National Defence. The measurement data were subsequently provided to Canada and the United Kingdom, and resultant analyses of these data continue to be shared between the U.S., Canada, and the U.K. under the auspices of The Technical Cooperation Program. This clutter measurement program was originally conceived at Lincoln Laboratory by William P. Delaney and subsequently directed by Carl E. Nielsen, Jr., David L. Briggs, and Lewis A. Thurman. Day-to-day assistance in managing and interpreting the large volume of analysis results was provided by John F. Larrabee and the late Paul C. Crochetiere. George McDowell and Seichoong Chang played important consultant roles during calibration and reduction of the data. Among others, people who have had significant involvement in computer programming and computer-related data reduction activities include Ken Gregson, Gerry McCaffrey, Sharon Kelsey, Charlotte Schell, Kim Jones, Bill Dustin, and Bob Graham-Munn. The skillful efforts of Ms. Pat DeCuir in preparing the manuscript are much appreciated.

TABLE OF CONTENTS

LIST OF ILLUSTRATIONS

LIST OF ILLUSTRATIONS (Continued)

LIST OF TABLES

1. INTRODUCTION

The performance of surface-sited radar against low-flying targets is often limited by ground clutter. As the radar beam scans over the ground, the amplitudes of the clutter returns received from all the spatially distributed resolution cells within the scan coverage on the ground vary over a wide range, from very weak to very strong. Radar designers and analysts need to be able to model ground clutter statistics to determine radar performance. MIT Lincoln Laboratory has completed a several-year program of collecting radar ground clutter measurement data from many sites widely distributed over the North American continent. This report provides general information describing clutter returns received from regions of visible ground based on these recent measurements. Although the primary purpose is to describe clutter amplitude distributions applicable to spatially distributed radar resolution cells, some brief information on temporal variations of clutter returns is also included.

1.1 BACKGROUND

A surface-sited radar often experiences ground clutter interference to ranges of many kilometers. Most of the relatively significant clutter comes from geometrically visible terrain. From most places on the surface of the earth, geometric visibility is spatially patchy; looking out from a site, high regions of terrain are visible and intervening low regions of terrain are masked. Thus clutter occurs within kilometer-sized macroregions of general geometric visibility, each containing hundreds or thousands of spatial resolution cells. The spatial patterns of occurrence of ground clutter can be predicted geometrically with reasonable accuracy using available digital terrain elevation data bases. Predicting, in this manner, the existence of some macroregion of ground clutter, it is subsequently necessary to be able to predict the amplitude statistics of the clutter as they exist within that region to estimate average signal-to-clutter ratios for the radar operating in that clutter. Thus the objective is to predict ground clutter amplitude statistics for distribution over spatial macroregions of visible terrain.

Dominant clutter sources within macroregions of general geometric visibility are often spatially localized or discrete, such that groups of cells providing strong returns are often separated by cells providing weak or noise-level returns. This report shows that a fundamental parametric dependence in low-angle clutter amplitude statistics is that of depression angle as it affects microshadowing in a sea (i.e., macroregion) of discrete clutter sources such that mean strengths increase, and cell-to-cell fluctuations decrease with increasing angle. Depression angle is the angle below the horizontal at which a clutter patch is observed at the radar.

The measures of clutter amplitude statistics used in this report are absolute measures not dependent on radar sensitivity. The Phase Zero and Phase One measurement radars were almost always sensitive enough to measure discernible returns from the dominant discrete clutter sources that occurred within visible macroregions, regardless of range to the region. Increasing sensitivity merely acts to reduce the relative proportion of cells at radar noise level (i.e., microshadowed cells) within such regions. The theoretical clutter amplitude distributions defined here for modeling application over such regions cover all the cells within the region, including those below noise level for any particular radar.

The subject of this report is ground clutter from visible regions of terrain. Ground clutter from regions well beyond the horizon is usually much weaker than that from directly illuminated regions.

Although weak, such interference is not necessarily inconsequential to radars operating against targets beyond the horizon. Long-range diffraction-illuminated ground clutter is being investigated using instrumentation other than that described here. However, these weak signals are understood fundamentally as clutter returns reduced by large propagation losses due to the indirect illumination, and they are not further considered here.

1.2 CLUTTER MEASUREMENT EQUIPMENT

The current program of radar ground clutter measurements went forward in two phases, Phase Zero, a pilot phase that was noncoherent and at X-band only, followed by Phase One, the full-scale coherent program at five frequencies (viz., VHF, UHF, L-, S-, and X-bands). Photographs of Phase Zero and Phase One measurement instruments are shown in Figures 1 and 2, respectively. The Phase Zero radar was a commercial marine navigation radar, in the receiver of which was installed a precision intermediate frequency (IF) attenuator to measure clutter strength. The Phase One radar was a modern, computer-controlled instrumentation radar with high data rate recording capability (i.e., linear receiver with 13-bit A/D converters in I and Q channels) and maintained coherence and stability sufficient for 60-dB, two-pulse-canceller clutter attenuation in postprocessing. A major report on the Phase One equipment and measurement program is available [1]. Important measurement parameters associated with each instrument are shown in Table 1.

Figure 1. Phase Zero equipment at Dundurn, Saskatchewan.

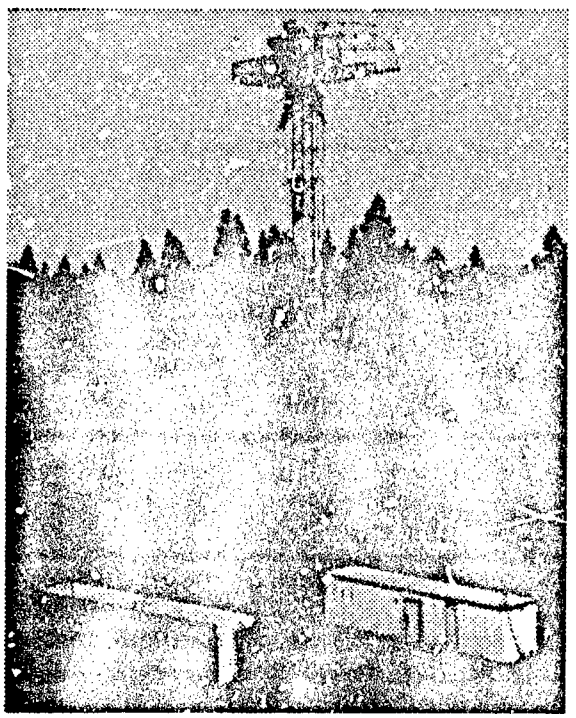

Figure 2. Phase One equipment at Brazeau, Alberta.

Both instruments were self-contained and mobile on truck platforms. Antennas were mounted on erectable towers and had relatively wide elevation beams that were fixed horizontally at 0° depression angle. That is, no control was provided on the position of the elevation beam. For most sites and landscapes, the terrain at all ranges from one to many kilometers was usually illuminated within the 3-dB points of the fixed elevation beamwidth. At each site terrain backscatter was measured by steering the azimuth beam through 360° and selecting a maximum range setting such that all discernible clutter within the field of view, typically from one to about 25 or 50 km in range, was recorded. Phase Zero and Phase One radars had uncoded, pulsed waveforms.

Phase Zero and Phase One instruments were internally calibrated for every clutter measurement. The Phase One instrument was externally calibrated at almost every site, using standard gain antennas and corner reflectors mounted on portable towers. The Phase Zero instrument utilized balloon-borne spheres to provide several external calibrations.

TABLE 1
Clutter Measurement Parameters

	Phase Zero	Phase One				
Frequency						
Band	X-Band	VHF	UHF	L-Band	S-Band	X-Band
MHz	9375	165	435	1230	3240	9200
Polarization	HH	VV or HH				
Resolution						
Range	9, 75, 150 m	15, 36, 150 m				
Azimuth	0.9°	13°	5°	3°	1°	1°
Peak Power	50 kW	10 kW (50 kW At X-Band)				
10 km Sensitivity	$\sigma^\circ F^4 = -45$ dB	$\sigma^\circ F^4 = -60$ dB				
Antenna Control	Continuous Azimuth Scan	Step or Scan Through Azimuth Sector (≤185°)				
Tower Height	50'	60' or 100'				
Data						
Volume	2 Tapes/Site (800 bpi)	~25 Tapes/Site (6250 bpi)				
Acquisition Time	½ Day/Site	2 Weeks/Site				

1.3 CLUTTER MEASUREMENT SITES

During the approximately five-year period from late 1979 to late 1984, large amounts of radar ground clutter measurement data were collected from many sites. The terrain at two measurement sites is shown in Figure 3. Figure 3(a) shows low-relief undulating prairie farmland at the Beiseker site located 75 km northeast of Calgary. The Phase One measurement equipment is visible as it was set up on this site. Figure 3(b) shows high-relief mountainous terrain at the Plateau Mountain site located 120 km southwest of Calgary, deep in the Canadian Rockies. Figures 3(a) and (b) are airborne views looking west. The level terrain in the foreground of Figure 3(b) is the top of Plateau Mountain; the lower part of the figure shows how the terrain drops off precipitously on its east side. Significantly different backscatter characteristics would be expected, and indeed were measured, from the terrain in Figure 3(a) compared with that of 3(b). This report shows that a useful first step in clutter prediction is to simply distinguish terrain type by whether it is low-relief as pictured in Figure 3(a) or high-relief as in 3(b).

Figure 4 shows the locations of all 107 sites at which radar ground clutter measurements have been made.[1] Table 2 provides the name, location by province or state and latitude and longitude, terrain-descriptive information in terms of land cover and landform, and effective height for several of the sites for which measurement results are subsequently discussed in this report.

Classes of land cover and landform referred to in Table 2 are briefly described in Tables 3 and 4, respectively. Table 2 provides land cover and landform information for each site in terms of the percent of occurrence of a particular category of classification across all the spatial clutter occurring at that site. The percent of occurrence of each classifier follows in parentheses.

Effective site height in Table 2 is the difference between the terrain elevation of the radar position and the mean of the elevations of all the discernible clutter cells (i.e., most of the visible terrain) that occurred at that site. Effective radar height is equal to effective site height plus antenna mast height. It is clear that by such definition, effective site height and effective radar height are with respect to illuminated terrain only and indicate how high the site or antenna is above the terrain causing clutter backscatter; they are not influenced by masked or shadowed terrain.

---

[1]It is apparent in Figure 4 that many of our measurement sites were in Canada. The Phase Zero and Phase One clutter measurement programs were jointly conducted by the United States and Canada. The resultant data are provided by Lincoln Laboratory to government authorities in Canada and the United Kingdom, and coordinated analyses of these data continue in all three countries under the auspices of the Technical Cooperation Program, Subgroup K (Radar Technology). Billingsley [2], Chan [3], Sarno [4], and Tonkin and Wood [5] illustrate some of the emphases that clutter analyses have been taking in the three countries.

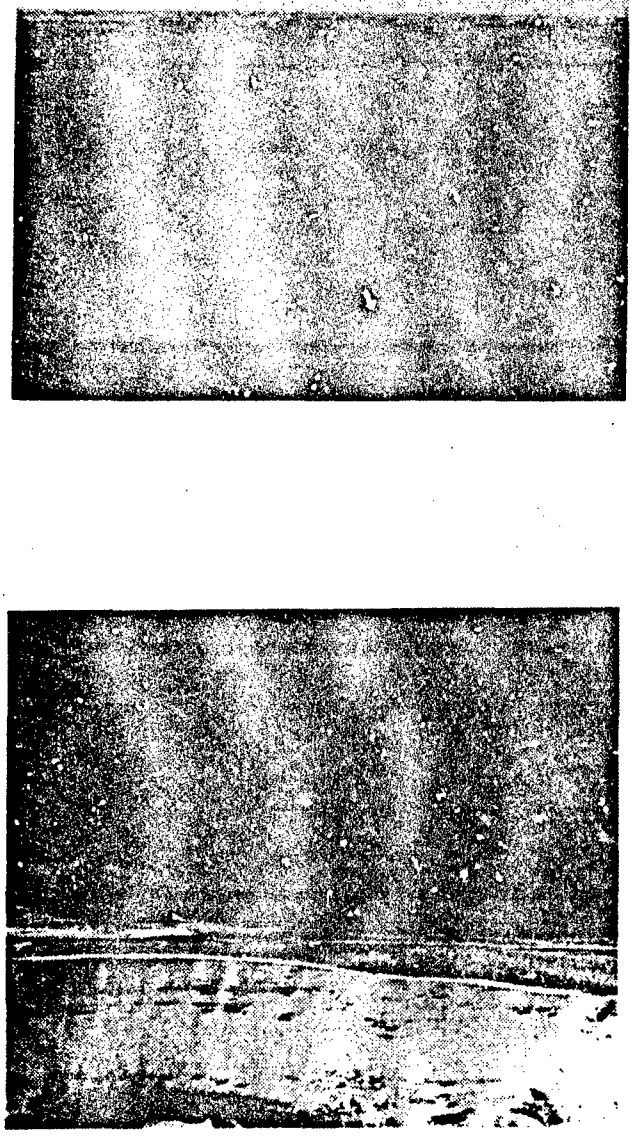

Figure 3. Two clutter measurement sites in Alberta, Canada: (a) low-relief farmland at Beiseker and (b) high-relief mountainous terrain at Plateau Mountain.

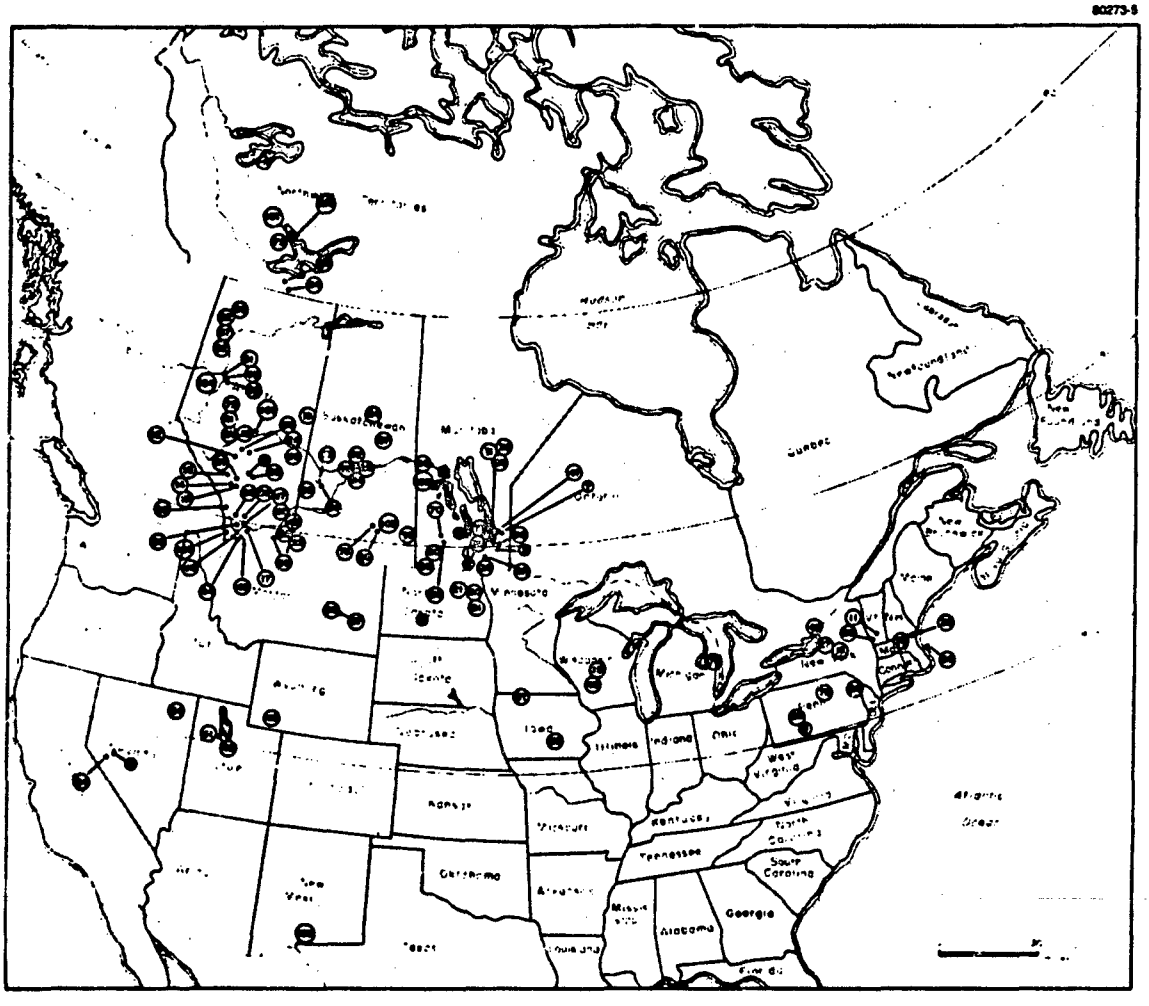

Figure 4. Location of 107 radar ground clutter measurement sites.

TABLE 2
Location and Description of 21 Radar Ground Clutter Measurement Sites

Site Name	Province or State	Latitude (°N)	Longitude (°W)	Land Cover Class Code (Percent Occurrence)	Landform Class Code (Percent Occurrence)	Effective Site Height (m)
Altona II	Man.	49.19	97.66	21(100)	1(100)	-2
Beiseker	Alta.	51.39	113.27	21(100)	3(43), 2(36), 9(9), 7(6), 1(4), 8(2)	76
Big Grass Marsh	Man.	50.39	98.85	41(31), 62(20), 31(19), 21(17), 33(13)	1(100)	-3
Brazeau	Alta.	53.04	115.43	43(64), 51(13), 62(9), 21(4), 42(4), 61(4), 41(1), 52(1)	3(31), 1(21), 4(16), 7(14), 2(12), 8(5), 5(1)	142
Burnstick	Alta.	51.97	114.78	43(63), 21(21), 62(16)	3(25), 5(25), 2(21), 8(15), 7(14)	64
Calgary West	Alta.	51.00	114.23	41(41), 31(28), 11(13), 12(9), 21(9)	3(52), 4(35), 2(9), 7(4)	109
Cazenovia	N.Y.	42.93	75.93	21(50), 41(50)	4(70), 2(10), 7(10), 3(5), 9(5)	12
Coaldale	Alta.	49.75	112.62	21(91), 11(9)	3(47), 1(37), 2(16)	-12
Cold Lake	Alta.	54.43	110.18	21(39), 43(39), 11(5), 52(5), 61(5), 12(3), 31(2), 62(2)	1(40), 3(33), 2(12), 5(9), 7(6)	25
Dana	Sask.	52.28	105.77	21(69), 41(29), 11(2)	3(41), 5(34), 1(15), 2(10)	44
Dundurn	Sask.	51.85	106.57	41(30), 21(23), 32(23), 52(8), 11(4), 14(4), 31(4), 51(4)	3(45), 5(35), 1(10), 2(10)	-3
Equinox Mt.	Vt.	43.16	73.12	43(91), 21(9)	7(65), 8(14), 5(11), 2(8), 6(2)	663
Gull Lake West	Man.	50.40	96.53	43(49), 21(21), 33(8), 62(8), 61(6), 12(4), 52(4)	1(67), 3(27)	28
Magrath	Alta.	49.41	112.97	21(64), 31(19), 51(11), 11(3), 32(3)	2(25), 3(20), 7(15), 9(15), 1(13), 4(8), 5(2), 6(2)	79
Penhold II	Alta.	52.18	113.97	21(64), 52(11), 41(8), 43(8), 11(3), 12(3), 62(3)	1(48), 3(28), 2(12), 7(7)	40
Plateau Mt.	Alta.	49.21	114.52	42(35), 31(29), 70(26), 41(9), 32(1)	8(91), 2(4), 3(4), 7(1)	279
Rouleau	Sask.	50.23	104.87	21(90), 11(5), 51(5)	1(95), 3(5)	20
Shilo	Man.	49.75	99.63	41(44), 21(26), 31(18), 32(6), 11(3), 12(3)	1(50), 3(36), 2(7), 5(7)	3
Strathcona	Alta.	51.03	114.17	11(33), 12(20), 41(15), 31(13), 51(11), 21(8)	7(33), 3(28), 4(19), 2(14), 1(3), 5(3)	72
Waterton	Alta.	49.15	113.83	31(27), 41(27), 33(16), 42(14), 70(8), 52(5), 40(3)	7(33), 4(26), 8(16), 2(10), 5(6), 1(3), 3(3), 6(3)	-88
Wolseley	Sask.	50.36	103.15	21(73), 41(21), 52(4), 11(2)	3(47), 5(33), 1(16), 2(4)	17

TABLE 3
Land Cover Classes

1	Urban or Built-up Land
	11 Residential
	12 Commercial
2	Agricultural Land
	21 Cropland
	22 Pasture
3	Rangeland
	31 Herbaceous
	32 Shrub
	33 Mixed
4	Forest
	41 Deciduous
	42 Coniferous
	43 Mixed
5	Water
	51 Rivers, Streams, Canals
	52 Lakes, Ponds, Sloughs
6	Wetland
	61 Forested
	62 Non-Forested
7	Barren Land

TABLE 4
Landform Classes and Descriptions

Landform Class	Terrain Relief (ft)	Terrain Slope (deg)	
1 Level	<25′	<1°	
2 Inclined	>50′	1° — 2°;	Unidirectional
3 Undulating	25′ — 100′	<1°;	Regular Sequences of Gentle Slopes; Wavelike
*4 Rolling	>150′	2° — 5°;	Regular to Irregular Sequences of Moderate Slopes
5 Hummocky	25′ — 150′	<2°;	Complex Sequences of Slopes
*6 Ridged	50′ — 500′	2° — 10°;	Sharp Breaks in Slope at Tops and Bottoms of Terrain Features
*7 Moderately Steep	>100′	2° — 10°;	Unidirectional
*8 Steep	>100′	10° — 35°;	Frequently Unidirectional
9 Broken	>50′	1° — 5°;	Short Dissected Slopes

[U] * Classes so indicated are "high-relief;" classes not so indicated are "low-relief."

2. PHASE ZERO X-BAND CLUTTER MEASUREMENTS

2.1 THE NATURE OF LOW-ANGLE CLUTTER

2.1.1 Clutter Physics

The major elements involved in low-angle clutter are shown in Figure 5. Attention is focused on directly illuminated clutter from large kilometer-sized patches of visible terrain. Within such patches, at the low illumination angles of surface-sited radar, the clutter sources are all the vertical features of discontinuity (i.e., things that stick up) on the landscape, either objects associated with the land cover such as trees or buildings, or the high points of the terrain itself. The nature of such sources is that they are usually spatially localized or discrete with regions of microshadow occurring between them where the receiver is at its noise floor. As the angle of illumination increases, the amount of microshadowing decreases. As a result, strengths in clutter amplitude distributions increase and spreads in clutter amplitude distributions decrease with increasing angle. These effects with angle constitute a major parametric dependence in low-angle clutter.

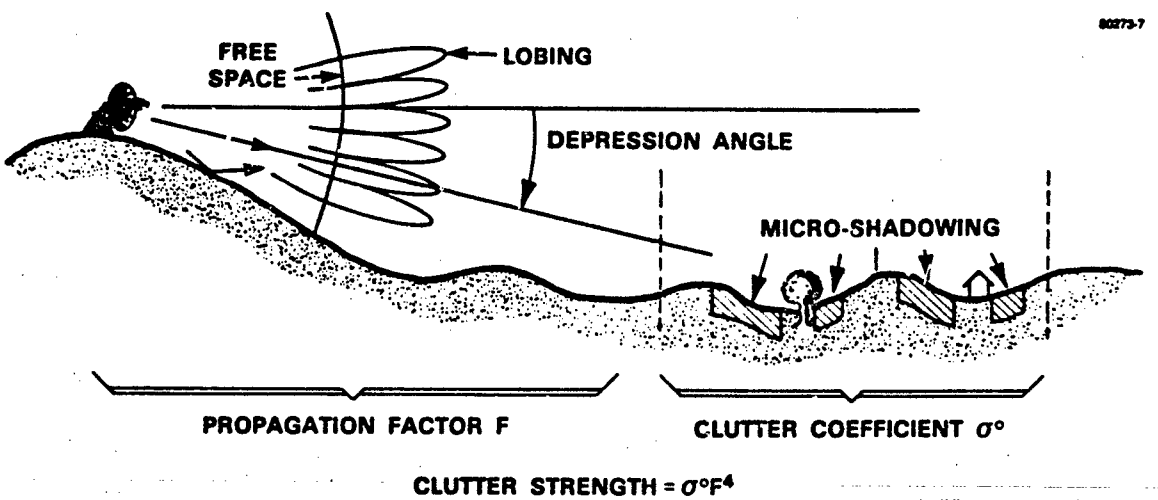

Figure 5. Clutter physics.

The terrain between the radar and the clutter patch influences the illumination of the clutter patch. For example, multipath reflections can interfere with the direct illumination and cause lobing on the free-space antenna pattern. All such propagation effects are included within the propagation factor F, which is defined to be the ratio of the incident field that actually exists at the clutter cell being measured to the incident field that would exist there if the clutter cell existed by itself in free space. What is measured as clutter strength is the product of the clutter coefficient itself, σ°, defined to be radar cross section (RCS) per unit ground area in the resolution cell, and the fourth power of the propagation factor. At

X-band, terrain reflection coefficients are often lower, and hence multipath effects diminished, from those that can exist at lower radar frequencies. When multipath propagation lobes exist at X-band, they are usually relatively narrow. Typical clutter sources such as trees and buildings over most visible terrain often subtend a number of such lobes when they exist. As a result, the effects of propagation are diminished and tend to average out at X-band, compared with lower frequencies where they can dominate. Throughout this report, clutter strength is given by $\sigma^{\circ}F^4$ in units of m^2/m^2.

2.1.2 Measured Ground Clutter Maps

Figure 6 shows Phase Zero X-band measurements of ground clutter in plan position indicator format at six Canadian sites. The maximum range in all cases is 47 km. These data are shown at close to full Phase Zero sensitivity so that cells with discernible clutter return from the ground are shown as white, and cells where the receiver is at its noise floor are shown as black. Range resolution is 150 m, azimuth resolution (i.e., 3-dB beamwidth) is 0.9°. Capsule descriptions of the six sites shown in Figure 6 are given in Table 2. At Altona, the terrain is very level cropland in Manitoba; clutter is measured there only from discrete vertical objects (such as barns, silos, telephone poles, isolated trees, etc.) out to a spherical earth horizon (nominally given by 16 km for the 50-ft Phase Zero antenna mast) except for the terrain feature (Pembina Hills) that rises to the far southwest. Only at such level sites is a spherical earth model of terrain very applicable in understanding low-angle microwave clutter, and at such level sites dominant clutter sources are often high cultural or natural discretes distributed over the spherical surface. At most other sites, even relatively low-relief sites, specific terrain features dominate in low-angle clutter measurements over what would be measured on a spherical earth. Thus, moving across Saskatchewan (Dana) and into Alberta (Penhold and Beiseker), the terrain becomes more undulating and rolling, and the influence of specific large-scale terrain features dominates over spherical earth effects in the clutter maps for these sites in Figure 6. For example, even in the relatively low-relief terrain at Beiseker, it is the terrain surfaces inclined toward the radar (e.g., to the north and south) from which clutter is received; these surfaces are shadowed (i.e., black) on their far sides. Moving on in Figure 6, Burnstick is a forested site in the foothills of the Rocky Mountains, and Plateau Mountain is a site high in the Rockies themselves. To the west at Plateau Mountain, clutter is measured from barren rock faces of high peaks in the Rockies, and to the east clutter is measured looking down at the prairie.

In all cases in Figure 6, the patterns of spatial occurrence of clutter are very patchy and granular. The nature of the clutter is on-again, off-again as it arises from discrete sources distributed on surfaces within line-of-sight visibility. The details of each pattern are specific to the terrain features at that site; however, two general observations can be made about all such patterns. First, the amount of clutter that occurs gradually diminishes with increasing range from the site. Second, where clutter occurs (i.e., white patches), its strength is relatively independent of range. Section 4.3 bases the development of simple non-site-specific modeling information on these two observations. But now attention is focused on the following question: Where clutter occurs (i.e., over spatial regions largely within geometric line-of-sight visibility in which a relatively high percentage of resolution cells contain discernible clutter), what are the spatial amplitude distributions of clutter strengths there?

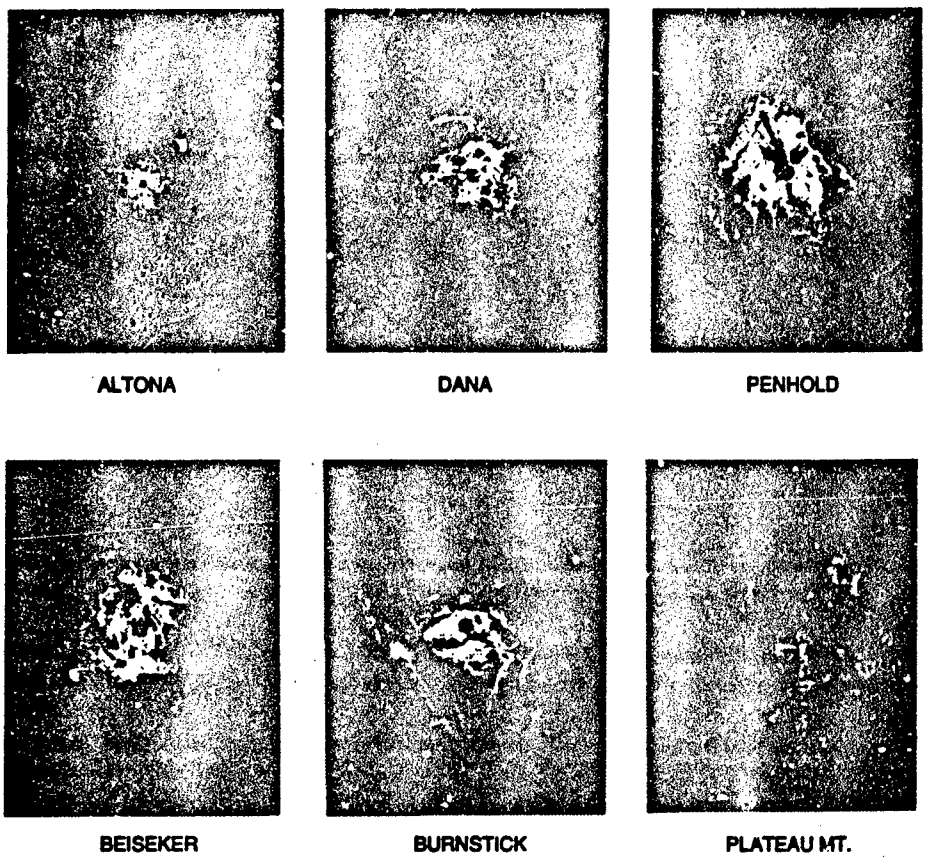

Figure 6. Ground clutter maps at six sites (X-band; 47-km range).

In Figure 6 the range resolution is 150 m. Figure 7 shows similar measurements at six sites at higher resolution, namely 9 m. At this increased resolution (and shorter range, namely 5.88 km), the discrete or localized nature of the actual clutter sources within regions of general terrain visibility is very evident. The pattern of vertical cultural objects on the level cropland at Altona is obvious. On the undulating terrain at Beiseker, terrain features are evident in the clutter map, but a rectangular pattern of cultural discretes is seen overlaying them. At ranges within 6 km, Dundurn is a military wasteland area of shrub and brush-covered sand dunes, typically 20 to 30 ft high, but without a road grid or cultural overlay; however, a very granular texture is also seen to the clutter pattern there, where the top of each sand dune gives rise to a discrete or localized clutter return. In observing this very granular clutter map for Dundurn, one is not inclined to attempt to bring detailed terrain slope and grazing angle to bear to explain or predict the strength from each individual dune.

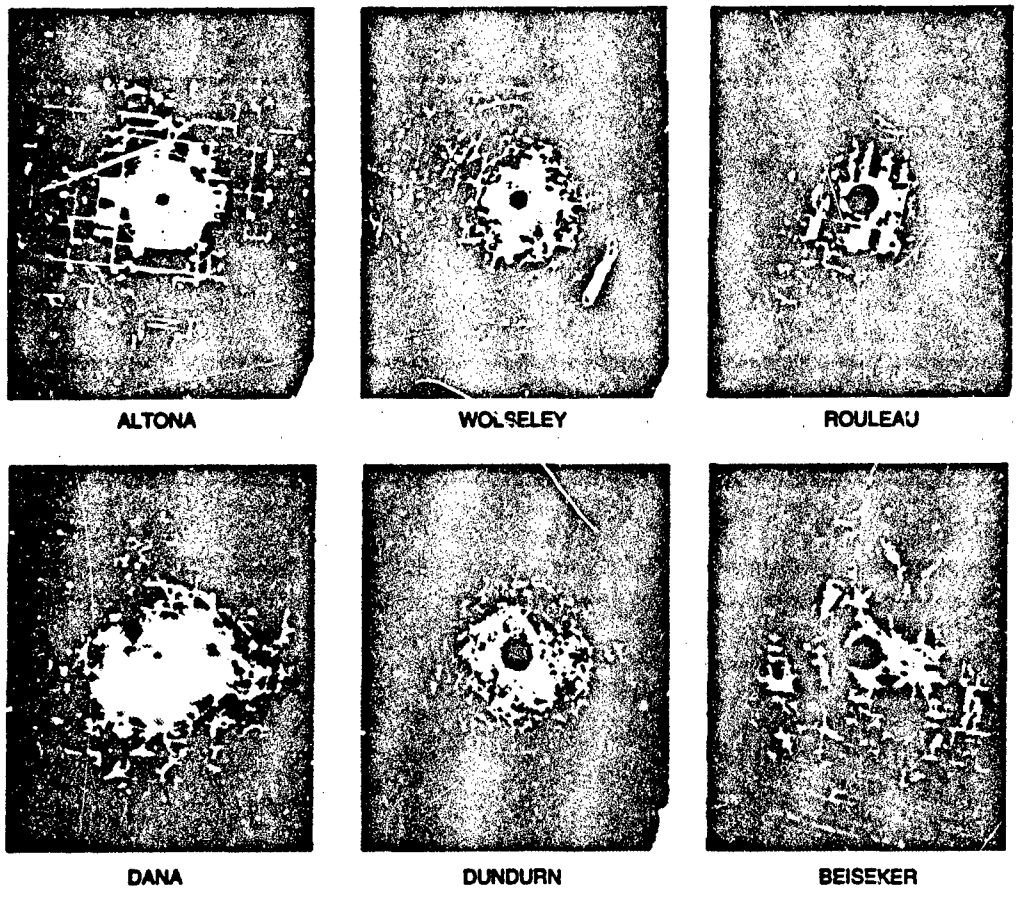

Figure 7. High-resolution ground clutter maps at six sites.

In totality, the high-resolution plots of Figure 7 illustrate what was stated earlier, that within directly illuminated clutter regions, the clutter sources are the discrete objects that stick up above the mean level of the surface. These discrete sources are densely distributed within illuminated regions. Clutter returns from the terrain surfaces themselves, as opposed to the objects sticking up from these surfaces, are much weaker and, in fact, are often below the sensitivity of the receiver. In viewing the clutter maps of Figure 7, one is inclined to envisage a sea of discretes as an appropriate physical model for low-angle ground clutter in contrast to the historical tendency in clutter modeling to associate the phenomenon primarily with area-extensive σ° backscatter from the terrain surfaces themselves (with a relatively few, very strong classical discretes such as water towers sometimes added in subsequently as an RCS adjunct).

2.1.3 Clutter Patches at Gull Lake West, Manitoba

Our approach to modeling clutter amplitude statistics is as follows. Within the clutter map measured at each site, macropatches of clutter are selected within spatial regions generally within line-of-sight illumination in which a relatively high percentage of resolution cells contain discernible clutter. The meaning of "relatively high" depends on the terrain type and corresponding nature of microshadow in the clutter map. Typically, relatively high might mean about 50%, but for high sites and/or steep terrain in which relatively full illumination exists it can approach 100%, and in level terrain in which only isolated discretes are illuminated it can be as low as about 25%. Overlaying and registering clutter maps onto air photos and topographic maps also ensures (in patch specification) that the terrain within each patch is, in large measure, uniform. Interpretation of the air photos and topographic maps provides descriptive information of the terrain within the patch. For each clutter patch, the distribution of clutter strengths occurring within the patch is obtained and stored in a computer file with the applicable terrain descriptors of the patch. The modeling task then becomes one of attempting to establish general correlative properties between the stored distributions of measured clutter strength and the corresponding terrain descriptions.

Next are shown some typical clutter patches and measured clutter patch spatial amplitude distributions from the Gull Lake West site in Manitoba. Figure 8(a) shows a measured clutter map of 11.8-km radius for Gull Lake West. Selected clutter patches within that area are shown in Figure 8(b). Figure 9 shows the measured amplitude distributions for six of the Gull Lake patches shown in Figure 8.

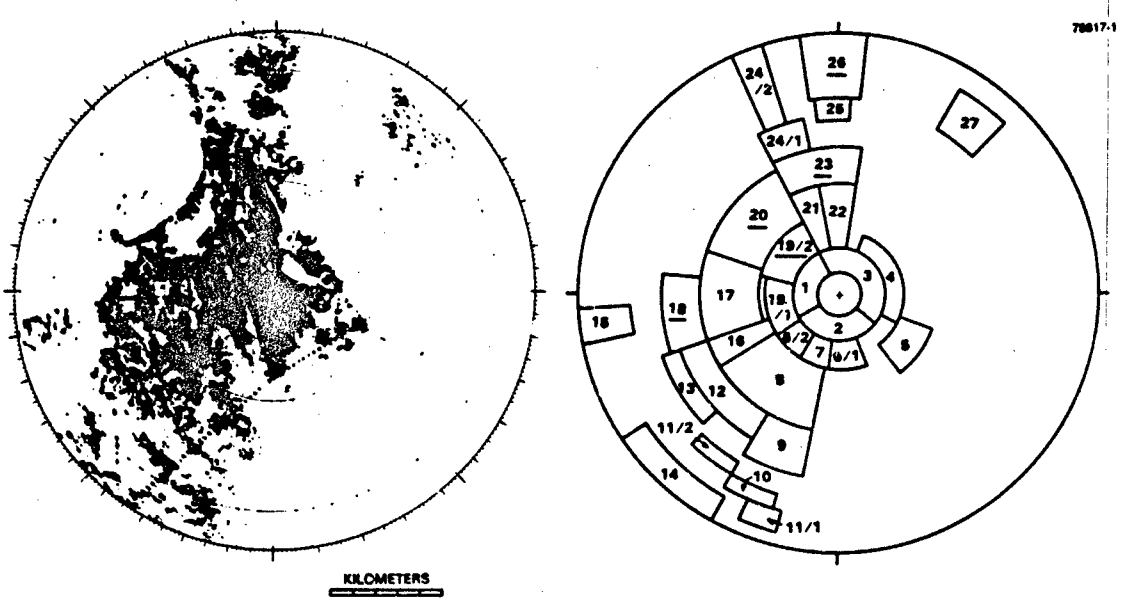

(a) PHASE ZERO X-BAND CLUTTER MAP, MAXIMUM RANGE = 11.8 km

(b) CLUTTER PATCH SELECTION

Figure 8. (a) Measured ground clutter map and (b) patches at Gull Lake West, Manitoba.

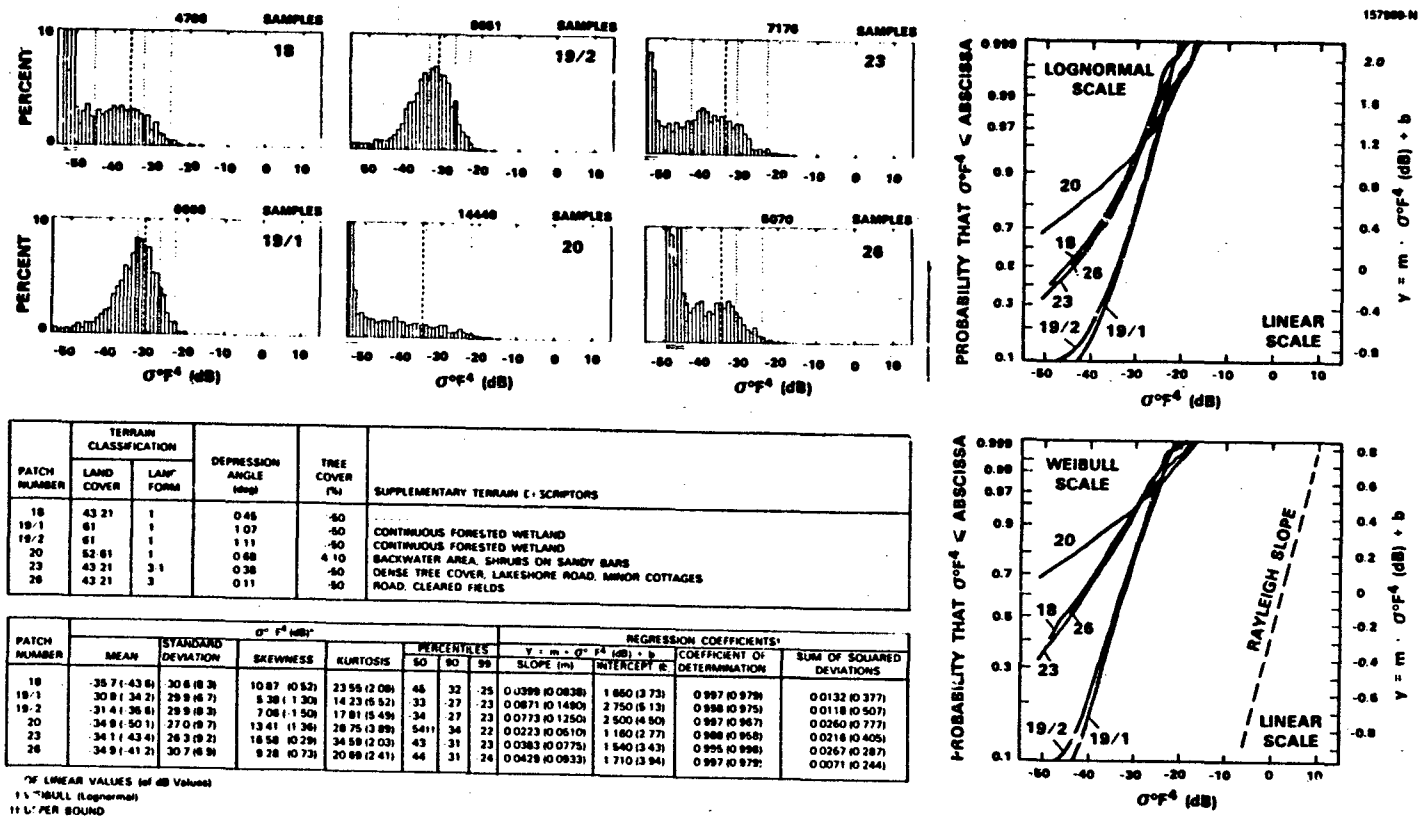

PATCH NUMBER	TERRAIN CLASSIFICATION: LAND COVER	TERRAIN CLASSIFICATION: LAND FORM	DEPRESSION ANGLE (deg)	TREE COVER (%)	SUPPLEMENTARY TERRAIN DESCRIPTORS
18	43 21	1	0 45	50	
19/1	61	1	1 07	50	CONTINUOUS FORESTED WETLAND
19/2	61	1	1 11	50	CONTINUOUS FORESTED WETLAND
20	52 61	1	0 68	4 10	BACKWATER AREA, SHRUBS ON SANDY BARS
23	43 21	3 1	0 38	40	DENSE TREE COVER, LAKESHORE ROAD, MINOR COTTAGES
26	43 21	3	0 11	50	ROAD, CLEARED FIELDS

PATCH NUMBER	σ° F⁴ (dB)* MEAN	STANDARD DEVIATION	SKEWNESS	KURTOSIS	PERCENTILES 50	90	99	REGRESSION COEFFICIENTS† y = m · σ° F⁴ (dB) + b SLOPE (m)	INTERCEPT (b	COEFFICIENT OF DETERMINATION	SUM OF SQUARED DEVIATIONS
18	-35 7 (-43 6)	30 6 (0 3)	10 87 (0 52)	23 55 (2 08)	46	32	25	0 0399 (0 0838)	1 660 (3 73)	0 997 (0 979)	0 0132 (0 377)
19/1	30 8 (34 2)	29 9 (6 7)	5 38 (1 30)	14 23 (5 52)	33	27	23	0 0871 (0 1480)	2 750 (5 13)	0 998 (0 975)	0 0118 (0 507)
19-2	-31 4 (36 6)	29 9 (6 3)	7 06 (1 50)	17 81 (5 49)	34	27	23	0 0773 (0 1250)	2 500 (4 50)	0 997 (0 967)	0 0260 (0 777)
20	-34 9 (50 1)	27 0 (8 7)	13 41 (1 36)	28 75 (3 89)	5411	36	22	0 0223 (0 0610)	1 160 (2 77)	0 988 (0 958)	0 0216 (0 405)
23	-34 1 (43 4)	26 3 (9 2)	16 58 (0 29)	34 59 (2 03)	43	31	23	0 0383 (0 0775)	1 540 (3 43)	0 995 (0 998)	0 0267 (0 287)
26	-34 9 (41 2)	30 7 (6 9)	9 28 (0 73)	20 69 (2 41)	44	31	24	0 0429 (0 0933)	1 710 (3 94)	0 997 (0 979)	0 0071 (0 244)

*F LINEAR VALUES (of dB Values)
† WEIBULL (Lognormal)
†† UPPER BOUND

Figure 9. Phase Zero clutter statistics and terrain classification of selected patches at Gull Lake West.

The terrain from which clutter at Gull Lake West was measured lies in the valley of the Red River and as a result is extremely level. The site itself at Gull Lake West lies on the western brow of a north-south situated ridge about 100 ft above the level terrain to the west, which the site overlooks. Thus the effect of the ridge is to extend the Phase Zero mast height from its nominal 50-ft value to a higher elevation of about 150 ft. Otherwise, the very level terrain at Gull Lake West in some respects represents a canonical situation in which complicating effects of terrain relief are absent. Thus the specific effects observed in the clutter distributions at Gull Lake West are largely caused by variation and complexity in land cover. Consideration of these effects can help provide a deeper understanding of the general low-angle clutter amplitude distributions presented later in this report.

In discussing these effects, patches 19/1 and 19/2 are considered first. These patches are level forested wetland, relatively uncomplicated by the presence of roads running through them, clearings, cultural discretes, and shadowing caused by variations in terrain elevation. Many of the taller trees making up this forested wetland are larch or tamarack. The other major component of the forested wetland is spruce. Also present is an understory of willow.

The radar overlooks these patches from its nearby ridge location at a depression angle of about 1°. At first consideration, 1° may not seem to provide much in the way of illumination angle, but it is enough to make all the difference in causing these patches to be fully illuminated obliquely from above, rather than from the side at grazing incidence as they would have been if the radar position had not had its 100-ft terrain elevation advantage. As a result, the clutter histograms for patches 19/1 and 19/2 in Figure 9 are uncontaminated by cells at radar noise level (i.e., $\sigma^\circ F^4$ bins containing one or more cells at radar noise level are doubly underlined; these bins appear to the left side of the histograms for the other four patches in the figure and obviously indicate the sensitivity limit of the radar in these histograms). That is, every cell in patches 19/1 and 19/2 provides a discernible clutter return, which is not the case for most low-angle clutter patches. In addition, patches 19/1 and 19/2 provide what appear to be rather nicely behaved histograms of traditional bell shape. In fact, and as expected for full illumination of relatively homogeneous tree foliage, the amplitude distributions for patches 19/1 and 19/2 are very nearly Rayleigh, which may be ascertained from their close match to the Rayleigh slope in the Weibull cumulative plot in Figure 9, as well as from the relative values of $\sigma^\circ F^4$ moments and percentiles listed.

What would not have been expected, perhaps, is that so few patches provide such nicely behaved, nearly Rayleigh statistics as do patches 19/1 and 19/2. Over large extents of composite landscape such as typically produce low-angle clutter in surface radars, most sites provide very little in the way of homogeneous terrain. For example, consider patch 18 at Gull Lake West. Although the terrain is level, the land cover is mixed between forest and cropland. At a depression angle of about 0.5°, the clutter return from the agricultural field surfaces is either masked by the surrounding trees or below sensitivity at this low angle. As a result, a considerable number of samples in the distribution are at noise level (spike at left side of histogram). To the right of the noise samples, the histogram is less bell-shaped and more spread out than those of patches 19/1 and 19/2 (dotted vertical lines indicating 50, 90, and 99 percentiles are more separated). The cumulative distribution for patch 18, plotted on the Weibull scale in Figure 9, is of considerably less slope than Rayleigh. Patches 23 and 26 are relatively similar to patch 18 in terrain

description, depression angle, and clutter amplitude distribution, and these three patch distributions as a set (e.g., bottom graph, Figure 9) characterize much of the clutter-producing terrain at Gull Lake West. Note that these cumulative distributions include all the samples from each patch, including those at radar noise level; however, the distributions are shown only above (i.e., to the right of) their regions of noise contamination. Thus, over the regions shown in Figure 9, these distributions are not affected by the sensitivity limit of the radar and are what would be measured by an infinitely sensitive radar. Even on canonically level terrain with an artificially high antenna mast, complexity and heterogeneity in land cover has introduced a considerable extra degree of spread in these three distributions (patches 18, 23, and 26) compared with homogeneous land cover (patches 19/1 and 19/2), all evident in comparing their cumulative amplitude distributions on the Weibull scale.

Figure 10 shows clutter strength versus range looking west at Gull Lake West. It is observed that between 2 and 3 km in range, a relatively constant level of return is received from the level forested wetland. In this region, only small-scale fluctuation is observed from range gate to range gate, indicative of local heterogeneity in the forest over such small areas. However, beyond 3.3 km in Figure 10, the nature of the clutter phenomenon changes dramatically. This region is characterized by extreme and rapid fluctuations in clutter strength as the various features of vertical discontinuity, many of which are tree lines, are encountered. Knowing how homogeneous tree or homogeneous cropland pixels backscatter does not provide much information on how important boundary pixels backscatter in transition zones, as shown in Figure 10, where forest meets cropland. Clearly, even for this canonically level terrain, a pixel-specific predictive approach would require an enormous amount of land cover information to be able to accurately predict the deterministic clutter strength profile shown across patches 17 and 18. Such an approach would be easier to apply if more terrain was, like patch 19/1, relatively homogeneous.

Referring back to Figure 7, to a large extent most of the dominant backscatter sources in low-angle ground clutter are the myriad features of vertical discontinuity that exist on landscape. A correct empirical approach in dealing with all these edges of features is to collect meaningful numbers of them together within macropatches, like patches 17 and 18 in Figure 10, and let the terrain classification system carry the burden of statistically describing the attributes of the discontinuous clutter sources within the patch at a gross overall level of description. Study of heterogeneous patches like 17 and 18 at Gull Lake West can help lead to a general understanding of the clutter spatial amplitude distributions that occur in radar receivers as their beams sweep over large extents of composite landscape.

In Figure 9, the cumulative distributions plotted on the Weibull scale appear more linear than those plotted on the lognormal scale. This is often (but not always) the case. To the extent that this is the case, Weibull formulations represent better engineering approximations to clutter spatial amplitude distributions than do lognormal formulations. Lognormal formulations of clutter amplitude statistics tend to provide too much spread in the statistics. Our measured amplitude distributions almost never pass rigorous statistical hypothesis tests for belonging to Weibull, lognormal, or other theoretical distributions that have been tried.

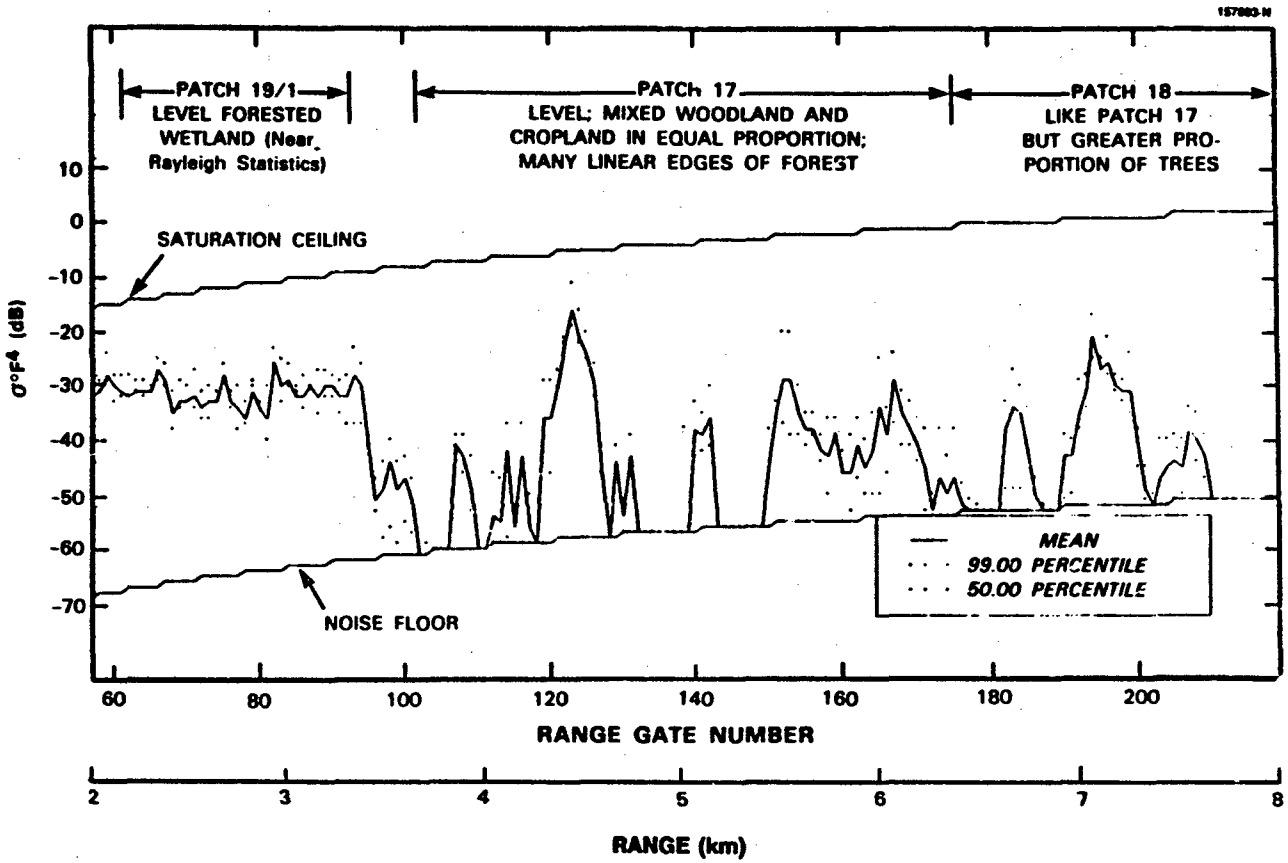

- DATA SHOWN FOR INDIVIDUAL RANGE GATE POSITIONS, AVERAGED OVER A 2° SECTOR, 271.5° TO 273.5° (10 Azimuth Samples/Gate)
- MEASUREMENT DATE, 23 FEBRUARY 1980; LEAFLESS DECIDUOUS TREES, SNOW COVERED FIELD SURFACES; SEE FIG. 5

Figure 10. Clutter strength versus range looking west at Gull Lake West.

2.1.4 Depression Angle

As is shown in Figure 5, depression angle is the angle below the horizontal at which a clutter patch is observed at the radar. More specifically, depression angle is defined as the complement of incidence angle at the backscattering terrain point under consideration. Incidence angle equals the angle between the projection of the earth's radius at the terrain point and the direction of illumination at that point, assuming a 4/3 earth radius to account for nominal atmospheric refraction. Thus our rigorous definition of depression angle is in a reference frame centered at the terrain point, not at the antenna. This definition includes the effect of earth curvature on the angle of illumination, but does not include any effect of the local terrain slope. Grazing angle is the angle between the tangent to the local terrain surface at the backscattering terrain point and the direction of illumination. Thus grazing angle does take into account the local terrain slope. At short enough ranges where earth curvature is insignificant, depression angle simplifies to be the angle below the horizontal at which the terrain point is viewed from the antenna.

To illustrate the effect of depression angle on low-angle clutter, results are shown from two sites. First results are shown from Shilo, Manitoba at low depression angle, 0.1° or 0.2°. Then results are shown from Cazenovia, New York at a depression angle of about 9°, which is a very high depression angle for surface-sited radar. In contrast to Gull Lake West, which was wooded terrain with occasional agricultural fields, the terrain at Shilo was open prairie farmland strongly supportive of multipath. Terrain relief at Shilo was low, less than 50 m over 10- to 20-km extents, but the terrain was not completely level. The site position itself provided little elevation advantage over surrounding terrain. A terrain elevation profile to the southwest at Shilo is shown in Figure 11, incorporating the curvature of a 4/3 radius spherical earth. Geometrical masking is also shown in this figure. In this southwest terrain profile, the depressional dip at about 4.5-km range is a river valley. From 5.2 to 13.4 km, the terrain gradually rises out of the river valley at an average terrain slope of 0.26°. Although this is a small angle, it is more than sufficient to bring this terrain into full visibility from the radar position. Small changes in terrain slope to the southwest at Shilo, for example, in the regions from 13.4 to 15.1 km and beyond 17.3 km, are enough to cause these regions to be masked, which leads to an important point that is often misconstrued at first consideration. Terrain slope and changes in terrain slope, even when quite small, are very important in how they directly and deterministically affect the spatial patterns of occurrence of the clutter. The effect of terrain slope on clutter strength, however, is an entirely different matter, which is discussed in Section 2.1.5.

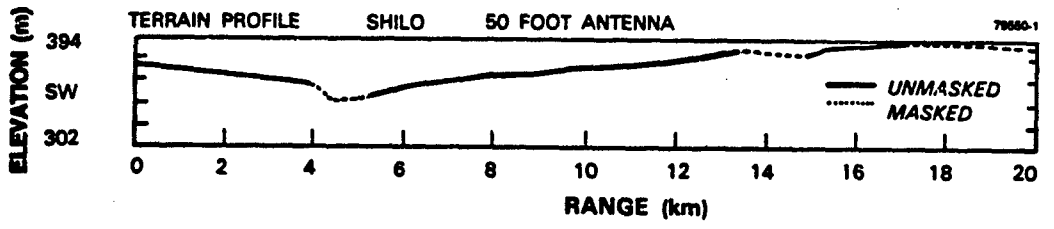

Figure 11. Terrain elevations and masking to the southwest at Shilo, Manitoba.

Figure 12 shows clutter strength versus range in a narrow azimuth sector to the southwest at Shilo. Only in the first 2 km on the relatively discrete-free prairie grassland that happens to occur in this near-in region is seen anything approaching a traditional deterministic effect between area-extensive σ° from the terrain surface and grazing angle in Figure 12. This close to the radar, the antenna mast height is sufficient to provide grazing angles greater than 0.5°. Thus as range decreases from 2 km, grazing angle increases from 0.5°, and clutter strengths rise. Even in this near-in region, the nature of the increase of σ° with grazing angle is not smooth and monotonic but shows wide fluctuations.

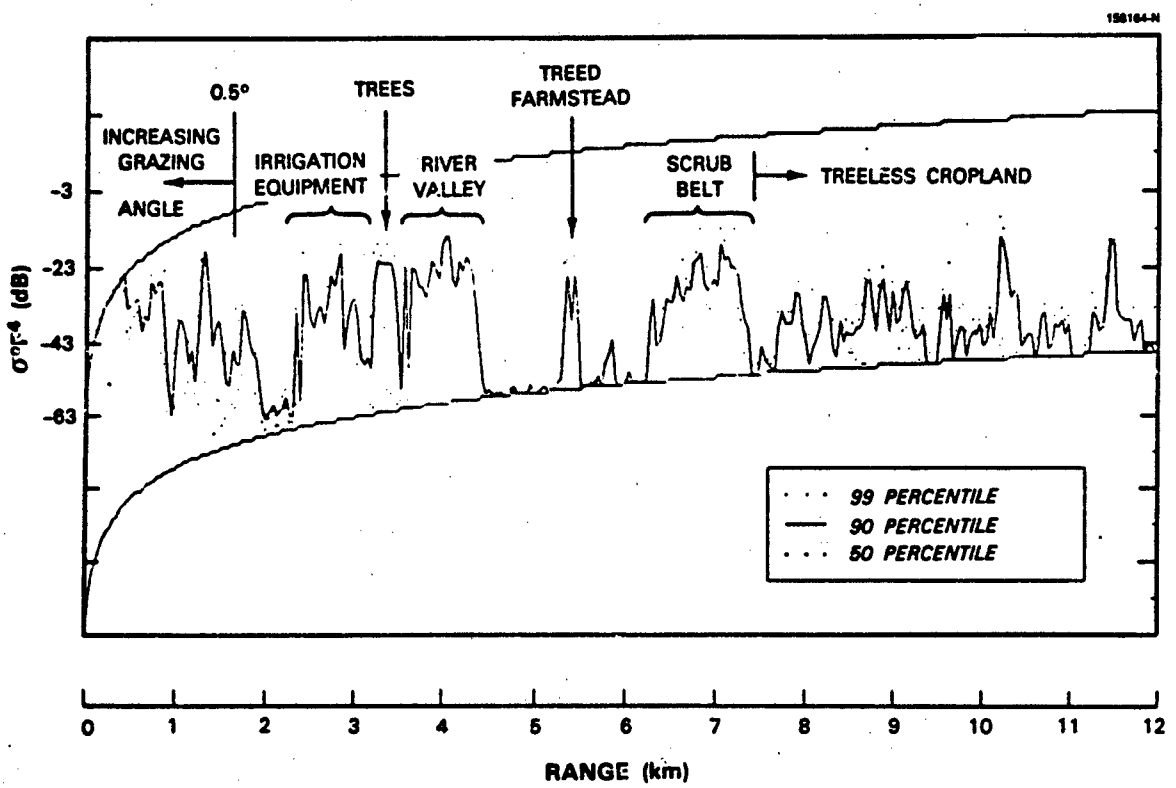

- DATA SHOWN FOR INDIVIDUAL RANGE GATE POSITIONS, AVERAGED OVER A 7° SECTOR, 232° TO 239° (31 Azimuth Samples/Gate)
- MEASUREMENT DATE, 3 MARCH 1980; LEAFLESS DECIDUOUS TREES, SNOW COVERED FIELD SURFACES

Figure 12. Clutter strength versus range to the southwest at Shilo.

Beyond 2 km, the clutter strengths in Figure 12 are dominated by discrete clutter sources. For example, the treeless cropland to the far southwest for which clutter data are shown is within geometric line-of-sight of the radar (i.e., from these fields the radar antenna is visible on the horizon). Thus these fields are under direct illumination by the radar at a depression angle of about 0.1°. Yet the radar is not sensitive to the backscatter from these field surfaces themselves. Rather, the clutter sources in these fields are all vertical discrete objects, including individual farmsteads (usually surrounded by trees as windbreaks) and other vertical features such as fence lines, telephone poles, bushes, and buildings.

The overall nature of the low-angle clutter amplitude phenomenon shown in Figure 12 shows extreme and rapid variation of clutter strength from range gate to range gate. These variations easily encompass 30 dB or more at a given percentile level of strength. The overall picture is not one of well-behaved or easy-to-describe statistics. Rather, there is patchiness and heterogeneity. An investigator would not start out being overly optimistic about capturing the effects shown here in a traditional grazing angle model based on terrain slope. This, however, is the phenomenon that seeks description.

Considered next is similar clutter strength versus range data from a much higher site at Cazenovia, New York. At Cazenovia the radar set-up is high on the side of a steep valley, as shown in the top sketch in Figure 13. The radar looks down into the valley at high airborne-like depression angles. Beneath the terrain profile in Figure 13 are $\sigma^\circ F^4$ data versus range shown in the same manner as in Figure 12 for Shilo, averaged azimuthally over an azimuth sector in individual range-gate positions. The dashed lines between the upper terrain profile and the lower clutter data trace are included merely to aid the eye in associating particular points within the data window on the terrain profile with corresponding points in the clutter data.

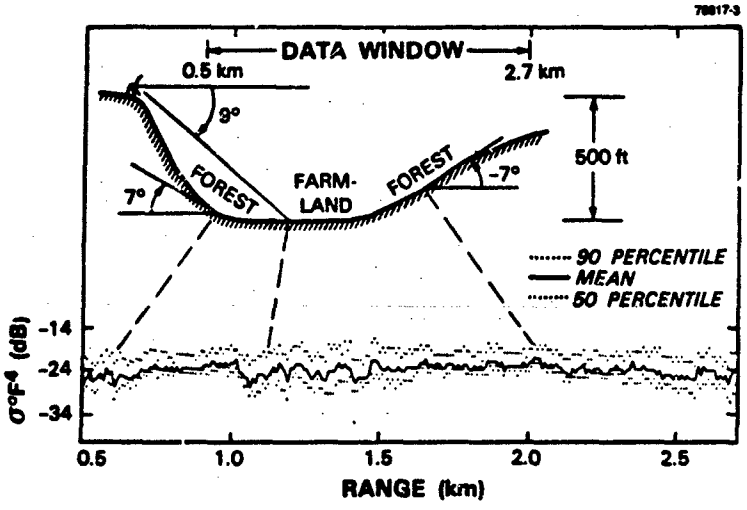

● DATA SHOWN FOR INDIVIDUAL RANGE GATE POSITIONS, AVERAGED OVER A 58° AZIMUTH SECTOR (9248 Azimuth Samples/Gate)

Figure 13. Clutter strength versus range at high depression angle at Cazenovia, New York.

The data in Figure 13 seem to belong to a completely different phenomenological regime than the data in Figure 12. The fluctuations of clutter strength with range are much less at the higher depression angle, more on the order of 6 dB than the 30-dB swings shown in Figure 12. The variation of clutter strength with range at high depression angle in Figure 13 is much less patchy, more homogeneous, and gives much more indication of being of a continuous process rather than the discrete-dominated process of Figure 12. The amount of shadowing (i.e., number of noise level cells) is dramatically reduced (essentially to zero) from Figure 12 to 13. Thus the most remarkable feature in the high-angle data of Figure 13 is the reduction of spread in clutter amplitudes exhibited at the higher illumination angle. Besides reduction in spread, the overall strength has increased with depression angle also, from about $\sigma^\circ F^4 \approx -33$ dB on the average in Figure 12 to about $\sigma^\circ F^4 \approx -24$ dB on the average in Figure 13. These two major effects of decreasing spread and increasing strength in clutter amplitude distributions as depression angle increases and shadowing decreases are basic effects in low-angle clutter that are generalized in subsequent sections of this report.

2.1.5 Terrain Slope

Depression angle does not depend on the local terrain slope at the backscattering terrain point, whereas grazing angle, defined as the angle between the tangent to the local terrain surface at the backscattering terrain point and the direction of illumination, does depend on the local terrain slope. If depression angle is a useful modeling parameter of low angle clutter, should not grazing angle be a better parameter? Intuition strongly suggests that the best measure of illumination angle in considering backscattering from a rough surface is the angle between the direction of illumination and the plane of the surface.

How should these important terrain slopes be computed or measured? At this point digital terrain elevation data are considered. Referred to as "DTED," these data are often provided as points of terrain elevation precise to 1 m on an approximately 100-m grid. In clutter modeling, can grazing angle be brought to bear to predict clutter strength, pixel by pixel in the DTED, based on the elemental terrain slopes provided by these data? If such an approach were successful, the DTED could then be allowed to carry the burden of describing terrain.

The practicality of this approach was investigated at six different sites of widely varying terrain type. At all of them, very little useful correlation was seen between clutter strength and grazing angle. Why was this the case? It is necessary to recall first that DTED describes only a bare earth and contains no information describing land cover, edges of land cover features, or discrete land cover objects. That is, the DTED bare earth does not attempt to represent the discrete land cover sources that dominate many of these measurements. Beyond this, however, investigations clearly revealed that many DTED cells provide markedly inaccurate estimates of detailed terrain slope at the scale of radar resolution. Specification of scale, accuracy, precision, and sampling interval in a hypothetical terrain elevation data base suitable for clutter strength prediction would be expected to result in much more stringent requirements than those of the currently available DTED. Again, even perfect terrain data still would contain no land cover information. Of course, the currently available DTED invites its use; however, DTED cannot be

faulted if, as here, it is applied to more demanding problems than it was designed to face. In any event, these DTED studies support the observation that "... in typical agricultural and rolling terrain... the grazing angle is not readily definable [6]."

The discussion returns to the implicit idea that at some level or some scale, terrain slope must strongly affect clutter strength. In contrast to DTED pixels, consider the reported clutter patches, typically sized to be several kilometers on a side. Recall that the landform within each patch is classified through interpretation of stereo aerial photographs and topographic maps. In this classification, terrain slope is the principal criterion. Of course, any patch several kilometers on a side presents various slopes to the radar, so one must think in terms of a distribution of slopes over each patch. Further, realize that this distribution of slopes over a patch depends on the measurement scale employed. That is, increasing magnification is expected to always reveal increasing detail and new structure in the surface (i.e., fractal phenomenon). Thus the actual distribution of slopes over a patch is regarded as an indeterminate quantity.

Through subjective interpretation of air photos and maps, however, one can at least roughly bound or set limits to the slopes existing within each patch, and subsequently, bin patches within classes defined by these slope limits. Table 5 shows six categories of landform in increasing order of terrain slope. Within the category of level terrain are Phase Zero measurements from 524 different patches. For each level patch, there exists a corresponding measured mean clutter strength. Figure 14 shows the cumulative distribution of mean clutter strengths from all 524 patches of level terrain. A great deal of spread is observed in this distribution of mean clutter strength measured from level patches. From maximum to minimum measured mean values, there is over 30 dB of variation. The cumulative distributions of mean clutter strength from the five remaining terrain types of Table 5 are also shown in Figure 14. If the median level in each distribution of mean clutter strength in the figure (indicated by the horizontal dashed line) is selected as a measure of centrality, then a statistically significant monotonic increase in mean clutter strength is seen with terrain slope. That is, at the median level the distributions are displaced increasingly to the right with increasing terrain slope over a range of 11 dB from minimum to maximum. Hence intuition is justified. These data unequivocally illustrate that clutter strength depends on terrain slope. The effect is strong enough to be observed through dispersive influences of land cover, terrain heterogeneity, and depression angle. Two other important facts are also observed: (1) there is much spread within the distribution of mean clutter strength for any given class of landform, and (2) although significant, there is relatively little separation between adjacent classes.

Similar to the way in which Figure 14 shows how Phase Zero mean clutter strengths separate in six classes of landform, Figure 15 shows how Phase Zero mean clutter strengths separate in six classes of land cover. As might be intuitively expected, the data of Figure 15 indicate that, in terms of mean clutter strength, urban terrain is stronger and wetland weaker than most other land cover types. The results in Figures 14 and 15 are derived from the same set of 2,177 clutter patch measurements described in Section 2.1.

TABLE 5
Six Categories of Landform in Increasing Order of Terrain Slope

Landform	Terrain Slope (deg)
Level (LEV)	<1
Undulating (UND)	<1
Inclined (INC)	1-2
Rolling (ROL)	2-5
Moderately Steep (MST)	2-10
Steep (STP)	10-35

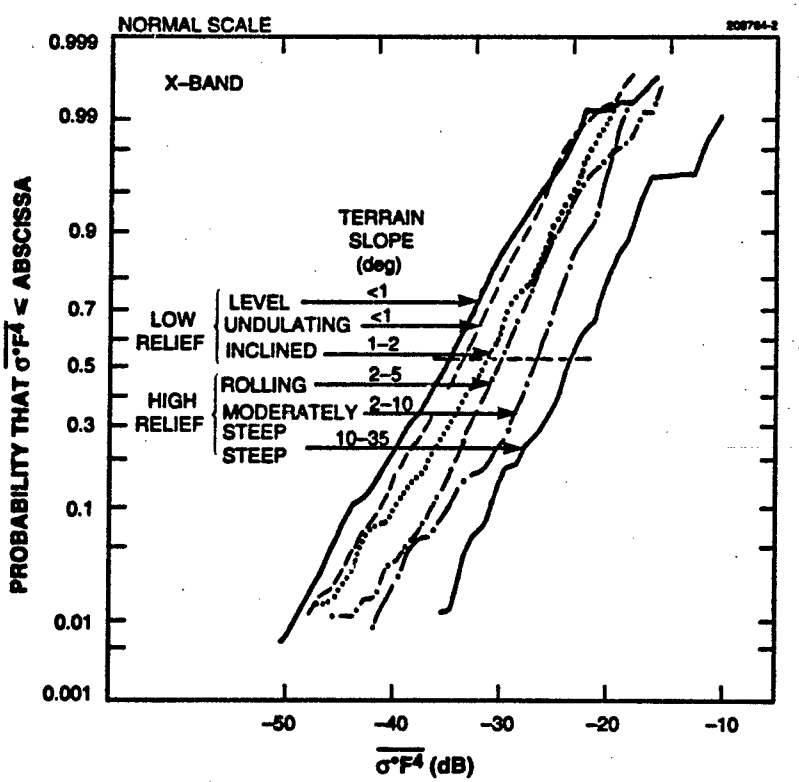

Figure 14. Cumulative distributions of X-band mean ground clutter strength by landform in rural terrain.

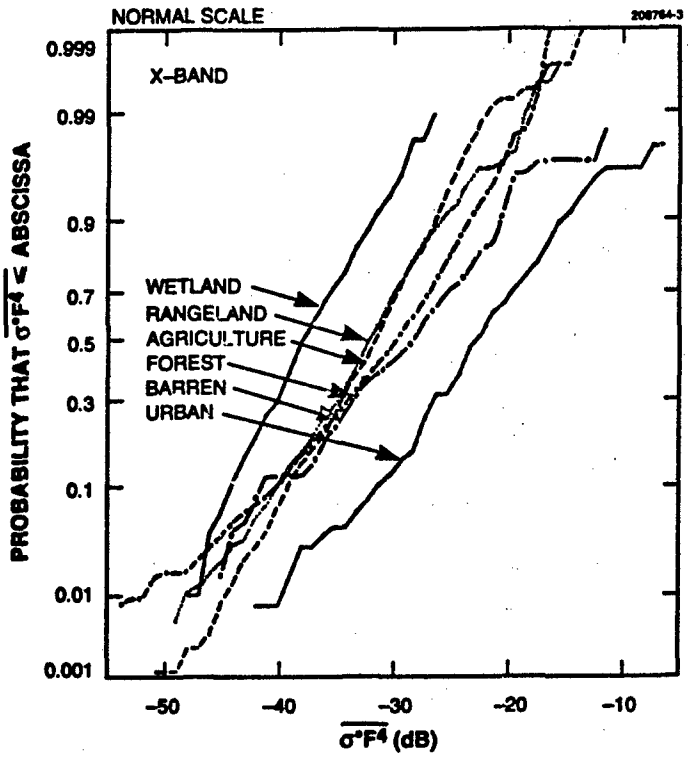

Figure 15. Cumulative distributions of X-band mean ground clutter strength by land cover.

2.1.6 Approach to Modeling

Assume that DTED is available for the site that is required to be modeled. The DTED can be used to define kilometer-sized clutter patches as regions of general geometric visibility. This is an appropriate use of DTED, well matched to the information content of the data base. Within these macroregions of visibility, one cannot accurately predict clutter strength pixel by pixel simply by association with the local terrain slope and grazing angle at the pixel. This is an inappropriate use of DTED because the sought after information is at a scale, accuracy, and precision not contained within the data.

Illumination angle, however, is of major importance in its effects on low-angle clutter amplitude statistics. Rather than grazing angle, results in this report are based on depression angle. Depression angle is a quantity that can be computed relatively rigorously and unambiguously from available information. For example, within a macropatch of visible terrain in DTED, depression angle (which depends on the pixel-level elevations over the patch and not the detailed rates of change of these elevations) is a quantity

that usually varies relatively slowly over the patch. If the mean depression angle over the patch is computed, this mean value is relatively insensitive to the questions of accuracy, precision, and scale that plague grazing angle.

But in using depression angle, how are the important effects of terrain slope incorporated? Reconsider the data in Figure 14 that statistically show that mean clutter strength increases with increasing terrain slope. As shown in the figure, terrain is simply separated into two categories, low and high relief. Low-relief terrain provides slopes of <2°; high-relief terrain provides slopes of >2°. Thus in Figure 14, level, inclined, and undulating terrain categories are all low relief; whereas rolling, moderately steep, and steep terrain categories are all high relief. This simple landform-descriptive scheme consisting of two, relatively general classes captures much of the statistical significance in the dependency of clutter strength on terrain slope, given the large spread within and little separation between more specific classes. In addition, this simple twofold scheme has the attendant advantage of liberating the user of these results from providing highly detailed descriptions of terrain.

Superficially, it may appear that terrain slope enters the current results only through specification of terrain relief as low or high. However, the further quantitative dependence of these results on depression angle also carries with it an implicit dependence on terrain slope, wherein higher terrain slopes generally occur at higher depression angles (i.e., high sites usually occur in hilly terrain). Thus results in this report take into account terrain slope, not in simplistic or idealized ways, but in practicable ways that have stood the test of trial in the empirical data of this study.

2.2 GENERAL SPATIAL AMPLITUDE STATISTICS

2.2.1 Amplitude Statistics by Depression Angle for Three General Terrain Types

Described here are spatial amplitude distributions of low-angle X-band ground clutter for three general terrain types, (1) rural/low relief, (2) rural/high relief, and (3) urban. These three terrain types are summarily described in Table 6 (but also see Table 4). These terrain types comprehensively include all

TABLE 6
Three General Terrain Types

1	Rural/Low-Relief (Slopes <2°; Relief <100 ft)
2	Rural/High-Relief (Slopes >2°; Relief >100 ft)
3	Urban

terrain, that is, any patch of terrain must be classified as one, and only one, of these three types. Thus rural terrain includes such diverse specific terrain types as agricultural, forest, rangeland, wetland, and barren. Urban terrain includes any kind of built-up land such as commercial, industrial, and residential. In terms of degrees of roughness of terrain surface, this classification system incorporates the following specific categories: level, undulating, hummocky, inclined, broken, rolling, ridged, moderately steep, and steep. Low relief encompasses the first five categories, and high relief encompasses the last four. Note that the actual distribution of slopes that exists within a macroscale clutter patch is specified, not the overall slope of the best-fit plane through the patch.

In data reduction and analysis, X-band clutter amplitude distributions were formed from 2,177 clutter patches, each generally several kilometers on a side. For each patch, detailed terrain descriptions at the specific level just described were determined. However, it was found that in the separation of clutter amplitude data into such specific and detailed terrain-descriptive classes, spread within class was broad, and separation between similar or neighboring classes was narrow, as illustrated by the results of Figures 14 and 15. Thus the three general terrain classes of Table 6 are utilized, which do provide significant and useful separation of X-band clutter data. A simple way of interpreting these three general terrain types is that only "mountains" (i.e., rural/high relief) and "cities" (i.e., urban) grossly warrant separation from all other terrain types (i.e., rural/low relief).

Empirical ground clutter spatial amplitude distributions are presented in Figure 16 by depression angle for rural/low- and rural/high-relief terrain. Similar results are presented in Figure 17 for urban terrain (in which the regime of the rural distributions is also shown lightly shaded for comparison). These distributions include all spatial samples within patches, including cells at radar noise level, but are only shown over $\sigma^\circ F^4$ regimes to the right of the highest noise-contaminated bin. Thus, where shown, these distributions are independent of Phase Zero sensitivity and represent what a theoretically infinitely sensitive radar would measure. It is seen that, within each of these three terrain types, the shape of the spatial amplitude distribution is strongly dependent on depression angle, such that there is a continuous rapid decrease in the spread of the distribution with increasing depression angle, even over the very small depression angles (e.g., usually $<1.5^\circ$ in low-relief terrain) associated with surface-sited radar. The distributions in Figures 16 and 17 are formed by combining like-classified clutter data from a large data set comprising 2,177 clutter patch amplitude distributions obtained from measurements at 107 sites. It is only by means of such extensive averaging that the smooth monotonic dependence of both strength (i.e., the distributions gradually move to the right with increasing angle) and spread (i.e., the slopes of the distributions gradually increase with increasing angle) emerge in these empirical distributions to provide a general predictive capability. These underlying fundamental trends are often obscured by specific effects in individual measurements.

Most (viz., 74%) of these measured data are contained in the rural/low-relief distributions of Figure 16. It is this parametric regime that is applicable to most surface radar situations and has traditionally been least well understood. The set of rural/low-relief distributions is extended in the rural/high-relief distributions (the latter accounting for 20% of the data), where higher depression angles are realized in high-relief terrain through higher site locations. Across the rural data set as a whole, the effect of continuously decreasing spread in the distributions with increasing angle is at the heart of understanding

low-angle clutter as a physical phenomenon dominated by microshadowing. The highest angle distribution (viz., 6° to 8° depression angle) almost achieves the Rayleigh slope, which indicates that the amount of microshadowing is relatively small at such high airborne-like angles. The resultant nearly full illumination, as expected, provides approximately Rayleigh statistics. The urban distributions of Figure 17 (which contain 6% of the measured data) also show monotonically decreasing spread with increasing angle, but contain significantly stronger clutter than the corresponding rural/low-relief distributions.

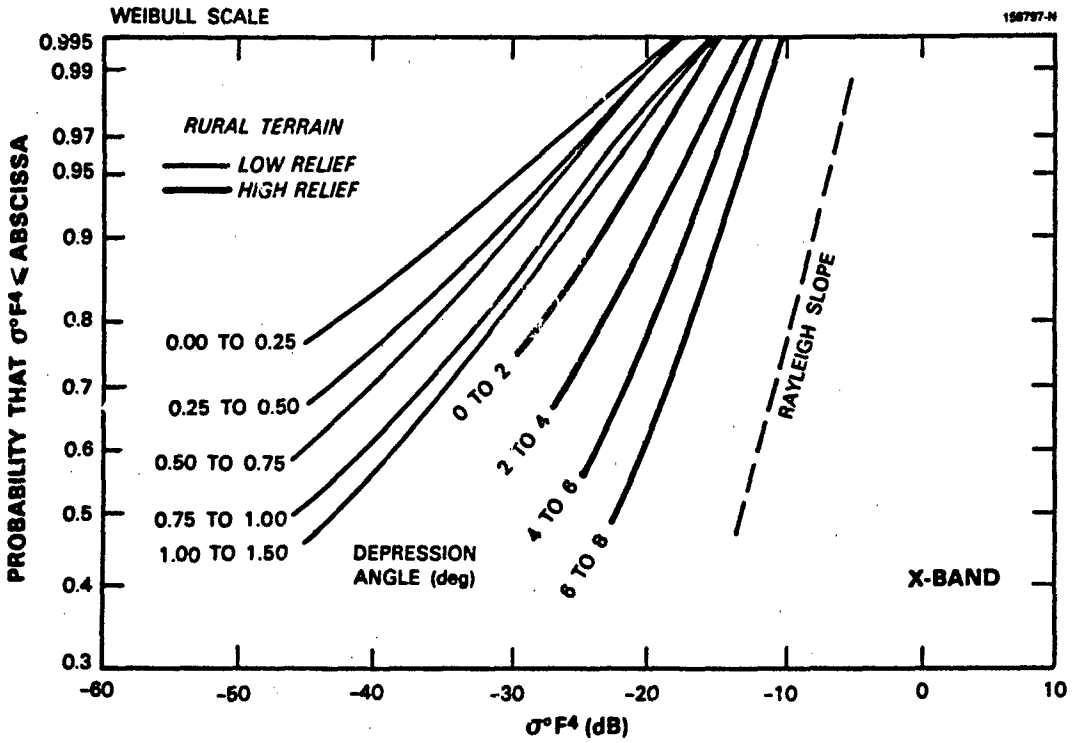

Figure 16. Cumulative ground clutter amplitude distributions by depression angle for rural terrain of low and high relief.

2.2.2 Weibull Parameters

In the empirical description and prediction of ground clutter spatial amplitude distributions, we utilize Weibull statistics [1,7]. Weibull distributions provide the wide degree of spread appropriate to low-angle ground clutter amplitude distributions. The Weibull cumulative distribution function may be written:

$$P(x) = 1 - \exp\left\{-\frac{\ln 2 \times x^b}{\left(\sigma^\circ_{50}\right)^b}\right\} .$$

σ°_{50} = median value of x

b = $1/a_w$

a_w = Weibull spread parameter.

The mean-to-median ratio for Weibull statistics is

$$\frac{\overline{\sigma^\circ_w}}{\sigma^\circ_{50}} = \frac{\Gamma\left(1+a_w\right)}{(\ln 2)^{a_w}} ,$$

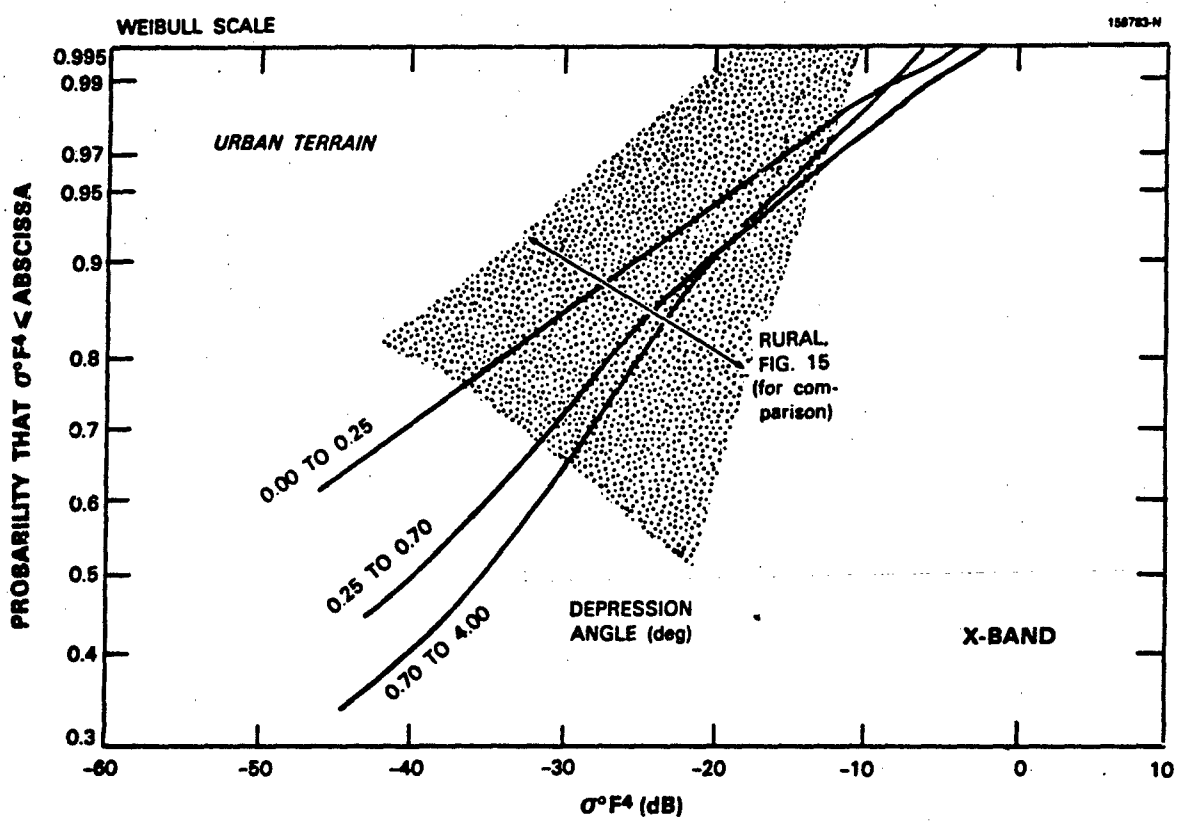

Figure 17. Cumulative ground clutter amplitude distributions by depression angle for urban terrain.

where $\overline{\sigma^\circ_w}$ is the mean value of x and Γ is the gamma function. Here the random variable x represents clutter strength $\sigma^\circ F^4$. Occasionally, $\sigma^\circ F^4$ is referred to as "effective clutter strength" to emphasize that it is this product, including propagation effects and not just the backscattering coefficient σ° itself, that is important to radar system performance.

Much of the information contained in the distributions of Figures 16 and 17 can be usefully approximated with Weibull statistics. Specific Weibull approximations for these ground clutter amplitude distributions are presented in Table 7, again by depression angle for each of the three general terrain types. The table shows that large spread parameters at low angles rapidly diminish with increasing angle, approaching the Rayleigh value of unity at the highest angles. At the same time, median clutter strengths rapidly increase with increasing angle. Mean clutter strengths increase more gradually with increasing angle, so spread in terms of mean-to-median ratio is also observed to rapidly decrease with increasing angle. This behavior mirrors that of K-distributions (which also decrease in spread and degenerate to Rayleigh), which arise out of theoretical investigations of low-angle clutter amplitude distributions [8,9]. To just describe these amplitude distributions, which is the intent here, Weibull distributions serve the purpose as well as K-distributions and are simpler to use.

TABLE 7
Statistical Attributes of X-Band Ground Clutter Amplitude Distributions for Rural/Low-Relief, Rural/High-Relief, and Urban Terrains by Depression Angle

Terrain Type	Depression Angle (deg)	Weibull Parameters a_w	σ°_{50} (dB)	$\overline{\sigma^\circ_w}$ (dB)	Ensemble Mean Clutter Strength (dB)	Percent of Samples Above Radar Noise Floor	Number of Patches
Rural/ Low-Relief	0.00-0.25	4.8	-60	-33	-32.0	36	413
	0.25-0.50	4.1	-53	-32	-30.7	46	448
	0.50-0.75	3.7	-50	-32	-29.9	55	223
	0.75-1.00	3.4	-46	-31	-28.5	62	128
	1.00-1.25	3.2	-44	-30	-28.5	66	92
	1.25-1.50	2.8	-40	-29	-27.0	69	48
	1.50-4.00	2.2	-34	-27	-25.6	75	75
Rural/ High-Relief	0-1	2.7	-39	-28	-26.7	58	176
	1-2	2.4	-35	-26	-25.9	61	107
	2-3	2.2	-32	-25	-24.1	70	44
	3-4	1.9	-29	-23	-23.3	66	31
	4-5	1.7	-26	-21	-22.2	74	16
	5-6	1.4	-25	-21	-21.5	78	9
	6-8	1.3	-22	-19	-19.1	86	8
Urban	0.00-0.25	5.6	-54	-20	-18.7	57	25
	0.25-0.70	4.3	-42	-19	-17.0	69	31
	0.70-4.00	3.3	-37	-22	-24.0	73	53

In Table 7, the measured mean clutter strength for each ensemble distribution is observed to closely match the mean strength of the approximating Weibull distribution, a first engineering indication that laying a best-fitting Weibull straight line over central parts of each measured distribution of Figures 16 and 17 produces approximating distributions of reasonable mean strength. Also, Table 7 strongly indicates that shadowing is a major causative agent for the variations that are observed with depression angle. That is, the incidence of microshadowed cells varies from as much as 64% at grazing incidence in low-relief terrain to as little as 14% at high angle in high-relief terrain. Condensing and coding properties of X-band low-angle ground clutter within Weibull coefficients as presented in Table 7 represents the fulfillment of much of what we initially set out to learn about the low-angle clutter phenomenon.

2.2.3 Mountain and Urban Clutter

Besides needing information that describes general clutter strengths, an analyst may also need to know something about worst-case situations. Provided here is additional specific information on how strong mountain or urban clutter can become.

The steepest, roughest terrain from which ground clutter was measured was that of the Canadian Rocky Mountains. One site, Plateau Mountain, is a flat-topped mountain high in the Rockies (8,125 ft above sea level), to which road access was available for the truckborne clutter measurement equipment. From Plateau Mountain the view to the west is of steep, barren rock faces from high peaks in the Rockies. The lower slopes of these mountains are often tree-covered with the trees gradually thinning out at the higher elevations. Measured clutter amplitude distributions from the five strongest of these Plateau Mountain clutter patches were selected. Descriptive information and mean clutter strengths for these five patches are provided in Table 8.

First consider patches 4/4, 4/5, 5/1, and 5/2. These four mountain patches represent very strong ground clutter. In terms of mean clutter strength, the strongest patch measured at Plateau Mountain was 4/4 at –9.6 dB, approximately 10 dB stronger than the strongest mean clutter from general rural terrain in Table 7. In perusing Table 8, it is seen that all four patches are steep, barren, mountain peaks with various incidences of trees on their lower slopes and observed at various depression angles. Mean clutter strengths from these four patches range from –9.6 to –10.8 dB. Taken together, these four patches may be thought of as representing a worst-case (i.e., strongest clutter) for rural terrain. The mean strength of the clutter in patch 15/3 is somewhat weaker at –16.2 dB. The information in Table 8 for patch 15/3 indicates that it is a steep, forested patch rather than a steep, barren patch and that it is observed at a relatively high depression angle of 2.2°.

The discussion continues with clutter measurements for three urban clutter patches. Table 9 shows terrain descriptions, depression angles, and mean clutter strengths for these three patches, which constitute backscatter measurements made from the town of Rosetown, Saskatchewan (population 2,500); the city of L. bridge, Alberta (population 55,000); and the city of Calgary, Alberta (population 600,000), respectively. All three urban areas exist on the relatively low-relief Canadian prairies. In each case, the patch was selected to include only relatively high commercial buildings within the urban complex, in contrast to lower outlying residential areas. Differences in clutter strength between commercial and residential urban clutter are discussed subsequently.

TABLE 8
Descriptions and Statistical Attributes of the Five Strongest X-Band Clutter Patches at Plateau Mountain

Patch Number*	Mean Clutter Strength of Patch (dB)		Number of Spatial Samples in Patch	Percent of Samples Above Radar Noise Floor	Depression Angle (deg)	Land-form	Land Cover	Percent Tree Cover η
	Including Samples at Radar Noise Floor	Excluding Samples at Radar Noise Floor						
4/4	-9.6	-9.0	264	86	1.6	8	7	$30 < \eta \leq 50$
4/5	-10.8	-9.5	336	74	0.6	8	7	$30 < \eta \leq 50$
5/1	-10.8	-8.7	216	62	1.2	8	7	$3 < \eta \leq 10$
5/2	-9.8	-9.0	264	84	0.8	8	7	$1 < \eta \leq 3$
15/3	-16.2	-16.1	784	99.5	2.2	8	41	$\eta > 50$

[U] *Except for patch 15/3, these patches all include exposed rock and near vertical rock faces at mountain summits; in patch 15/3, the terrain constitutes forested slopes (still steep) at lower elevations.

TABLE 9
Descriptions and Statistical Attributes of Three Urban Clutter Patches at X-Band

Site	Patch Number	City or Town	Mean Clutter Strength of Patch (dB)	Number of Spatial Samples in Patch	Percent of Samples Above Radar Noise Floor	Depression Angle (deg)	Land-form	Land Cover	Percent Tree Cover η
Rosetown North[a]	13/2	Rosetown	-4.6	384	77	0.18	1	12	$1 < \eta \leq 3$
Lethbridge West[b]	12	Lethbridge	-5.1	3066	74	0.29	1	12	$1 < \eta \leq 3$
Strathcona[c]	7	Calgary	-13.4	6328	70	1.21	1-3	12-11-51	$1 < \eta \leq 3$

[U] Notes:

a. Commercial sector of Rosetown.

b. Industrial sector, some open development land, TV tower.

c. Downtown Calgary, high rise buildings, Bow River and parks near river, railroad, some residential (minor).

Although the data in Table 9 are from three commercial patches, the physical differences are great. Rosetown is a small prairie town, providing services to the local agricultural community. Its commercial sector is physically very small but includes grain elevators illuminated at low depression angle. The mean clutter strength of –4.6 dB for the Rosetown patch is the single strongest mean clutter strength that exists within the data base of 2,177 Phase Zero patch measurements; however, it is not particularly exceptional—there are many other relatively small, relatively strong clutter patches from small prairie towns, often including grain elevators.

It may be preferable to base the worst-case urban clutter strength estimate on larger urban patches than Rosetown, allowing for much more extensive statistical averaging to take place within the distributions. Lethbridge is a moderate-sized regional city in southern Alberta. The industrial area constituting its urban clutter patch is approximately 10 times larger than Rosetown but, as was the Rosetown patch, is illuminated at quite low depression angle. Notwithstanding the substantial physical differences in these two patches, their clutter amplitude distributions and mean strengths are very similar. The Calgary patch in Table 9 is approximately twice as large as the Lethbridge patch. Calgary is a major city, and the Calgary patch was selected to include, for the most part, just its high-rise central urban core. Thus the Calgary patch is quite different, physically, from both the Lethbridge and the Rosetown patches. At Calgary, the radar position was on a hill in the outskirts of the city, 490 ft higher than the average terrain height at the city center. Thus the depression angle at which the radar viewed the ground at the city center was substantial, 1.2°, although the highest buildings in the city core were more than 500 ft high. The hilltop location may have resulted in less multipath augmentation and in many surfaces being illuminated at more oblique angle than the near-grazing-incidence illumination at Rosetown and Lethbridge and may be the cause of the somewhat weaker mean clutter strength for Calgary (in Table 9) compared with Rosetown and Lethbridge.

Taken together, these three patches would seem to provide a reasonable indication of how strong urban clutter can become. Compared with the general urban distributions of Table 7, the data in Table 9 indicate that worst-case urban clutter can be 10 dB stronger in mean strength than more general urban levels. This is roughly the same conclusion reached about severe mountain clutter compared with more general high-relief clutter. In terms of mean clutter strength, severe urban clutter can be 5 dB stronger than severe mountain clutter.

In considering urban clutter, attention has been restricted to relatively strong urban clutter from commercial sectors. Considered now are the differences in urban clutter strength between residential sectors (expected to be weaker) and commercial sectors (expected to be stronger). Table 3 indicates that within the general land cover class of urban, the more specific subclasses of residential and commercial are employed. All the measured clutter amplitude distributions from patches classified by land cover as residential were combined into one ensemble amplitude distribution, and all measured distributions from patches classified by land cover as commercial were combined into another ensemble amplitude distribution. In terms of mean clutter strength over the complete ensemble distributions, the results indicate that clutter from commercial sectors is 3.4 dB stronger than clutter from residential sectors. This may be regarded as a general result based on measurements from many clutter patches.

2.2.4 Farmland and Forest

The simple terrain-descriptive scheme of Table 6 provides the useful general trends in low-angle clutter statistics formulated empirically in terms of Weibull statistics shown in Table 7. The simple scheme is based on distinguishing terrain in only three types. Although Weibull statistics and three terrain types are enough to show fundamental trends in low-angle clutter, the resultant simple construct cannot contain, of course, all the complex higher-order attributes of the real phenomenon. Examples of additional effects in measured clutter amplitude distributions are next provided, illustrating how increasing fidelity in terrain-descriptive information can reveal higher-order trends in clutter statistics.

Figure 18 shows general X-band ground clutter results obtained through ensemble combination of many Phase Zero measurements. In this figure, $\overline{\sigma^\circ_w}$ and a_w are shown as a function of depression angle for various rural terrain types. First, following the simple terrain-descriptive scheme, within rural terrain, if terrain type is distinguished in two major categories of relief, as low (terrain slopes <2°) and high (terrain slopes >2°), in both categories of relief $\overline{\sigma^\circ_w}$ increases and a_w decreases with increasing depression angle; and $\overline{\sigma^\circ_w}$ is significantly greater and a_w significantly less in high-relief terrain than in low-relief terrain, for a given depression angle.

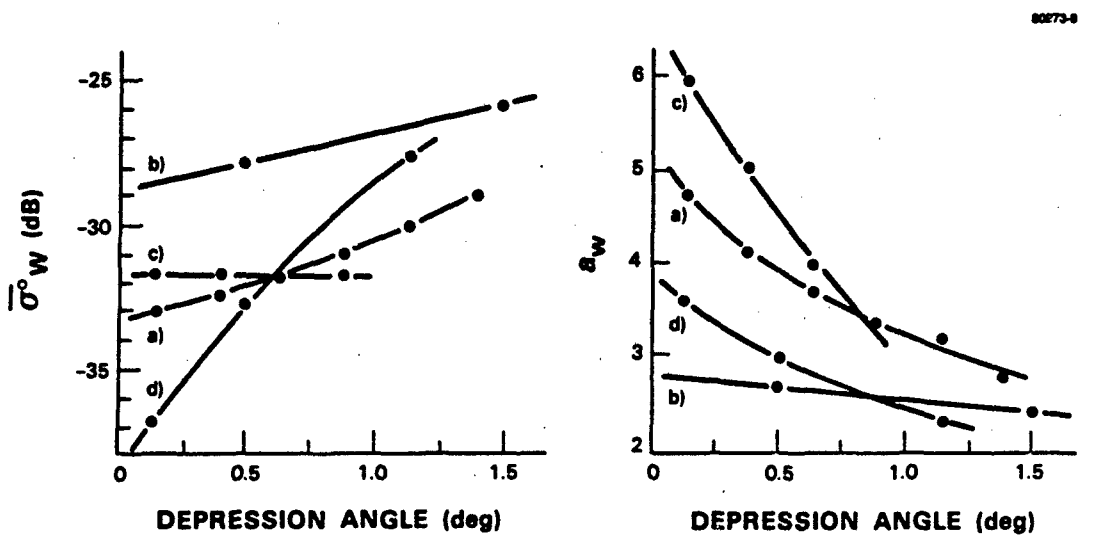

Figure 18. X-band ground clutter results for (a) rural/low-relief terrain, (b) rural/high-relief terrain, (c) level farmland, and (d) level forest.

Second, if within general rural/low-relief terrain specific subcategories of level farmland and level forest are separated out, Figure 18 shows that with increasing depression angle in level farmland $\overline{\sigma^\circ_w}$ does not vary at all, but a_w decreases very quickly, whereas in level forest $\overline{\sigma^\circ_w}$ increases and a_w decreases.

The reasons for this are as follows. In level farmland, dominant clutter sources are large, discrete, vertical objects. At low angles strong returns are received from these discrete sources but much (e.g., 75%) of the intervening terrain is either shadowed or provides very weak returns due to the illumination being at grazing incidence. As a result, in level farmland at low depression angle clutter amplitude distributions have very large spread. As depression angle increases, the intervening terrain between strong discrete sources comes under stronger illumination. The weak returns from these regions rapidly increase, and as a result spreads in amplitude distributions rapidly decrease, but the strong returns from the discrete objects at the high ends of the distributions tend to be relatively independent of depression angle and continue to dominate their mean strengths.

In contrast, level forest is much more a homogeneous scattering medium, not dominated by large discrete objects. Nevertheless, at low angles in level forest, there still occurs a large amount (e.g., 50%) of microshadowing. As angle increases, the shadowing gradually decreases. As a result the amplitude distributions gradually tighten up, and their mean strengths—not dominated here by large singular discrete sources—gradually rise.

2.3 DEPRESSION ANGLE CHARACTERISTICS

Throughout this report, the importance of depression angle on low-angle ground clutter amplitude distributions is emphasized. In Section 2.3, characteristics were provided defining these distributions as a function of depression angle for increasing specificity of terrain type. That discussion continues here, but moves in the opposite direction and focuses on general effects of depression angle on clutter amplitude distributions independent of terrain type. In addition, the median strengths in these distributions, previously tabulated in Table 7, are brought back into the discussion to help further their understanding.

Figure 19 shows mean and median clutter strengths as a function of depression angle, inclusive of all terrain types. The results of Figure 19 are based on Phase Zero measurements of 1,926 macropatches from 86 sites. Figures 20 and 21 show the ratio of standard deviation-to-mean versus depression angle and the incidence of occurrence of microshadowing within clutter patches versus depression angle, respectively, for the same set of Phase Zero data upon which the results in Figure 19 are based. At very low angles, clutter is caused to a very great extent by discrete sources distributed over a nonbackscattering surface. As discussed in Section 2.2, and as shown in Figure 21, as angle rises through the low-angle regime, the percent of cells containing discernible clutter rises very quickly as the shadowed terrain between discrete sources rapidly comes into view. As a result, the median clutter strength, which was driven down by the large number of shadowed cells at very low angles, also rises relatively quickly with increasing depression angle as shown in Figure 19. Median clutter strength does not rise quite as abruptly as the shadowing function, because even when terrain comes into visibility at very low angle, the area-extensive backscatter from the terrain surfaces themselves, as opposed to the discrete objects on them, is very weak. With increasing angle, however, as the shadowing function levels off, the median clutter strength continues to rise as area-extensive backscatter rises with increasing angle. The ratio of mean-to-median in Figure 19 and the ratio of standard deviation-to-mean in Figure 20, which are measures of spread in clutter amplitude distribution, both decrease strongly with increasing angle as the shadowed and weak samples at the low end of the distributions rise towards the stronger values, which are dominating

the mean. In the high angle limit of 8° for the data in Figures 19 and 20, both these measures of spread begin to approach their limiting values associated with Rayleigh statistics.

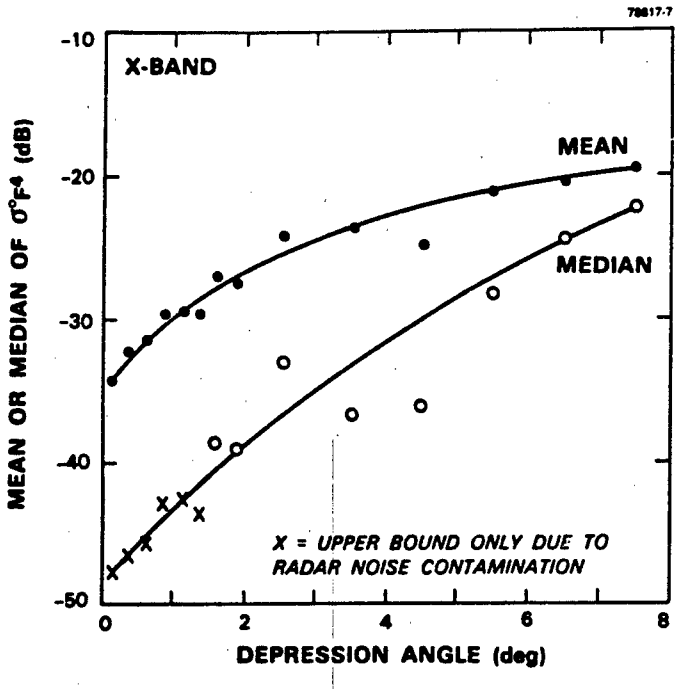

Figure 19. General variation of ground clutter strength with depression angle.

In modeling ground clutter at the high depression angles associated with airborne platforms, clutter strength is often approximated as being directly dependent on the sine of the depression angle. Such a model is referred to as "constant γ," where $\sigma^\circ = \gamma \cdot \sin\theta$. Typical decibel values of γ (i.e., 10 $\log_{10}\gamma$) in current use for rural terrain are –10 and –15 dB [6,10,11]. The mean clutter strength curve above 1° in Figure 19 is very accurately represented by $\sigma^\circ = \gamma (\sin\theta)^{1.2}$ with a decibel value of γ equal to –8.9 dB. Note that the exponent to which sin θ is raised in this latter expression is 1.2; that is, the sin θ dependence of the Phase Zero data in Figure 19 above 1° (457 macropatches) is somewhat stronger than the linear dependence often assumed [6,10,11]. Fitting the constant-γ model with linear sin θ dependence to the mean clutter strength data above 1° in Figure 19 leads to a decibel value of γ of approximately –11 dB, although doing so results in a poorer fit to the data. A summary of simple semiempirical clutter models such as the constant-γ model and its variations that have been utilized historically to fit various experimental data sets is provided in Ruck [12].

At lower angles, however, where most clutter occurs in surface-sited radar (1,472 macropatches in Figure 18), mean clutter strength is much stronger than would be predicted by the sine of the depression angle dependency, the latter, of course, becoming vanishingly small as depression angle approaches zero. Strong mean clutter at low angles is the consequence of domination of the low-angle phenomenon by

discrete clutter sources. There has been occasional speculation in the clutter literature as to whether clutter strengths might "come back up" at very low angles because of possible specular incidence on discretes [13]. The data of Figure 19 indicate that, although mean clutter strength remains relatively high at low angles, its general characteristic is to always decrease with decreasing angle, with no reversal occurring in this characteristic at very low angle.

Mean clutter strength is observed to vary over a range of 15 dB with depression angle in Figure 19 from –34.2 dB at grazing incidence in the 0° to 0.25° depression angle regime to –19.3 dB in the 7° to 8° depression angle regime. This mean strength variation of 15 dB with depression angle is the strongest general parametric variation observed of any single parameter in the Phase Zero X-band data. The effect of higher average terrain slopes at higher depression angles is implicit in this dependence. The dependence may be summarized by saying that it is depression angle as it influences shadowing on a sea of discretes that most directly affects strength in low-angle ground clutter.

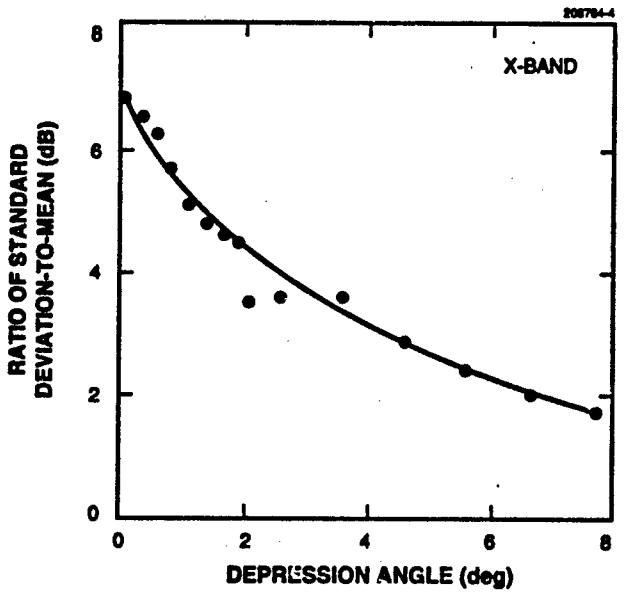

Figure 20. General dependence of ratio of standard deviation-to-mean in ground clutter spatial amplitude statistics on depression angle.

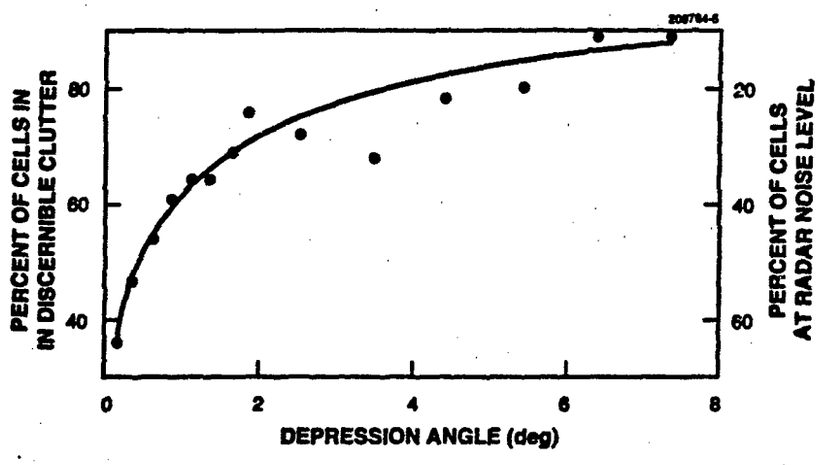

Figure 21. General incidence of microshadowing within clutter patches as a function of depression angle.

3. PHASE ONE MULTIFREQUENCY CLUTTER MEASUREMENTS

3.1 REPEAT SECTORS

To this point, the discussion has been on the initial clutter measurement data base that was obtained with the X-band Phase Zero instrumentation radar. With Phase Zero, a large primary file, consisting of 2,177 different clutter patch measurements has been under analysis. With this large number of terrain samples, even after separating into different categories of terrain type and depression angle, there are still many samples left in any given category and hence good statistical definition in the results. That is, with a lot of averaging at work in these data, even small differences in results are statistically significant.

A limitation of the Phase Zero results is that they are directly applicable only at X-band. In contrast, the full-scale Phase One instrumentation radar operated in five frequency bands—VHF, UHF, L, S, and X [1]. With Phase One, there are thus far 42 terrain patches under analysis, one per site from each of the 42 Phase One sites. This particular patch at each site is referred to as the "repeat sector" patch. Backscatter measurements were performed on each repeat sector patch across a 20-element radar parameter matrix (viz., five frequencies, two polarizations, two range resolutions), and each such measurement was performed several times to get day-to-day variations in clutter statistics. This Phase One repeat sector data base that is currently under analysis constitutes a comparable amount of data to the Phase Zero data base and allows one to address trends of variation with frequency, resolution and polarization. It is important to realize, however, that when looking for such trends and separating the 42 repeat sector patches into various categories of terrain type and depression angle, in contrast to Phase Zero there often may not be very many terrain samples per category. As a result, this study reaches for multifrequency characteristics, often on the basis of a few examples of an observed trend rather than with the statistical rigor of Phase Zero. Currently, preparations are being made to bring all the Phase One, 360° survey data at each site under analysis, in addition to the repeat sector data. In so doing, the Phase One analyses will eventually obtain the important Phase Zero statistical advantage of very many terrain samples.[2]

3.2 PROPAGATION AND ABSORPTION

This section begins with a brief review of the fundamental mechanisms at work in low-angle ground clutter. The point of view is to consider what might cause major parametric trends in the Phase One repeat sector results, particularly when radio frequency (RF) ranges from VHF to X-band, a span approaching two orders of magnitude.

Thus far it has been shown that a fundamental parametric dependence in low-angle clutter amplitude statistics is that of depression angle as it affects microshadowing among dominant discrete clutter sources, such that mean strengths increase and cell-to-cell fluctuations decrease with increasing angle. Depression angle continues to be an important parameter at all frequencies in the Phase One results.

---

[2]At this current time of revision of Technical Report 786 (i.e., September 1992), analysis of the extensive Phase One survey data is completed, and a report on the results, viz., Technical Report 958 [14], is being prepared.

Because of the heterogeneous process involved, wherein groups of cells providing strong returns are often separated by cells that provide weak or noise-level returns, the spatial resolution of the radar plays a fundamental role in the amount of spread in clutter amplitude distributions from spatial macroregions. Also at all frequencies, increasing resolution results in less averaging within a cell, more variability from cell to cell and hence increased spread in the distributions.

Within the context of the above mechanisms, frequency itself does not generally play as fundamental a role as do depression angle and resolution. Averaged across all the multifrequency measured data, independent of terrain type, mean clutter strength shows no significant trend of variation with frequency. One reason is that in composite terrain, clutter sources tend to be vertical objects and edges of vertical features (e.g., tree lines) that are large with respect to RF wavelength, VHF through X-band.

However, two strong trends with frequency occur in particular circumstances. One is directly the result of the intrinsic backscattering coefficient itself, σ°, having an inherent frequency-dependent characteristic. Thus at high depression angles in forested terrain, our propagation measurements have shown that forward reflections are minimal (i.e., $F \sim 1$), and in such terrain σ° decreases strongly with increasing frequency. This result is due to the absorption characteristic of forest increasing with frequency, and hence the diffusely radiative characteristic of forest (including the backscatter direction) decreasing with frequency.

The other trend with frequency is the result of a general propagation effect entering clutter strength $\sigma^\circ F^4$ through the propagation factor F. As discussed previously, at low depression angles in level open terrain, strong forward reflections cause multipath lobing on the free space antenna pattern. In contrast to X-band, however, at low frequencies such as VHF, these lobes tend to be broad for typical antenna heights. As a result, at such low frequencies returns from most clutter sources are received well on the underside of the first multipath lobe, and effective clutter strengths are much reduced. As frequency increases the multipath lobes become narrower, and typical clutter sources such as buildings or trees subtend a number of such lobes with the result that at higher frequencies the overall multipath effect on illumination averages out and has little net influence on the effective clutter strength. Thus at low angles on level open terrain, there is a characteristic of strongly increasing mean clutter strength with frequency introduced through the propagation factor. Because this characteristic is caused by the interference between the direct and the multipath rays, it depends on geometric factors such as antenna mast height (50 to 60 ft in these measurements) and range to the clutter patch. In inclined or rolling open terrain of increased relief, multipath is as likely to reinforce as to cancel clutter returns, even at low frequencies.

Polarization has very little general effect on ground clutter amplitude statistics. In the distribution of differences of vertically polarized mean clutter strength minus horizontally polarized mean clutter strength across the entire multifrequency repeat sector clutter measurement data base, the median difference is only 1.5 dB. However, occasional specific measurements can show more significant variation with polarization.

3.3 PHASE ONE RESULTS

Phase One made measurements at 42 different sites, largely in the 1982 to 1984 time period [1]. Figure 22 shows measured ground clutter maps for all five Phase One frequencies at one of these sites, Peace River South, high on the east bank of the Peace River in Alberta. The maximum range in these maps is 23 km. Clutter is shown as white where $\sigma^\circ F^4 > -40$ dB. To the west in each map is the well-

illuminated river valley; to the east, level terrain is illuminated at grazing incidence. As patterns of spatial occurrence of ground clutter, all five clutter maps are quite similar. The reason for this similarity is that the relatively strong clutter shown in Figure 22 largely comes from visible terrain. At all five frequencies in the figure, the nature of the clutter tends to be granular and patchy. However, the granularity is greater at grazing incidence to the east, less at the higher depression angles to the west. As has been discussed, such effects are principally due to depression angle as it affects microshadowing. Also obvious in Figure 22 is the effect of increasing azimuth beamwidth with decreasing frequency, causing increasing azimuthal smearing of the clutter. This effect is that of spatial resolution, such that decreasing resolution results in decreased spreads in clutter amplitude distributions.

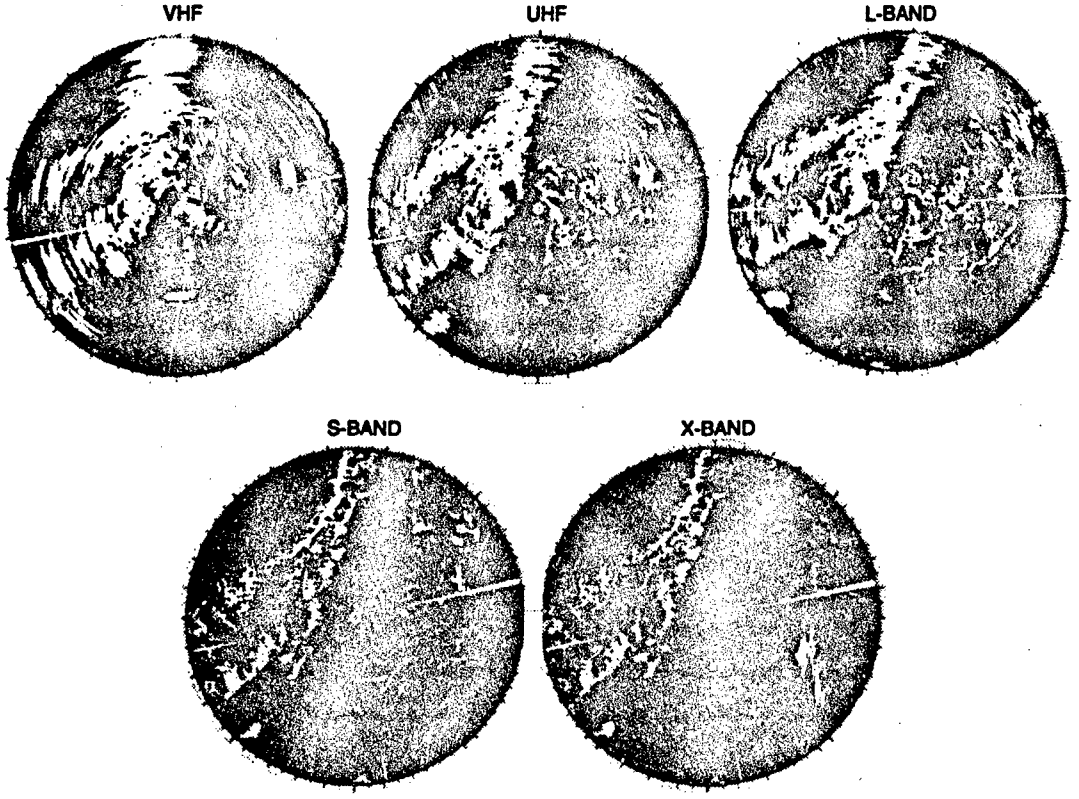

Figure 22. Measured multifrequency ground clutter maps at Peace River, Alberta.

The primary Phase One data thus far under analysis are from the repeat sector at each of the 42 sites. As previously discussed, the repeat sector is a concentration in which measurements were repeated a number of times. Typically, the repeat sector is about 20° in azimuth extent and occurs at ranges beginning a few kilometers from the radar and extending 5 or 10 km.

Figure 23 shows Phase One repeat sector measurements of mean ground clutter strength versus frequency for various terrain types. Depression angle, resolution, and polarization are also carried as parameters. First the data are separated into the three major terrain categories of rural/low relief, rural/high relief, and urban. Within the set of rural/low-relief data in Figure 23(a), which is applicable to mixed composite terrain at intermediate depression angles, little general frequency dependence is observed. However, in rural/high-relief terrain, and in particular, the extreme high-relief subcategory of mountains shown in Figure 23(a), a strongly decreasing trend of mean clutter strength with increasing frequency is seen. Figure 23(b) shows that through the microwave bands, mean clutter strengths in urban terrain are relatively frequency independent and stronger than in rural terrain. At VHF, however, mean strengths from urban terrain spread over many decibels. This spread is caused by specific propagation influences at VHF, in which broad multipath lobes can either increase or decrease the effective gain of the measurement over the whole repeat sector.

Next, Figure 23 separates the Phase One measurements into rural subcategories of forest and farmland. Figures 23(c) and (d) show mean clutter strength in forested terrain as a function of frequency in three regimes of depression angle. At high depression angles greater than 1°, there is a strong decreasing trend of mean clutter strength with increasing frequency, which is due to the increasing absorption characteristics of the forest with increasing frequency. It is believed that the decreasing trend of mean strength with frequency in mountain terrain in Figure 23(a) is also largely due to the vegetative absorption effect because the mountain repeat sectors, even though they contained high barren peaks and rock faces, also presented steeply inclined forested surfaces at their lower elevations. At intermediate depression angles in forested terrain, Figure 23(d) shows little variation of mean strength with frequency, indicating that at the lower angles there occurs less penetration of energy into the forest vegetation and hence decreased influence of its absorption and reradiation characteristics. At even lower angles near grazing incidence, Figure 23(c) shows an opposite trend of increasing strength with increasing frequency, indicating that at such low angles forward reflections are beginning to occur at low frequencies.

Next, Figures 23(e) and (f) show mean clutter strength in farmland terrain as a function of frequency in two regimes of depression angle. Throughout the microwave regime in these figures, little general dependence of mean strength is seen with either frequency or depression angle. However, at low depression angle on level farmland, Figure 23(e) indicates that as frequency decreases below L-band through UHF to VHF, the effective mean clutter strength drops off dramatically, an effect due to the decreasing intensity of illumination caused by increasing multipath.

In agreement with the Phase Zero data of Figure 18, the Phase One repeat sector data set of Figure 23 indicates that at X-band in forested terrain, mean clutter strength increases significantly with depression angle, but at X-band in farmland terrain, mean clutter strength is relatively independent of depression angle. Effects of polarization and resolution on mean clutter strength are generally relatively small in Figure 23. However, occasional specific measurements show more significant variation with these parameters. As one extreme example, Figure 23(a) shows measurements from two different sites, indicating that at VHF in steep mountainous terrain, vertically polarized backscatter is about 6 dB stronger than horizontally polarized.

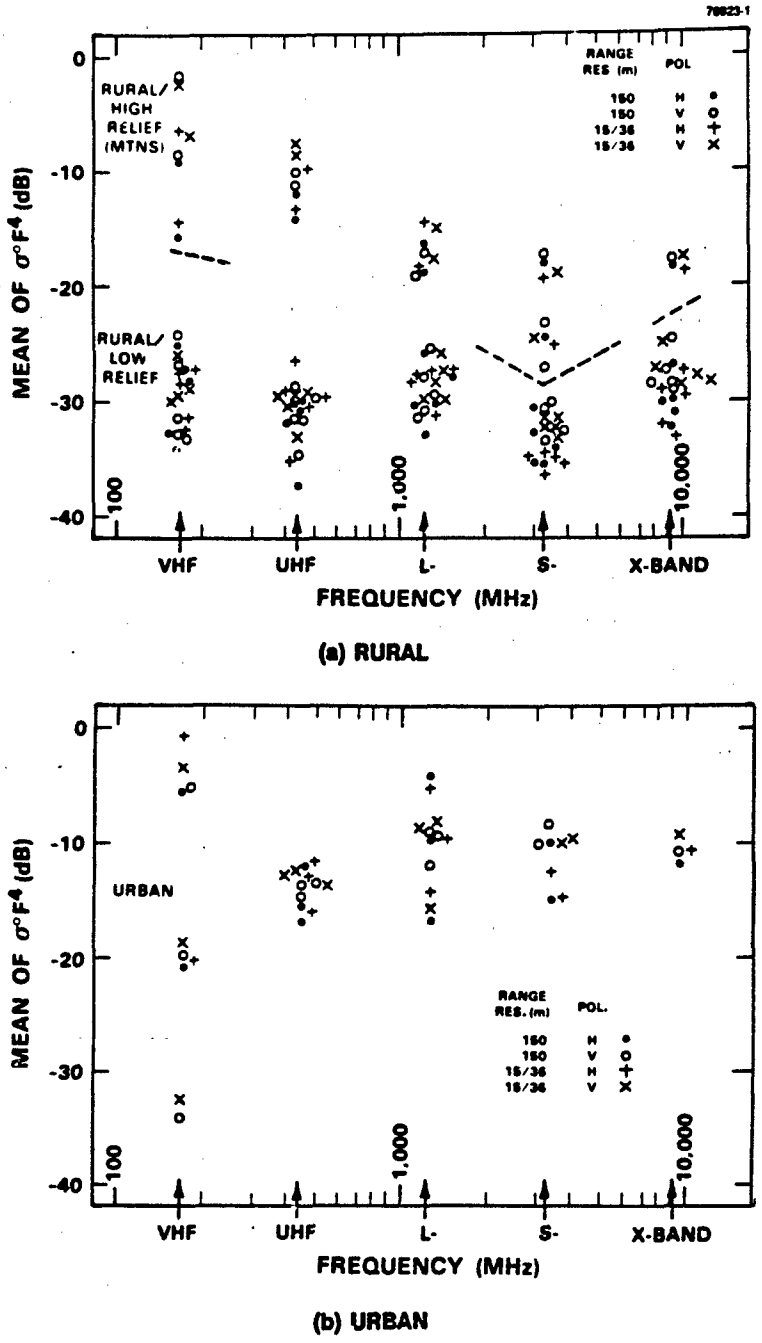

Figure 23. Phase One measurements of mean ground clutter strength versus frequency in (a) rural and (b) urban terrain.

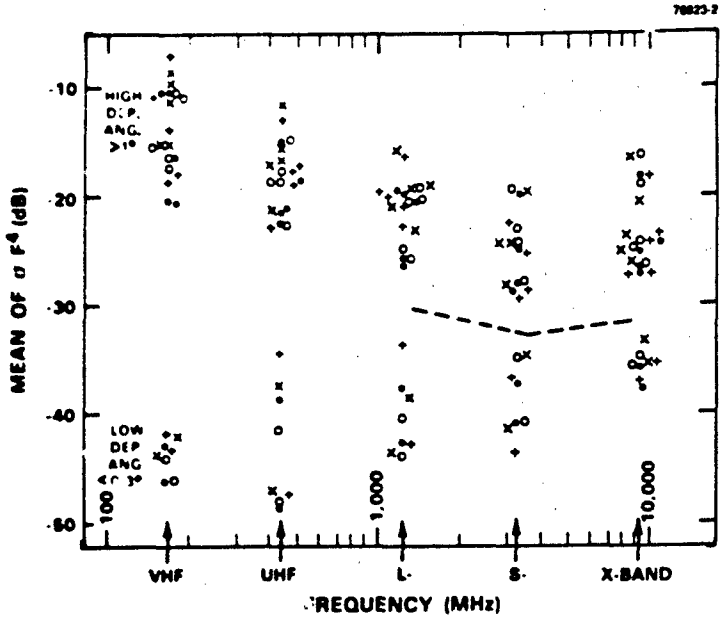

(c) FOREST: LOW AND HIGH DEPRESSION ANGLES

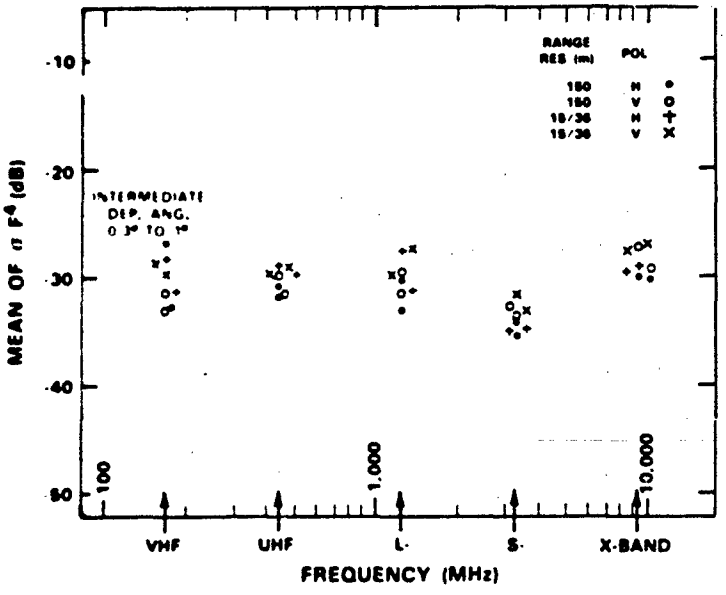

(d) FOREST: INTERMEDIATE DEPRESSION ANGLE

Figure 23 (Continued). *Phase One measurements of mean ground clutter strength versus frequency in forested terrain at (c) low/high and (d) intermediate depression angles.*

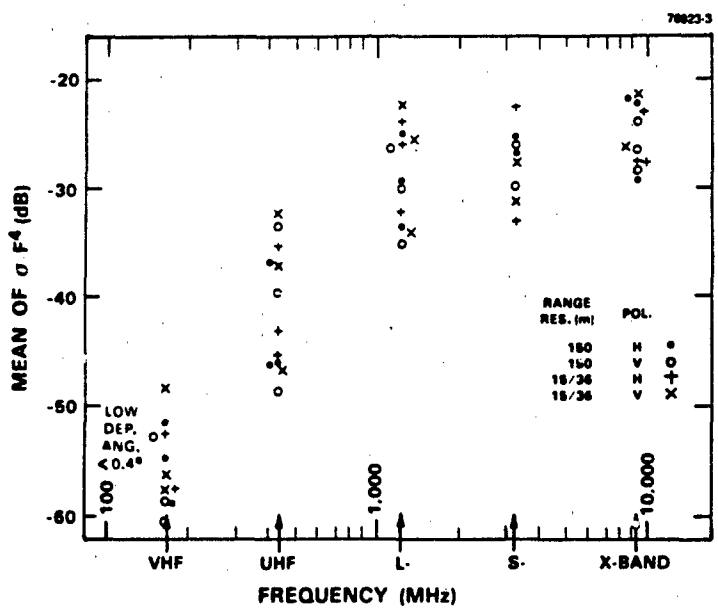

(e) FARMLAND: LOW DEPRESSION ANGLE

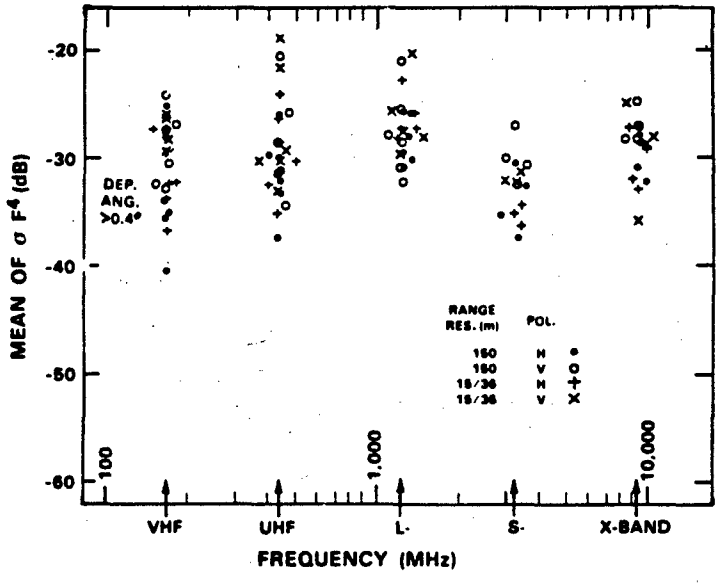

(f) FARMLAND: INTERMEDIATE AND HIGH DEPRESSION ANGLES

Figure 23 (Continued). Phase One measurements of mean ground clutter strength versus frequency in farmland terrain at (e) low and (f) intermediate/high depression angles.

4. CLUTTER MODELS

4.1 MODELING RATIONALE

Low-angle ground clutter is a patchy phenomenon. Areas of the ground that are geometrically visible to the radar usually cause relatively strong clutter returns, and areas of the ground that are geometrically shadowed or masked to the radar usually cause relatively weak clutter returns, often below the sensitivity of the radar. Using DTED allows, at gross level, the deterministic prediction and distinction between macroregions of general visibility and macroregions of shadow, where *macro* implies kilometer-sized regions that encompass hundreds or thousands of spatial resolution cells. Such specific prediction of the gross pattern of spatial occurrence of ground clutter at a given site is essentially what is meant here by site-specific study.

Predicting, in this manner, the existence of a macropatch of clutter at some site, a description is subsequently needed of the statistics of the clutter returns that are expected from within the patch. Thus Section 4.2 provides modeling information to describe clutter amplitude distributions occurring over macrosized spatial regions of visible terrain. These distributions are characterized by broad spread. The degree of spread in the distribution is fundamentally controlled by depression angle, that is, the angle below the horizontal at which the patch is observed at the radar. Depression angle is a quantity that can be computed relatively rigorously and unambiguously from DTED, depending as it does simply on range and relative elevation difference between the radar antenna and the patch. The fundamental dependence of spread in the clutter amplitude distribution on depression angle is significant even for the very low depression angles (i.e., typically <1°) and small patch-to-patch differences in depression angle (i.e., typically fractions of 1°) that occur in surface-sited radar. The patch-specific modeling information for ground clutter amplitudes presented in Section 4.2 is tied tightly to this basic dependence on depression angle, such that amplitude distributions are specified in terms of small and precise gradations of depression angle for various terrain types.

Let us reflect on this approach to modeling low-angle ground clutter. As a physical phenomenon, the two most salient attributes of low-angle ground clutter are, first, patchiness in spatial occurrence and second, extremely wide cell-to-cell statistical fluctuation in strength within a patch. Concerning spatial patchiness, it is emphasized that clutter does not always exist, and it is the patch-specific on-again, off-again macrobehavior of clutter that at first level determines the performance of a given radar against a given low-altitude aircraft at a given site. Concerning wide cell-to-cell variations of clutter strength within macropatches, it is emphasized that what appears at first consideration to be a phenomenon of extreme variability and little predictability turns out in the end, after analyzing much data, to be generally dependent on very fine differences in depression angle. Use of site-specific DTED allows the capture of both these basic attributes of low-angle ground clutter, its spatial patchiness (approximately computed simply as geometric visibility), and (through depression angle) its expected range of amplitudes within a patch. Therefore, this approach to modeling low-angle clutter is regarded as a major advance over more general

approaches that do not distinguish between macroregions of clutter occurrence and macroregions of shadow. This approach allows an analyst to predict, within macroregions, where a surface-sited radar can be expected to encounter clutter interference and where the radar will be free of such interference; and, given that the radar is experiencing clutter, what, on the average, the expected statistics of signal-to-clutter ratio will be across the macroregion of clutter.

Clutter returns within patches are often highly spatially correlated. This report discusses the fact that the dominant clutter sources within macroregions of general geometric visibility are usually spatially localized or discrete, such that groups of cells providing strong returns are often separated by cells providing weak or noise-level returns. The occurrence of noise-level returns sprinkled within macroregions of general geometric visibility is referred to as "microshadowing," where *micro* implies resolution-cell-sized areas. The high degree of spatial microcorrelation of strong discrete sources within macropatches results from the fact that such sources exist as vertical features of discontinuity in landscape that often occur in definite patterns, for example, along the leading edge of a tree line or the clustering of vertical objects along roads and field boundaries. If an analyst is interested in the actual microstatistics, for example, of break-lock in a surface radar tracking a target across a given clutter patch, the information in this report does not go that far. The kind of detail and fidelity in terrain description that are required to predict microstatistics of spatial correlation of clutter amplitudes within macropatches are regarded as a second sequential major hurdle to cross in clutter modeling. Limitations to be encountered in attempting this second advance have begun to be actively explored. It is not yet known how well microspatial correlation can be predicted, but it is a very challenging task that immediately takes exploratory operations out to the limits of current resources in terms of available information and computer processing. In contrast, the first major advance in low-angle clutter fidelity, which is the field-of-investigation of this report, comes relatively easily once DTED is in play.

The allusion to general non-site-specific and non-patch-specific approaches to clutter modeling does not imply that such approaches are without value. Section 4.3 moves from measurements in which the patch-specific parameter of depression angle is the fundamental controlling parameter to nonspecific modeling information based on relatively general parameters such as site height, terrain roughness, and terrain type (e.g., forest, agricultural, etc.). However, it is true that such nonspecific approaches are, indeed, relatively abstract and conceptually vague in quantitative study. This is the logical penalty that non-site-specific approaches must pay as the price for generality. This penalty comes about because, instead of aggregating system performance measures after realistic clutter computations at many individual sites, the non-site-specific approach attempts to aggregate and generalize clutter influences before a one-time assessment of system performance. That is, the non-site-specific approach takes the easy way of attempting to a priori average the clutter first, whereas the site-specific approach takes the harder but more rigorous way of a posteriori averaging the actual site-specific performance measures to reach generality.

4.2 SITE-SPECIFIC MODEL

Comprehensive multifrequency modeling information for predicting ground clutter amplitude statistics as they occur over spatial macroregions of geometrically visible terrain is presented in Table 10.[3] This information is provided within a context of Weibull statistics [1,7], where $\overline{\sigma^\circ_w}$ is the Weibull mean strength and a_w is the Weibull spread parameter. In developing such a model, there are three categories of descriptive parameters available. First are parameters which are descriptive of the radar. The important radar parameters affecting clutter statistics are radar frequency as it affects $\overline{\sigma^\circ_w}$ and radar spatial resolution as it affects a_w.

Second are parameters descriptive of the geometry of illumination of the clutter patch. We use depression angle, a quantity relatively simple and unambiguous to determine, depending as it does simply on range and relative elevation difference between the radar antenna and the backscattering terrain point. Our attempts to use grazing angle have met with little additional success, partly due to difficulties associated with scale, precision, and accuracy in unambiguously defining local terrain slope and partly because dominant clutter sources tend to be vertical discrete objects associated with the land cover.

One burden in formulating the model in terms of depression angle rather than grazing angle is the need to contend with negative depression angles, a practical complication that does not intrude in the theoretical concept of measuring grazing angle above the local surface. Negative depression angle occurs when terrain is observed by the radar at elevations above the antenna. From simple geometry, if terrain is visible at negative depression angle, it must be of terrain slope greater than the absolute value of the depression angle at which it is observed.

Third are parameters descriptive of the terrain within the clutter patch. The clutter model of Table 10 is comprehensive in terms of addressing all terrain types. Most terrain types in the model involve several depression angle regimes. In this model, the important general terrain types are threefold, namely (1) rural/low-relief terrain in which terrain slopes are <2°; (2) rural/high-relief terrain in which terrain slopes are >2°; and (3) urban terrain. Most of the current measured data are from rural/low-relief terrain. Within general rural/low-relief terrain, the model further distinguishes the three specific important subclass terrain types of continuous forest, open farmland, and open wasteland (e.g., desert, marsh) or grazing land with very low incidence of large discrete vertical objects (e.g., farmstead buildings, feed storage silos, isolated trees, etc.) such as typically occur in farmland. Within rural/high-relief terrain, particularly separated out are the two subclass terrain types of continuous forest and mountains. Within urban terrain, separated out is the subclass of urban terrain as observed on open low-relief terrain supportive of multipath. Concerning the several subcategories of terrain contained within each of the three general terrain types in Table 10, the general category (a) is applicable only if the terrain in question fails to meet the specification of any of the subsequent specific subcategories within a group. That is, the general category applies to mixed or composite terrain that is neither completely open nor completely tree covered. The subcategorization of terrain within each major group becomes increasingly important with decreasing frequency. As discussed earlier, for logical completeness a fourth general category comprising terrain observed at negative depression angle is required. To repeat, terrain observed at negative depression angle is usually relatively steep.

---

[3]This model and its validation are discussed further in Billingsley [2]. New, more comprehensive clutter modeling information based on the Phase One 360° survey data is currently being prepared for publication in Technical Report 958 [14].

TABLE 10
Multifrequency Weibull Parameters of Ground Clutter Amplitude Distributions

Terrain Type	Depression Angle (deg)	$\overline{\sigma^{\circ}_{W}}$ (dB)					a_W	
		Frequency Band					Resolution (m^2)	
		VHF	UHF	L-	S-	X-BAND	10^3	10^6
Rural/Low-Relief								
a) General Rural	0.00 to 0.25	-33	-33	-33	-33	-33	3.8	2.5
	0.25 to 0.75	-32	-32	-32	-32	-32	3.5	2.2
	0.75 to 1.50	-30	-30	-30	-30	-30	3.0	1.8
	1.50 to 4.00	-27	-27	-27	-27	-27	2.7	1.6
	>4.00	-25	-25	-25	-25	-25	2.6	1.5
b) Continuous forest	0.00 to 0.30	-45	-42	-40	-39	-37	3.2	1.8
	0.30 to 1.00	-30	-30	-30	-30	-30	2.7	1.6
	>1.00	-15	-19	-22	-24	-26	2.0	1.3
c) Open farmland	0.00 to 0.40	-51	-33	-30	-30	-30	5.4	2.8
	0.40 to 0.75	-30	-30	-30	-30	-30	4.0	2.6
	0.75 to 1.50	-30	-30	-30	-30	-30	3.3	2.4
d) Desert, marsh, or grassland (few discretes)	0.00 to 0.25	-68	-74	-68	-51	-42	3.8	1.8
	0.25 to 0.75	-56	-58	-46	-41	-36	2.7	1.6
	>0.75	-38	-40	-40	-38	-26	2.0	1.3
Rural/High-Relief								
a) General Rural	0 to 2	-27	-27	-27	-27	-27	2.2	1.4
	2 to 4	-24	-24	-24	-24	-24	1.8	1.3
	4 to 6	-21	-21	-21	-21	-21	1.6	1.2
	>6	-19	-19	-19	-19	-19	1.5	1.1
b) Continuous forest	any	-15	-19	-22	-22	-22	1.8	1.3
c) Mountains	any	-8	-11	-18	-20	-20	2.8	1.6
Urban								
a) General Urban	0.00 to 0.25	-20	-20	-20	-20	-20	4.3	2.8
	0.25 to 0.75	-20	-20	-20	-20	-20	3.7	2.4
	>0.75	-20	-20	-20	-20	-20	3.0	2.0
b) Urban, observed on open low-relief terrain	0.00 to 0.25	-32	-24	-15	-10	-10	4.3	2.8
Negative Depression Angle								
a) All, except mountains and high-relief continuous forest	0.00 to -0.25	-31	-31	-31	-31	-31	3.4	2.0
	-0.25 to -0.75	-27	-27	-27	-27	-27	3.3	1.9
	<-0.75	-26	-26	-26	-26	-26	2.3	1.7

The clutter model of Table 10 consists of 27 combinations of terrain type and depression angle. For each combination, the model provides Weibull mean clutter strength as a function of radar frequency f, VHF through X-band, as $\overline{\sigma^{\circ}_{w}}(f)$, and provides the Weibull spread parameter as a function of radar spatial resolution A over the range between 10^3 and 10^6 m^2, as $a_w(A)$. The spread parameter is obtained from linear interpolation on $\log_{10}(A)$ between the values provided for $A = 10^3$ m^2 and $A = 10^6$ m^2. The total matrix of information in Table 10 contains all the important trends that have been observed in our measured clutter amplitude distributions.

Many of the important parametric trends of variation in the data of Table 10 are plotted in Figure 24. These trends are now discussed in some detail. In this figure, in general rural terrain of both low and high relief, mean clutter strength increases with depression angle but is invariant with frequency. That is, within the shaded region clutter strength rises with increasing depression angle both within the rural/low- and within the rural/high-relief regimes. In continuous forest, however, mean clutter strength depends both on depression angle and frequency; whereas in open farmland, mean clutter strength is invariant both with depression angle and frequency, except at low depression angle on level terrain where a significant multipath propagation loss occurs at low frequencies. Note that at intermediate depression angles in Figure 24, both forest and farmland fall in closely with general rural/low-relief terrain in terms of mean clutter strength.

Urban complexes observed on low-relief open terrain provide large mean clutter strengths at high frequencies partly because of their broadside aspect, but at low frequencies these large returns are decreased significantly through multipath loss. However, in more general composite terrain, mean clutter strength from urban complexes is 10 dB weaker than at high frequency on open terrain and is frequency invariant.

On discrete-free desert, marsh, or grassland, mean clutter strength is weaker than for other terrain types. Again, at low and even intermediate depression angles, there is a large multipath loss due to decreased illumination at the lower frequencies, and this loss is greater and extends to higher frequencies than in farmland because the clutter sources are much lower in such terrain (e.g., a sagebrush bush) than in farmland (e.g., a silo). Note that propagation loss itself would continue to decrease mean clutter strength from UHF to VHF at low and intermediate depression angles on open desert, marsh, or grassland; however, data from four different sites and at all parametric variations of polarization and resolution indicate that, in such terrain, mean clutter strength actually rises slightly from UHF to VHF.

If mean clutter strength is compared between desert and forest at X-band, at low and intermediate depression angles, mean strength in desert terrain is 5 or 6 dB weaker than in forest terrain, but at high depression angle >1° (and on the basis of two different Phase One desert measurement sites at all combinations of polarization and resolution), mean strength in desert is equal to that in forest terrain (i.e., at X-band, looking down at sagebrush vegetation is equivalent to looking down at a forest canopy).

The data in Figure 24 cover 66 dB of variability in mean clutter strength, from mountains at VHF to desert at UHF. Of course, cell-to-cell variability in amplitude statistics is even greater. Table 10 shows that spreads in clutter amplitude distributions due to cell-to-cell variability decrease both with increasing depression angle and with decreasing spatial resolution. Over and above these basic dependencies,

Table 10 shows that a_w in open farmland is greater than in general rural/low-relief terrain, whereas a_w in continuous forest is less than in general rural/low-relief terrain, and that a_w in rural/high-relief terrain is less than in rural/low-relief or urban terrain.

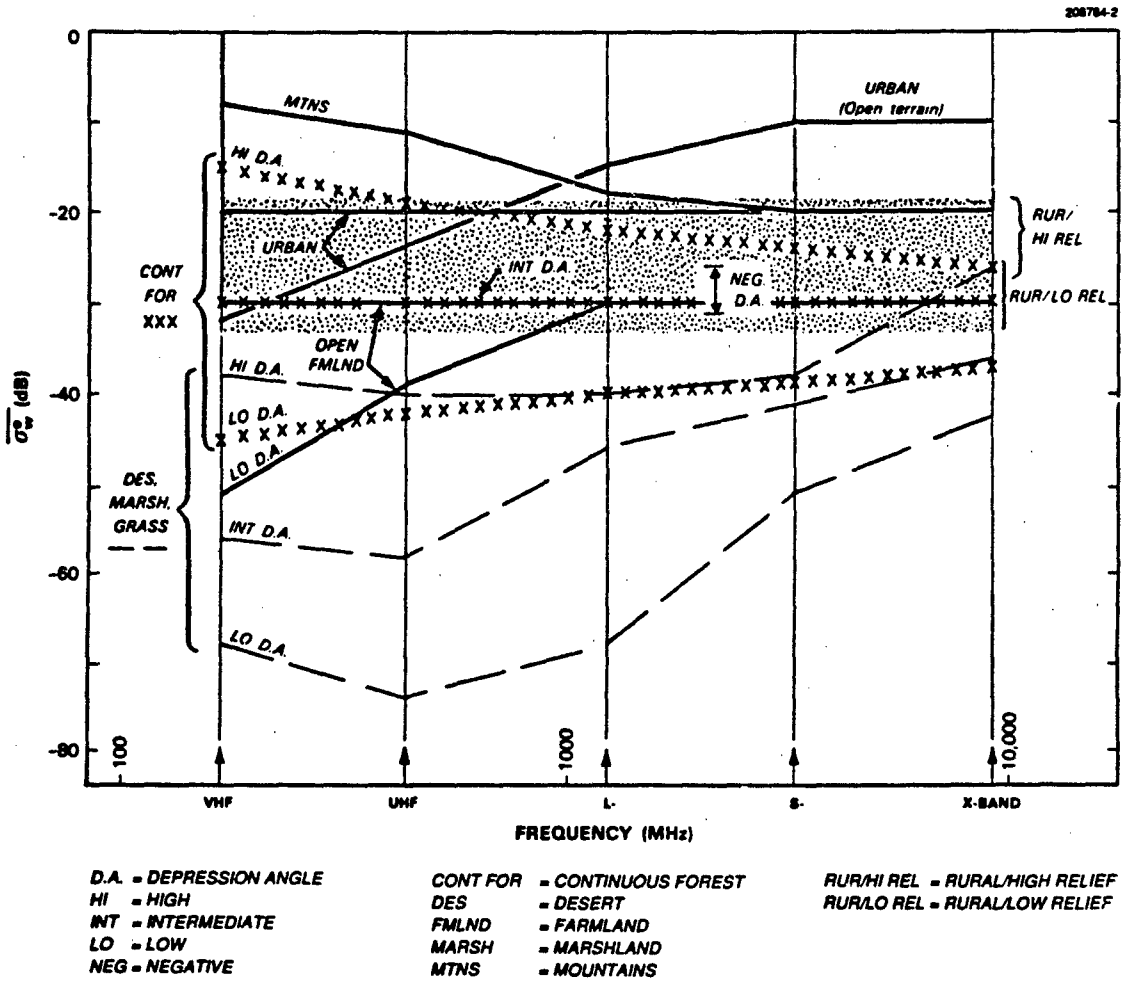

Figure 24. Weibull mean clutter strength versus frequency for all terrain types.

4.3 NON-SITE-SPECIFIC MODEL

In Section 4.2, the measured data were used to develop a clutter model for use in determining site-specific radar system performance, where the actual terrain at the radar site is deterministically represented through digitized terrain elevation data. Such a site-specific clutter model can provide, with reasonable fidelity, detailed measures of clutter-limited radar performance as a particular low-altitude aircraft flies past a particular radar at a particular site. At a higher level of abstraction, however, there

remains a need for a non-site-specific clutter model for use in computing the limiting effects of ground clutter on system performance in a generic sense, independent of how specific terrain features vary from site to site. This section brings the large data base of Phase Zero ground clutter measurements statistically to bear to provide a simple non-site-specific X-band clutter model that captures the important statistical and parametric variations in the data base.

4.3.1 Phase Zero Results

Figure 25 shows measured clutter maps for six different sites. The details of each pattern of spatial occurrence of clutter are specific to the terrain features at that site. However, two general observations can be made about all such patterns. First, at each site the patches of clutter become fewer and farther between with increasing range so that the amount of clutter that occurs gradually diminishes with increasing range from the site. Second, the amount of clutter that occurs is a strong function of the effective height of the radar, including the height of the hill on which the radar is situated. Effective radar height is defined with respect to visible terrain and includes the antenna mast height as defined in Section 1.3. It is obvious in Figure 25 that higher radars see clutter to longer ranges.

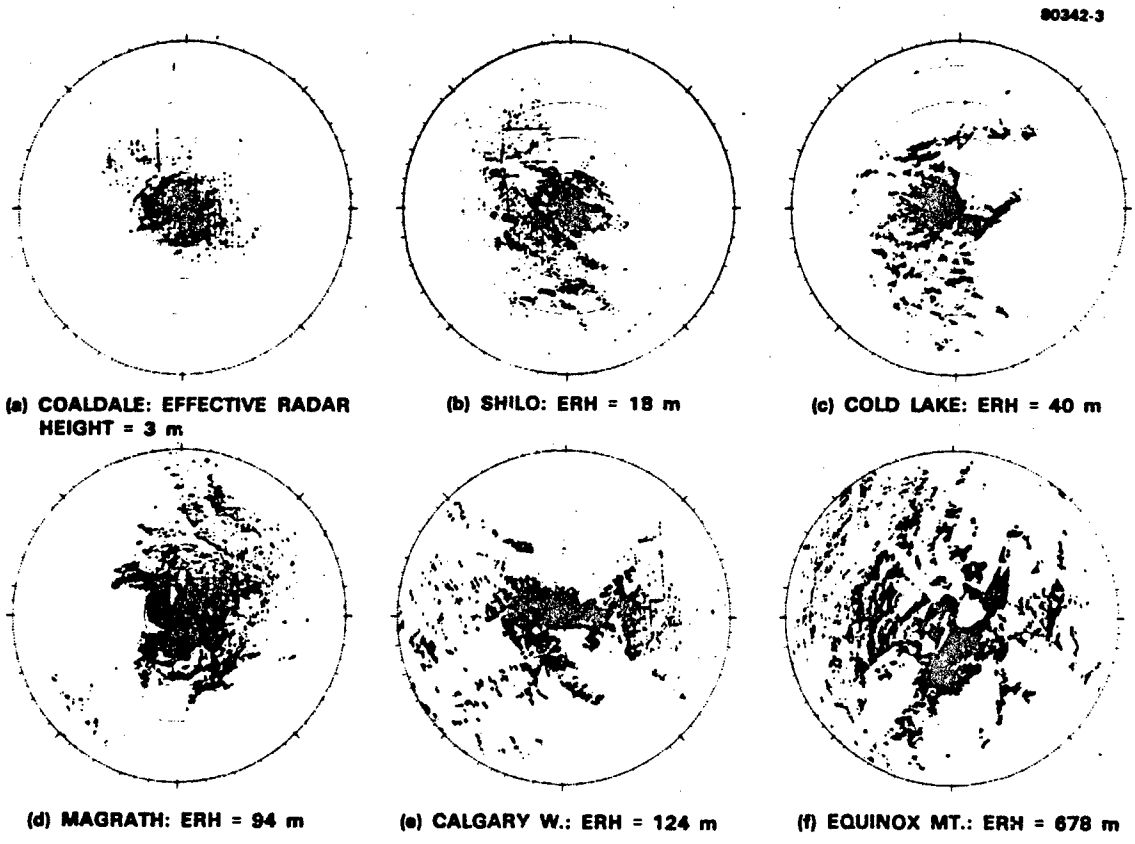

Figure 25. Phase Zero clutter maps for six sites. In each map, maximum range = 47 km (10-km range rings). Results shown are for full Phase Zero sensitivity.

Figure 26 provides general information on clutter extent and strength by averaging measurements like those of Figure 25 from many sites. Figure 26(a) shows percent of circumference in clutter versus range averaged across 86 sites. The resultant clutter visibility curve is approximately linear over most of its extent as displaved on the logarithmic vertical scale employed in Figure 26(a). This linearity indicates that in general the amount of ground clutter that occurs in surface radar decreases exponentially with increasing range. Thus the data of Figure 26(a) quantifies the first observation of the preceding paragraph. The curve of Figure 26(a) represents the best non-site-specific information that the large Phase Zero data base can deliver when brought to bear to answer the general question, "How far out does ground clutter go?" Because ground clutter diminishes gradually (i.e., exponentially) with increasing range, this question must be answered conditionally in terms of a threshold on how much clutter is of concern. As an example, Figure 26(a) indicates that in general 10% of circumference is in clutter at 19-km range.[4]

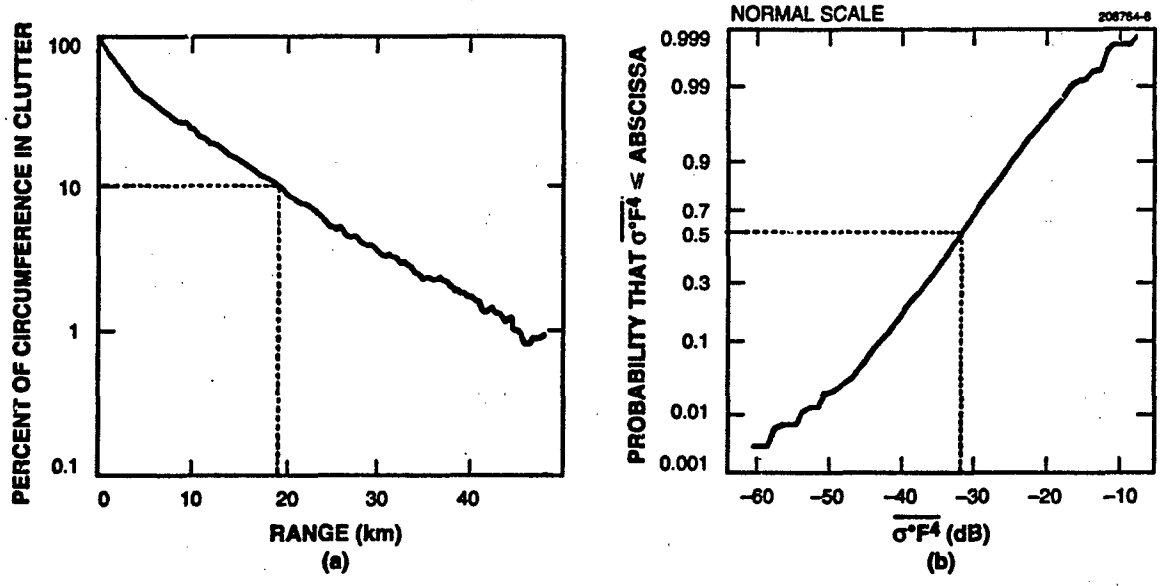

Figure 26. General spatial extent and strength of low-angle radar ground clutter: (a) decrease of clutter occurrence with range and (b) distribution of mean strengths of ground clutter patches.

[4]Percent circumference in clutter represents the probability of discernible clutter P_c versus range R. $P_c(R)$ is dependent on radar sensitivity. If it is assumed that clutter arises only from geometrically visible terrain and that over visible terrain clutter is Weibull-distributed, then it is straightforward to numerically extrapolate the Phase Zero clutter visibility data of Figure 26 to radars of higher sensitivity. In this extrapolation, $P_c(R) = F_v(R) \cdot P_D(R)$, where $P_v(R)$ is the probability that the terrain is geometrically visible, and $P_D(R)$ is the probability that the clutter strength is above radar noise level given that the terrain is visible. $P_D(R)$ is simply the Weibull cumulative (integral) distribution function with radar noise level at range R as the lower limit of integration. $P_D(R)$ is easily numerically evaluated, once the Weibull coefficients of the clutter and the noise level of the radar are specified. If the ratio of $P_D(R)$ for a radar of increased sensitivity to $P_D(R)$ for Phase Zero sensitivity is computed, then clutter visibility $P_c(R)$ for the radar of increased sensitivity is simply the product of this ratio and $P_c(R)$ for Phase Zero as given by the data in Figure 26. The validity of such extrapolation of Phase Zero clutter visibility data to higher sensitivity radars is dependent on the goodness of the assumptions, which deteriorate with large departure from Phase Zero sensitivity.

Phase Zero clutter amplitude distributions are analyzed over macropatches of clutter visibility, as discussed previously. Figure 26(b) shows the cumulative distribution of mean clutter strengths, one mean value per clutter patch, over all the 2,177 patches for which Phase Zero clutter amplitude distributions were formed. These 2,177 macropatches were selected from 96 different measurement sites. The curve of Figure 26(b), as plotted on a logarithmic (i.e., decibel) abscissa, is essentially linear over most of its central extent. This linearity implies that the distribution of mean strengths of clutter patches (in units of m^2/m^2) is lognormal. The data in Figure 26(b) represent Phase Zero's best answer to the next general question, "How strong is ground clutter?" Figure 26(b) indicates that mean ground clutter strength varies over five orders of magnitude. Thus this question also must be answered conditionally in erms of probability of occurrence. The median or 50-percentile value of mean clutter strength in this figure is –31 db (i.e., half of all measured values of mean clutter strength occurred above –31 db, half below). The mode or most frequently occurring value of mean clutter strength in Figure 26(b) is –40 dB.

4.3.2 Simple Clutter Model

In developing a non-site-specific clutter model, the first issue that must be confronted is terrain visibility. As previously discussed, from most places on the surface of the real earth, geometric visibility to terrain is spatially patchy. Looking out from the site, high regions are visible and intervening low regions are masked. Most of the relatively significant clutter comes from the geometrically visible terrain. As range increases, the visible terrain patches become fewer and farther between until beyond some maximum range, no more terrain is visible. Thus on the real earth, geometric terrain visibility and hence the spatial occurrence of clutter is a gradually diminishing function of increasing range.

By a simple non-site-specific clutter model is meant a model that is spatially homogeneous and isotropic. The sort of earth that provides this kind of clutter is a cue ball earth. That is, if the site-specific macroscopic terrain features that exist at every real site are suppressed, what remains is a cue ball, conceptually devoid of all macrofeature, but uniformly microrough to account for homogeneous and isotropic diffuse clutter backscatter. On such a cue ball devoid of macroscale terrain features, the clutter patches observed at real sites expand to encompass all of the terrain out to a single-valued horizon, R_C. The resulting binary visibility function is imparted to the simple clutter model. There may be a temptation to spatially dilute the clutter amplitude statistics as actually measured within large macropatches of visibility with the large amounts of macroshadow that exist on the real earth between the patches. Such spatial dilution would artificially diminish clutter strengths with increasing range in a way that would certainly not be measured by a real radar on a real earth-sized cue ball.

Such considerations lead to the simple non-site-specific clutter model shown in Figure 27. This simple model provides homogeneous clutter within a circular region centered at the radar. The mean clutter strength within this region is given by $\overline{\sigma^\circ_w}$, and the radial extent of the region is given by the clutter cut-off range R_C. The statistically important effect of increasing macroshadow with increasing range shown in Figure 26(a) is used to set the radial extent of the homogeneous clutter region R_C. This setting of R_C is done as a statistical threshold on clutter visibility in the measured data. That is, the user first specifies the minimum spatial amount of clutter that begins to degrade the user's system (e.g., 20%). Then the range at which that amount of clutter generally occurs in the measurements is used as the clutter cut-off range R_C in the simple model (e.g., 12 km).

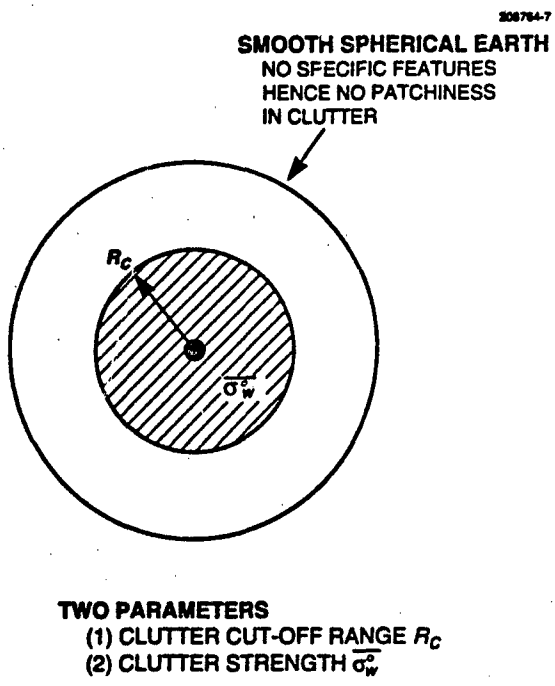

Figure 27. Non-site-specific clutter model.

The effective height of the radar above the surrounding terrain is the major parameter affecting how far ground clutter occurs. This effect is illustrated by the data of Figure 28, in which the exponential decrease of clutter occurrence with increasing range shown in Figure 26(a) is parameterized in five regimes of effective radar height, using the same 86-site set of data upon which the result of Figure 26(a) is based. Figure 28 may be compared with Figure 25. Again it is obvious that higher radars see clutter to longer ranges. The simple model incorporates this important effect of radar height by parameterizing the statistical procedures for setting clutter cut-off range to be dependent on radar height in the measured data.

The results of these procedures for specifying clutter cutoff range R_C in the non-site-specific model are summarized in Table 11. If 20% of circumference in clutter on the real earth is accepted as a baseline threshold above which clutter is expected to have substantial impact on radar system performance, Table 11 indicates that at a general radar height of 40 m, this threshold in clutter occurrence will be exceeded at ranges $\leqq$ 12 km. If it is known that the radar is substantially lower or higher than this general height of 40 m, the clutter cutoff range decreases to 7 km or increases to 22 km, respectively, for the same baseline threshold in clutter occurrence. If the threshold in clutter occurrence rises to as much as 50%, clutter extents above such a high threshold are relatively benign, 3 or 4 km, whereas if the threshold in clutter occurrence drops to as little as 2%, clutter extents are quite severe, ranging from 21 to 48 km,

depending on radar height. Note that except for this latter severe situation, clutter extents as derived empirically in Table 11 from clutter visibility on the real earth are usually much less than range to the spherical earth horizon on a cue ball, illustrating that on the real earth, terrain relief usually dominates over earth sphericity in influencing terrain visibility and horizons.

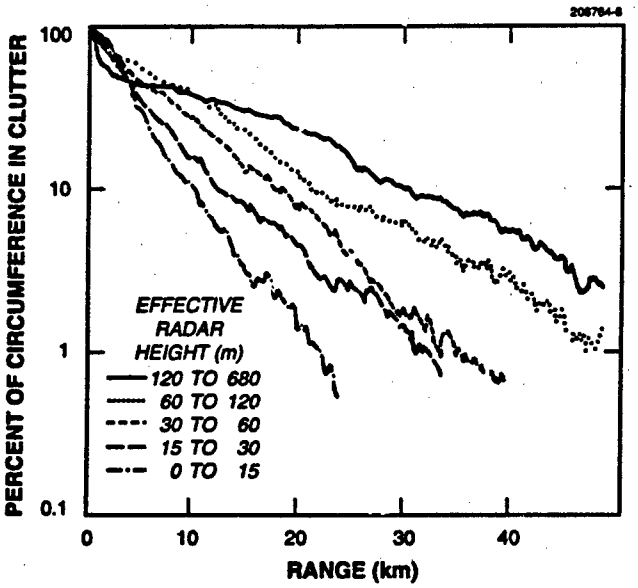

Figure 28. Average ground clutter occurrence versus range as a function of effective radar height.

With the radial extent of the homogeneous clutter region determined in this manner for the simple model, the mean strength of the clutter $\overline{\sigma^\circ_w}$ that exists within this region must be specified. To do so, clutter amplitude statistics as measured over many macropatches in the measured data are used as illustrated by the data of Figures 14, 15, and 26(b). Table 12 provides a resulting matrix of information showing how mean clutter strength varies with terrain type and probability of occurrence. If the 50-percentile level is accepted as a baseline probability of occurrence, then in completely general or non-terrain-specific circumstances the data suggest $\overline{\sigma^\circ_w} = -31$ dB as the best single measure of mean clutter strength. However, if it is known that the terrain is either relatively low or high relief or urban, mean clutter strength $\overline{\sigma^\circ_w}$ may be adjusted to –33, –27, or –23 dB, respectively, at the same 50 percentile probability of occurrence. Proceeding to a worst case/best case parameter study, if 90- and 10-percentile probabilities of occurrence are accepted as reasonable measures of strong and weak mean clutter strengths, respectively, then by these measures the data in Table 12 show how strong and how weak mean clutter strength can become both in general circumstances and for the three main terrain types.

TABLE 11
Clutter Cut-Off Range R_C for Use in Non-Site-Specific Clutter Modeling

Percent of Circumference in Clutter for Ranges ⩽ Cut-Off		Clutter Cut-Off Range R_c (km)			
		Effective Radar Height			
Empirical Threshold Underlying Model Development	Applicable to Cue-Ball Model	Low (15 m)	General (40 m)	High (200 m)	Clutter Visibility Variations
⩾50	100	3	4	3	Benign (least)
⩾20	100	7	12	22	Baseline
⩾2	100	21	37	48	Severe (most)
Spherical Earth Horizon (km)		16	26	58	

TABLE 12
Mean Clutter Strength for Use in Non-Site-Specific Clutter Modeling

Percent of Measured Patches with $\overline{\sigma^\circ_w}$ ⩽ Tabulated Value	Mean Clutter Strength $\overline{\sigma^\circ_w}$ (dB)				Clutter Strength Variations
	Terrain Type				
	Rural/ Low-Relief	General	Rural/ High-Relief	Urban	
10	-41	-40	-34	-31	Benign (weakest)
50	-33	-31	-27	-23	Baseline
90	-26	-23	-20	-15	Severe (strongest)

4.3.3 Further Considerations

Clutter Strength versus Range. Ground clutter strength depends principally on the depression angle at which the backscattering terrain point is illuminated as it varies with terrain elevation from point to point over a site. The simple non-site-specific model does not incorporate local variability in terrain elevation, and hence would be able to bring in depression angle only as a very slowly diminishing function with increasing range on a spherical earth. Is this small rate of change of illumination angle with range sufficient to cause an observable general dependence of clutter strength with range in our measurements? To begin to answer this question, consider again the measured clutter maps of Figure 25. These measurements are shown at full Phase Zero sensitivity. When the clutter in these maps is shown only above a gradually increasing threshold in clutter strength, the density of the clutter sources within patches gradually diminishes relatively uniformly over the whole map, indicating that within patches of visibility, clutter strength is relatively independent of range. That is, the clutter does not disappear at the longer ranges first. Plots of clutter amplitude versus range such as are shown in Figures 10, 12, and 13 also do not indicate any general diminishment of clutter strength with range through patches of clutter occurrence, even at long ranges.

Further results generalizing the lack of range dependency in clutter strength are provided in Figure 29. Clutter amplitude statistics combined from 10 different sites are separated into 4 annular regimes of range—from 5 to 15 km, 15 to 25 km, 25 to 35 km, and 35 to 45 km. Care must be taken to properly normalize the results. First, because the amount of clutter rapidly diminishes with increasing range, only those cells in which discernible clutter signals are measured above the radar noise floor are included. Second, because radar sensitivity diminishes with increasing range, the results are normalized to range-independent sensitivity by further conditionally limiting included cells to be only those in which clutter signals are stronger than system noise at the longest ranges, that is $\sigma^\circ F^4 > -24$ dB. The results of Figure 29 indicate that there is essentially no dependence with range in the resulting clutter amplitude statistics.

Because clutter strength shows no major dependence upon range, $\overline{\sigma_w^\circ}$ in our simple model abruptly transitions from a constant nonzero m^2/m^2 value within R_C to zero m^2/m^2 beyond R_C. This abrupt transition keeps the simple non-site-specific nature that was initially postulated as a requirement of the model before the user in the results of system studies implementing the model. When step function performance characteristics are unacceptable, it is not realistic to arbitrarily decrease clutter strength $\overline{\sigma_w^\circ}$ with increasing range in the simple model to introduce more acceptable, continuous characteristics with range and avoid step function characteristics. In reality, it is the spatial occurrence of clutter, not its strength, that diminishes with range. Thus when step function performance characteristics are unacceptable, a more sophisticated clutter model, incorporating a gradually diminishing clutter occurrence or visibility function must be employed. The site-specific clutter model discussed in Section 4.2 incorporates gradually diminishing terrain visibility with increasing range as determined by line-of-sight geometric terrain visibility in DTED. In addition, under current development is a non-site-specific clutter model that represents patchiness in spatial extent mathematically, based on the empirically observed exponential decrease of clutter visibility with range shown in Figures 26(a) and 28 [5].

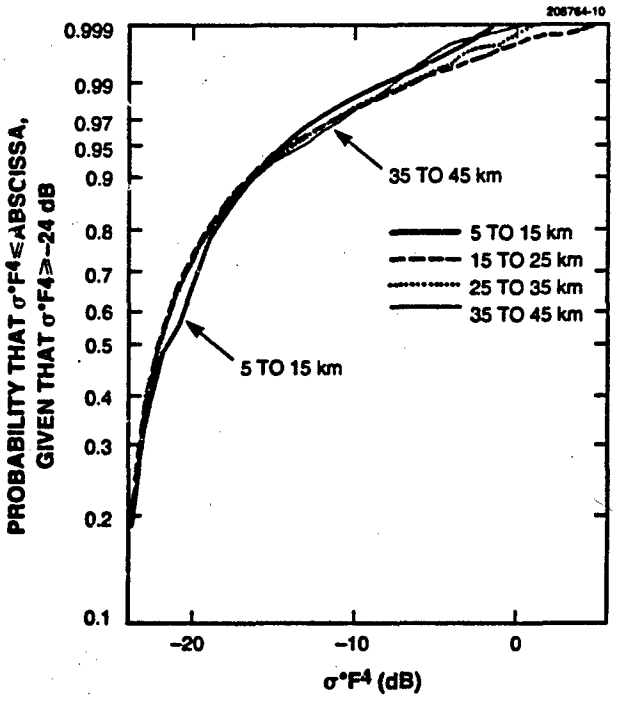

Figure 29. Clutter amplitude statistics in four regimes of range.

Spread in Clutter Amplitude Statistics. Ground clutter amplitude distributions have wide spread resulting from cell-to-cell spatial variation within macropatches of clutter occurrence. This wide spread is illustrated by the data in Figure 30, which show percentile levels between 50 and 90 in ground clutter amplitude distributions both for general terrain and for the three primary terrain types. Each percentile value plotted in Figure 30 is the median of the set of corresponding individual percentiles from all clutter patches of that class within the overall set of 2,177 clutter patch amplitude distributions. Figure 30 typically shows about 16 dB of variation between 50- and 90-percentile levels. Furthermore, this figure also shows that the mean value, indicated by a vertical arrow, is usually close to the 90-percentile level (except for rural/high-relief terrain in which illumination angles are higher and hence the influence of discrete sources, which tend to dominate the mean, are reduced).

Should a percentile level lower than the mean be used in selecting a value for σ°_{w} in the simple model? This question has no simple answer. The data displayed in Figure 30 illustrate the conceptual difficulty of modeling a widely varying dynamic random process with a single deterministic number. However, some guidance may be offered toward answering this question. In a recent system study simulating the existence of low-altitude targets at a number of Phase One clutter measurement sites, the

resultant radar performance, averaged over all sites, was approximately the same as would be computed if a constant clutter strength of $\sigma^{\circ}_{w} \approx -38$ dB were used over all visible terrain. This value of clutter strength occurs at the 70-percentile level on the general terrain curve of Figure 30, approximately halfway between the mean and the median. Recall that the most probable value of mean clutter strength in the general data of Figure 26(b) is −40 dB, perhaps a fortuitous concurrence. The reader is cautioned that this is a particular result of only one study. In any case, the data of Figure 30 allow investigators to adjust modeling values of σ°_{w} away from the mean values shown in Table 12, if they so desire.

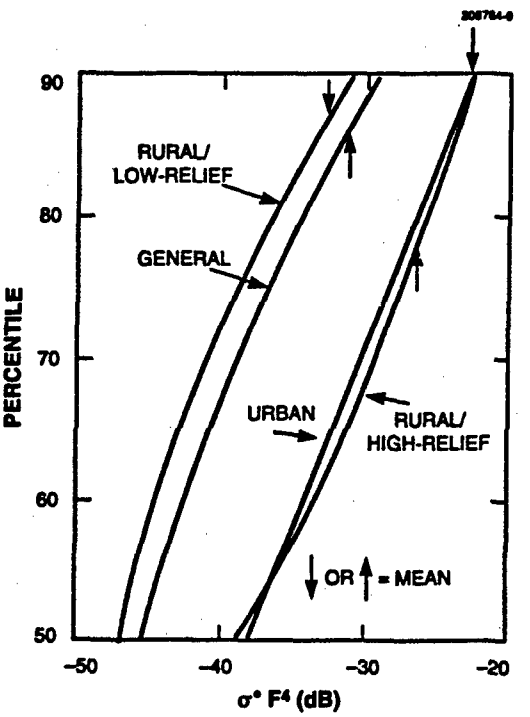

Figure 30. Clutter strength as a function of percentile level in the amplitude distribution.

Data Base Depth. The easy-to-use data for R_C and $\overline{\sigma^{\circ}_{w}}$ in Tables 11 and 12 capture the most important first-level effects for non-site-specific modeling application contained in the large data base of measurements. Additional skins of the onion may be peeled back to reveal ever increasing specificity of information. For example, consider the distributions of mean strength in six classes of landform and land cover provided earlier in Figures 14 and 15, respectively. One can imagine similar distributions by

landform and land cover for median strength or for other statistical measures of the patch amplitude distributions. The data in Tables 13 and 14 provide quantitative measures of distributions of means, ratios of standard deviation-to-mean, medians, and various percentile levels, by landform and land cover, respectively. Thus the data of Tables 13 and 14 may be drawn upon to expand the simplified information of Table 12 to other probabilities of occurrence, other measures of strength (e.g., median), and other landform and land cover types.

The statistical attributes shown in the second column of Tables 13 and 14 are now defined more explicitly. Observe in Figures 14 and 15 that the distributions are approximately lognormal. As a result, it is useful to define the mean and standard deviation of the normally distributed logarithmic quantity. These two quantities are shown as the first (i.e., top-most) and second attributes for each patch amplitude statistic. The third attribute shown is the median, which itself just transforms logarithmically. If the logarithmic quantity is normally and hence symmetrically distributed, its mean and median must be identical. The data in Tables 13 and 14 indicate that these two quantities (i.e., the first and third attributes, respectively) are, indeed, often nearly equal. Once it is assumed that the distribution is approximately lognormal, all other attributes of the distributions of both the logarithmic quantity and the more fundamental underlying linear quantity immediately follow from the first and second attributes provided in Tables 13 and 14. However, the fourth and final attribute for each patch amplitude statistic shown is the actual empirical mean of the basic linear quantity, which can be used either directly in its own right or as a further check on the degree of goodness of the approximating lognormal distribution.

Now consider some of the trends with landform contained in the data of Table 13, where terrain slopes rise monotonically with landform class, left to right, from less than 1° for level terrain to between 10° and 35° for steep terrain (see Figure 14). Consider the median of M samples within a particular landform class of a given statistic (e.g., mean) of a clutter amplitude distribution as an easy-to-understand attribute, in that half the samples occur above the median level and half below. The median attribute is shown in increasing order of landform as the third row of numbers for each patch amplitude statistic in Table 13. Thus, as terrain slopes rise from level to steep, the third rows of the table show that (1) mean strengths rise over the 10-dB range from –33 to –23 dB; (2) median strengths rise over the 15-dB range from –48 to –33 dB; (3) spreads in amplitude distributions as measured by ratio of standard deviation-to-mean fall from 7 to 3 dB, spreads as measured by ratio of 99.9 to 50 percentile fall from 33 to 24 dB, and spreads as measured by ratio of mean-to-median fall from 15 to 10 dB. All these trends are monotonic with increasing terrain steepness as specified by the median value from a large number M of individual patch measurements within each landform class.

In considering increasing specificity of information, recall that all the non-site-specific information presented in this section has been derived from X-band measurements. However, when considering that mean strengths from the three general terrain types of rural/low relief, rural/high relief, and urban are largely frequency independent, and that the simple model is already averaging out much fine-scaled variation, it is not unrealistic to apply the simple model across the general microwave regime. Investigators who wish to introduce more specific frequency dependence in non-site-specific investigation may, as a beginning, be guided by the multifrequency mean data of Table 10.

TABLE 13
Various Average Measures of Ensembles of Clutter Patch Amplitude Statistics by Landform

Patch Amplitude Statistic	Attribute of Set of Patch Amplitude Statistics Over M Patches	Landform					
		Level	Undulating	Inclined	Rolling	Mod. Steep	Steep
Mean $\bar{x}^m$	$\bar{\bar{x}}\|_{dB}^M$	-33.1	-32.0	-30.2	-28.9	-26.4	-22.8
	SD $[\bar{x}\|_{dB}]^M$	6.9	6.1	5.9	4.8	4.7	5.1
	$[\bar{x}\|_{dB}]_{50}^M$	-33.	-32.	-30.	-29.	-26.	-23.
	$\bar{\bar{x}}^M\|_{dB}$	-23.9	-26.6	-26.7	-26.0	-24.5	-19.7
Standard Deviation to Mean x_σ^m	$\bar{x}_\sigma\|_{dB}^M$	7.3	7.0	6.0	4.6	3.9	2.9
	SD $[x_\sigma\|_{dB}]^M$	2.9	3.1	2.8	2.1	2.1	1.9
	$[x_\sigma\|_{dB}]_{50}^M$	7.	7.	5.	4.	4.	3.
	$\bar{x}_\sigma^M\|_{dB}$	8.4	8.2	7.0	5.2	4.5	3.3
Median x_{50}^m	$\bar{x}_{50}\|_{dB}^M$	-47.5	-45.8	-42.7	-41.4	-38.1	-35.0
	SD $[x_{50}\|_{dB}]^M$	6.8	7.5	8.7	9.3	10.3	12.6
	$[x_{50}\|_{dB}]_{50}^M$	-48.	-46.	-44.	-42.	-36.	-33.
	$\bar{x}_{50}^M\|_{dB}$	-41.1	-39.3	-35.1	-33.1	-30.0	-24.5
nth Percentile to 50 Percentile $x_{n/50}^m$ n = 90,99,99.9	$\bar{x}_{n/50}\|_{dB}^M$	14.4,26.2,32.7	14.9,25.2,31.6	14.8,23.6,29.1	16.4,23.1,27.3	15.6,21.8,25.6	16.4,22.0,24.1
	SD $[x_{n/50}\|_{dB}]^M$	5.9,7.0,8.4	5.2,6.9,8.6	5.4,7.6,9.2	7.0,8.0,8.6	7.7,9.0,9.7	10.2,11.5,12.2
	$[x_{n/50}\|_{dB}]_{50}^M$	14.,26.,33.	14.,25.,32.	15.,23.,29.	16.,23.,27.	14.,20.,24.	13.,19.,22.
	$\bar{x}_{n/50}{}^M\|_{dB}$	19.1,32.8,40.6	18.5,30.6,39.5	18.1,30.2,38.0	22.5,29.8,34.7	23.4,30.6,36.2	27.2,34.4,37.5
Number of Patches M		571	556	338	216	152	94

TABLE 14
Various Average Measures of Ensembles of Clutter Patch Amplitude Statistics by Land Cover

Patch Amplitude Statistic	Attribute of Set of Patch Amplitude Statistics Over M Patches	Land Cover					
		Wetland	Rangeland	Agricultural	Forest	Barren	Urban
Mean $\bar{x}^m$	$\bar{\bar{x}}\|^M_{dB}$	-37.5	-32.0	-31.8	-30.7	-29.1	-22.4
	SD $\|\bar{x}\|_{dB}\|^M$	4.9	6.0	5.1	7.3	7.8	7.0
	$\|\bar{x}\|_{dB}\|^M_{50}$	-38.	-32.	-31.	-30.	-29.	-23.
	$\bar{\bar{x}}^M\|_{dB}$	-34.6	-27.5	-28.5	-26.2	-22.3	-16.7
Standard Deviation to Mean x^m_σ	$\bar{x}_\sigma\|^M_{dB}$	5.5	5.8	7.9	4.3	6.6	7.1
	SD $\|x_\sigma\|_{dB}\|^M$	2.0	2.8	2.9	2.2	3.4	2.3
	$\|x_\sigma\|_{dB}\|^M_{50}$	5.	5.	8.	4.	6.	7.
	$\bar{x}^M_\sigma\|_{dB}$	6.1	6.8	8.9	5.0	8.2	7.7
Median x^m_{50}	$\bar{x}_{50}\|^M_{dB}$	-48.3	-44.7	-47.2	-41.5	-42.4	-39.0
	SD $\|x_{50}\|_{dB}\|^M$	6.6	8.1	6.8	10.3	10.1	8.1
	$\|x_{50}\|_{dB}\|^M_{50}$	-48.	-46.	-47.	-43.	-45.	-38.
	$\bar{x}^M_{50}\|_{dB}$	-42.3	-36.6	-41.0	-31.3	-29.4	-32.7
nth Percentile to 50 Percentile $x^m_{n\ 50}$ n = 90,99,99.9	$\bar{x}_{n\ 50}\|^M_{dB}$	13.5,22.5,27.3	15.2,23.7,29.0	15.5,27.1,34.3	14.4,21.4,25.1	14.2,24.3,30.2	16.3,29.2,34.8
	SD $\|x_{n\ 50}\|_{dB}\|^M$	4.7,5.7,6.3	6.6,7.7,9.0	5.8,6.5,7.8	6.4,7.6,8.4	7.3,8.5,9.8	5.3,8.2,9.6
	$\|x_{n\ 50}\|_{dB}\|^M_{50}$	13.,22.,27.	14.,23.,29.	15.,27.,35.	13.,21.,24.	12.,23.,31.	16.,29.,36.
	$\bar{x}_{n\ 50}{}^M\|_{dB}$	16.7,26.2,31.3	21.9,31.0,38.6	19.7,32.2,40.6	20.6,28.4,33.0	22.6,31.6,39.0	20.6,35.8,43.4
Number of Patches M		92	371	788	684	115	122

4.3.4 Simple Model Summary

The rationale guiding the development of the simple, non-site-specific clutter model presented in this section is now summarized. The objective is to invest the model with important general attributes as they have come to be understood in investigating the large data base of Phase Zero clutter measurements. Of first-order importance is to distinguish between where the clutter occurs and its strength, given that it occurs. The simple model maintains this distinction by first specifying clutter cut-off range based on the measurements of clutter visibility and then specifying clutter strength based on measurements of clutter amplitude statistics within macropatches of occurrence. Furthermore, this model brings in the important parameters of radar height as it influences clutter extent and terrain type as it influences clutter strength. In this empirical manner, the model maintains its focus on the important first-level parameters in the real clutter phenomenon and statistically provides baseline central values of clutter strength and extent as they occur at real sites.

The model does more than this, however. In addition to providing central measures, the model also specifies the distributions. As a result, besides providing information on baseline values of strength and extent of clutter, the model also provides parametric information on how severe (i.e., strong clutter to long range) or how benign (i.e., weak clutter to short range) the clutter can become, all in terms of specifiable probability of occurrence. It is this depth of statistical information in the simple model incorporating the extreme variability of the clutter phenomenon in quantitative terms of probability of occurrence, more so than the baseline central values of the model, that set it apart from previous single-point approaches in the literature.

4.4 EFFECTS OF WEATHER AND SEASON

In Sections 4.2 and 4.3, a matrix of information was provided for predicting strengths of ground clutter returns from visible terrain. For example, Table 10 provides a manageable set of empirically derived numbers that establishes an orderly rationale for specification of ground clutter amplitudes over their many order-of-magnitude range of variation. The effects of season or weather are not allowed for anywhere in the predictive rationale. Are there important trends in the measurements as a result of seasonal or weather-related change? What are the ranges of variability, or error bounds, in the modeling information presented as a result of these effects?

The data do not indicate significant trends with season or weather. Why? Throughout this report, the emphasis has been on the importance of spatially localized or discrete sources in low-angle clutter statistics. Many of the measurement sites were on low-relief prairie farmland in western Canada. At the beginning of this program, for example, when standing in an Alberta wheat field and seeing nothing but wheat to far horizons, clutter modeling was thought of in terms of dielectric constant of wheat, moisture content of soil, and fields high in mature wheat versus harvested fields in stubble versus plowed or snow-covered fields, all of which led to an expectation of significant seasonal variations in clutter strength. Vertical discrete objects were not considered to be of foremost importance because visually, they seemed relatively sparse. It turned out that when radar measurements actually were made at such sites to ranges of 25 or 50 km or more (much greater than visual range standing in a wheat field), the incidence of discrete sources was large and their effect was dominant. Not all discretes are evident visually. For example, when looking visually to a far horizon,

what appears to be continuous terrain is often a series of discrete or localized hill tops, and furthermore, actual discrete land cover elements are often invisible at long range.

In the early days of radar, general acceptance of the idea that "angels" (i.e., nonzero Doppler echoes) were caused by birds came slowly because there did not appear to be that many birds, but over hundreds and thousands of square kilometers of radar coverage, there can be enormous numbers of birds to account for angels and similarly, there are enormous numbers of stationary discrete or localized vertical scattering features dominating zero-Doppler ground clutter statistics. Thus it is not so much the wheat field itself as the fence around it, the road and telephone line through it, the occasional storage granaries or trees around ponds that are in it, that act as clutter sources. The dramatic seasonal variations that occur in the physical appearance of the surface of the wheat field have relatively little effect on the returned clutter statistics. The actual vertical sources tend to be relatively unchanged, summer and winter. Thus, in general there is little seasonal variation in ground clutter strengths, usually on the order of 3 dB or so, with no noticeable trends. Occasionally, when in specific situations there have been stronger seasonal variations in clutter strength (but always <10 dB), they have been the result of seasonal effects in multipath propagation, which is much more directly dependent on the state of the field surface itself.

Tree lines are very common discrete clutter sources. A tree line within a large regional clutter patch contributes strong clutter cells to the overall patch amplitude distribution, independent of whether the trees happen to be in leaf or bare, wet or dry. Seasonal and weather effects only cause minor variations in these strong contributions. Of more significance in th distributions is whether the tree line exists or not, or more generally, the relative incidence of occurrence of tree lines on landscapes. Information is available on how clutter amplitude distributions vary with percent tree cover, which indicates that the dominant sources causing much of the wide spread typically observed in these distributions for agricultural terrain are isolated trees.

Nevertheless, season and weather do act to introduce variation in ground clutter. What are the ranges of variability, or error bounds, in prediction that are caused by these changes? Figure 31 shows cumulative distributions of both day-to-day and seasonal variations in mean clutter strength as measured by Phase One. The data in the figure show central differences in decibel units. The day-to-day variations shown are based on repeat sector measurements over the two- to three-week stay at every Phase One site. On the basis of these measurements, the 1-σ day-to-day variability in mean clutter strength, largely due to changes in weather, can be specified as 1.1 dB. The seasonal variations shown in Figure 31 are based on seven repeated visits by the Phase One equipment to selected sites for the purpose of investigating seasonal variability. On the basis of these measurements, the 1-σ seasonal variability in mean clutter strength is 1.6 dB. This definition of diurnal and seasonal variability in terms of probability of occurrence brings statistical order to a historical literature characterized more by individual examples. Such long-term temporal variations in mean clutter strength from macroregions of terrain may be contrasted with the spatial region-to-region 1-σ variability that is specified to be 3.2 dB on the basis of patch-to-patch variations in repeat sector clutter patch mean strength within a given category of terrain classification.

In light of such variability, the reader is cautioned that the numbers comprising the clutter modeling information of this report need to be regarded as statistical averages. These averages certainly establish important trends. Any specific clutter measurement, however, whether new or historical, may vary considerably from these predicted average numbers.

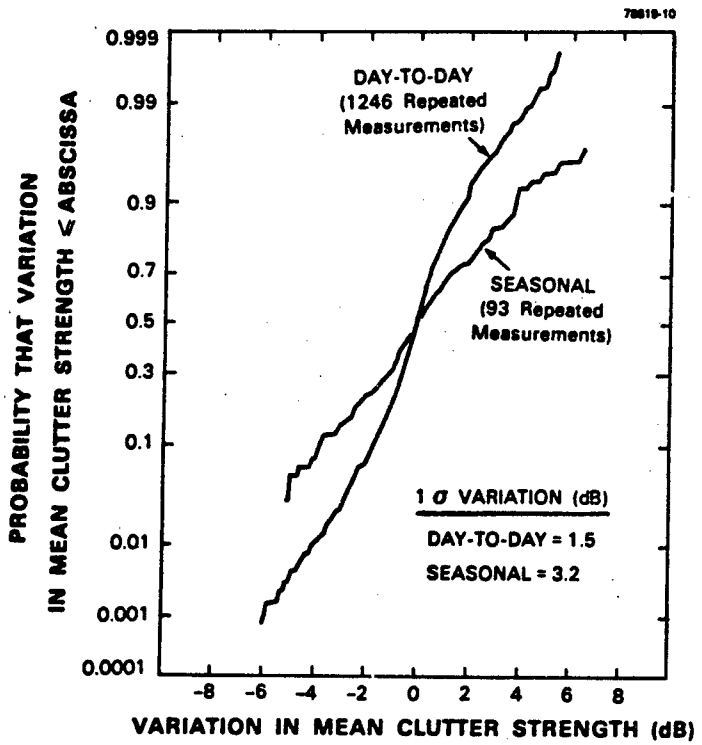

Figure 31. Diurnal and seasonal variability in mean ground clutter strength.

5. TEMPORAL CLUTTER STATISTICS

Until now, this report has been concerned with clutter amplitude statistics resulting from cell-to-cell spatial variations in ground clutter signals. The subject now turns to temporal variations in the received signals returned from particular cells [3,15]. Important attributes of temporal statistics are (1) temporal amplitude statistics, (2) spectral characteristics, and (3) correlation times. Figure 32 presents some preliminary information describing the relative frequency of occurrence of temporal amplitude statistics between cells with Rayleigh (i.e., windblown clutter) and Ricean (i.e., fixed discretes) statistics. Ricean statistics describe ground clutter temporal variations quite accurately as the return of a dominant steady reflector or fixed discrete in a varying background. Rayleigh statistics are a limiting case of Ricean statistics with steady signal equal to zero. The data in Figure 32 indicate that, over a population of 988 relatively strong clutter cells selected from three rural sites, more than 40% of the cells are Rayleigh (i.e., have ratios of standard deviation-to-mean = 0 dB), and the remainder are generally Ricean (i.e., have ratios of standard deviation-to-mean <0 dB), with increasingly strong Ricean cells occurring less frequently. For example, Figure 32 shows that 1% of cells are strongly enough dominated by fixed discretes to have a dominant-to-Rayleigh reflector ratio as high as 50. The reason that 40% of the clutter cells in the figure contain only windblown foliage with dominant-to-Rayleigh reflector ratio equal to zero is that there are some trees on these farmland landscapes. Where trees occur, even at relatively low incidence of occurrence, they tend to dominate as strong clutter sources.

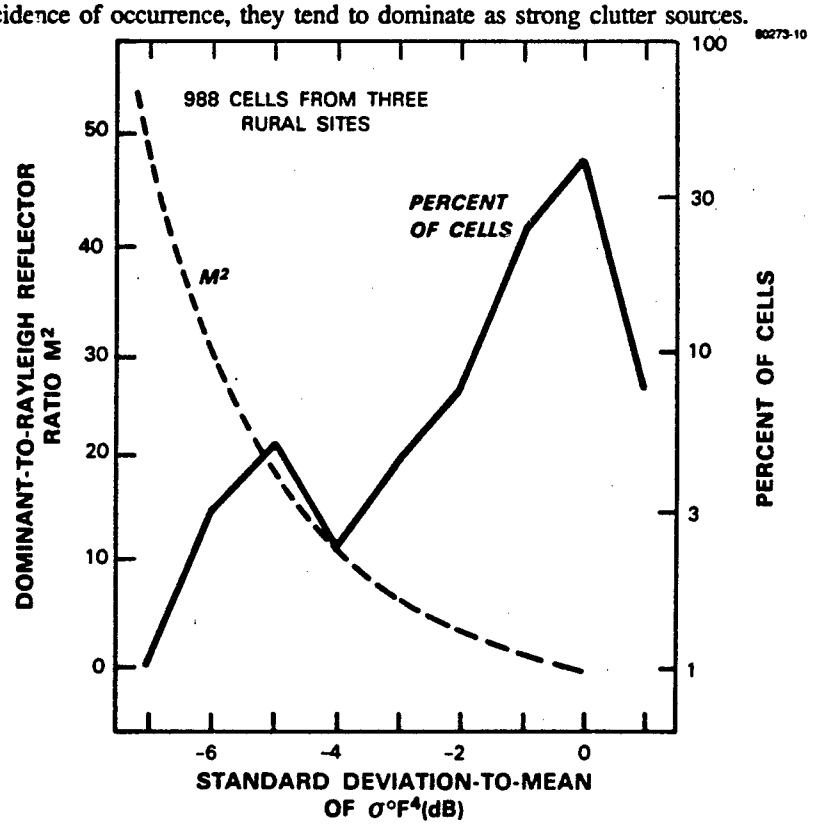

Figure 32. Frequency of occurrence of Rayleigh versus Ricean cells in X-band ground clutter.

For Rayleigh cells containing windblown trees, the wind-induced motion causes Doppler-shifted energy in the power spectra of the received temporal signals. Figure 33 shows two examples of X-band spectral results from a forested cell measured on two days, 17 and 25 April 1985. This cell contains mixed deciduous and evergreen trees to an approximate height of 60 or 70 ft. On 17 April the winds were quite strong; at the time of this X-band experiment, wind speed was recorded at 10 kn, gusting to 20. In contrast, 25 April was a very still day and the winds were recorded as "calm" at the time of our experiment.

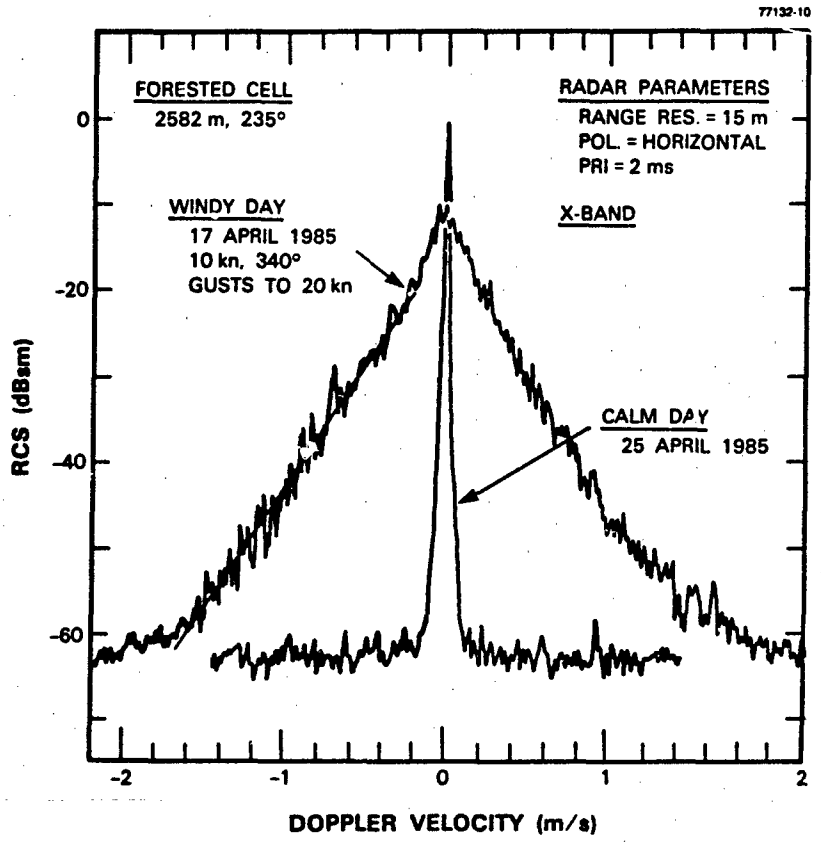

Figure 33. Power spectra of X-band radar returns from windblown trees.

The spectra of Figure 33 are computed directly as fast Fourier transforms (FFTs) of the temporal pulse-by-pulse return, including the dc component, calibrated in radar cross section (RCS) units of meters squared. The spectral content is displayed in decibels with respect to 1 m^2 (i.e., in decibels per meter squared or dBsm). The method used to generate these spectra is that of modified periodograms, where the temporal record of 30,720 pulses is divided into contiguous groups of 1,024 samples, a 1,024-point

complex FFT is generated for each group, and the amplitudes of the resultant set of FFTs are arithmetically averaged together in each Doppler cell to provide the spectrum illustrated. Thus in Figure 33 each spectrum shown is the result of averaging 30 individual spectra from an overall RCS record of 1.024-min duration and 2-ms pulse repetition interval (PRI). In the generation of each spectrum, a 4-sample Blackman-Harris window or weighting function is utilized, with highest sidelobe level at –74 dB and with 6 dB per octave falloff.

The results of Figure 33 illustrate the differences in spectral content of the X-band reflections from this cell between when the tree branches are relatively motionless and when they are undergoing relatively strong, wind-induced, random motion. It is graphically apparent in these results how much of the dc or zero-Doppler return on the calm day is converted to ac return distributed over Doppler velocities up to 2 m/s on the windy day. The windy day spectrum shown in the figure is one of the widest spectra so far found in the clutter data base. In this windy day data, the rate of decay of spectral energy with increasing Doppler velocity in the tail of the spectrum is approximately exponential as indicated by the straight line drawn through the left side of the spectrum. The Phase One system noise levels are evident in both the calm and windy day results of Figure 26 at a level of about –64 dBsm.

Much of the data are represented by the results of Figure 26 in that rates of decay of spectral energy with increasing Doppler velocity in radar returns from windblown trees are often observed to be reasonably well approximated as exponential in the tails of the spectral distributions well removed from the zero-Doppler region. To model this phenomenon, L-band has been chosen, where a considerable number of measurements are available from a forested cell. In the tail region of the power spectrum, where the exponential approximation is valid, the spectrum is represented as

$$P(v) = A\, e^{-\beta |v|}, \; v > 0.2 \text{ m/s} \quad ,$$

where

P	=	power spectral density (W/Hz)
v	=	Doppler velocity (m/s)
β	=	exponential decay factor
A	=	arbitrary constant.

For each of 23 different L-band experiments [15], the best exponential approximation to the spectral tail was determined, and the corresponding decay factor β was noted. These 23 values of β were separated into three groups by wind speed—windy (15 to 25 kn), breezy (10 to 11 kn), and light air (5 to 8 kn). Then the mean β within each group was determined. The resulting mean values of β and corresponding rates of exponential decay of spectral tails in the three regimes of wind speed are shown in Figure 34. These exponential decay factors apply only in the tail regions of spectra for Doppler velocities $v > 0.2$ m/s, well removed from zero-Doppler velocity. The spectral modeling information of Figure 34 has the advantage of statistical generality, obtained by averaging over a number of like-classified measurements.

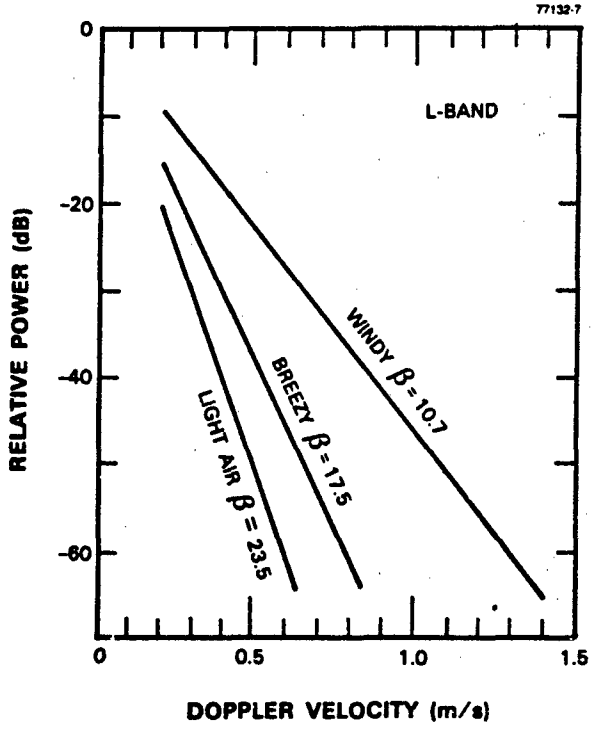

Figure 34. Approximate rates of exponential decay in the tails of L-band spectra from windblown trees in three regimes of wind speed.

The question now is, how long does it take for radar returns from windblown trees to decorrelate, which is complementary to the question of spectral extent in such returns. The normalized autocorrelation function was computed for all five Phase One frequencies for the returns from the forested cell as measured on the windy day of 17 April [15]. The time of day (hr:min) at which data collection commenced for each of these five experiments was as follows: X-band, 10:24; S-band, 11:30, L-band, 14:12, VHF, 15:00; UHF, 15:27. Each of these five experiments consisted of 30,720 pulses at PRIs of 2, 10, 10, 6, and 2 ms for VHF, UHF, L-, S-, and X-bands, respectively. For all five experiments, the polarization was horizontal and the range resolution was 150 m. Correlation times $\tau_{1/\varepsilon}$ and $\tau_{1/2}$ are defined as the times required for the normalized correlation function to decrease to $1/\varepsilon$ (= 0.368) or 1/2 (= 0.5), respectively. Table 15 gives these measures of time required for decorrelation of the radar returns from windblown trees. If the scattering centers and their motion were the same at all five frequencies, simple Doppler considerations would lead to the expectation that correlation times would decrease inversely with RF frequency, all else being equal. There is an approximate trend indicative of this effect in the data of Table 15. The results of this table do not scale exactly linearly with frequency, however, because (1) the

experiments were conducted at different times and thus under different specific wind conditions on 17 April, (2) the cell sizes and hence scattering center ensembles were different (e.g., due to azimuth beamwidth varying with frequency band), and (3) the scattering centers and their velocities are expected to vary with RF wavelength (i.e., twigs at X-band, branches at L-band, limbs at VHF).

TABLE 15
Correlation Times for Radar Returns from Windblown Trees on a Windy Day

Frequency Band	Correlation Time (s) $\tau_{1/2}$	$\tau_{1/e}$
VHF	4.01*	5.04*
UHF	0.69	0.94
L-Band	0.67	0.95
S-Band	0.062	0.081
X-Band	0.033	0.049

Note: * = extrapolated estimate

The correlative properties of radar returns from windblown trees shown in Table 15 apply for the particularly windy day of 17 April. Correlation times from windblown trees increase with decreasing wind speed. As an example, to quantify this effect, normalized autocorrelation functions were computed for the L-band returns from the same forested cell, measured on three different days under three quite different wind conditions [15]. The windy day was 17 April, the breezy day was 10 April, and the light air day was 5 June. Each experiment consisted of 30,720 pulses at pulse repetition intervals of 10, 2, and 10 ms for the windy, breezy, and light air days, respectively. In these results, the correlation times $\tau_{1/e}$ on the windy, breezy, and light air days were 0.95, 2.11, and 5.56 s, respectively. These results clearly show that temporal correlation in L-band radar returns from windblown trees increases with decreasing wind speed.

6. SUMMARY

Lincoln Laboratory wishes to quantify the performance of surface-sited radar against low-flying aircraft. Ground clutter often limits the system performance of surface radars as they attempt to detect and track low-altitude aircraft in a background of ground clutter interference over ranges from as close as a few kilometers to as great as 25 or 50. To understand such interference, ground clutter measurements were made at many sites. The objective of this clutter measurements program has been to develop clutter modeling capabilities that provide accurate predictions of clutter effects in typical surface radars for a variety of terrain types. Thus the interest is mainly in ground clutter as it affects such radars, typically at grazing incidence over many square kilometers of composite heterogeneous terrain.

Analyses of this extensive new base of clutter measurements have led to an understanding of a basic unifying mechanism underlying what appears at first consideration to be extreme variability and little predictability in low-angle clutter spatial amplitude distributions. This understanding is based on the fact that at the very low angles of illumination of surface radar, ground clutter largely consists of backscatter from a sea of discrete vertical clutter sources. Numerous low reflectivity or shadowed cells occur between cells containing discrete clutter sources, even though the overall region from which the clutter amplitude distribution is being formed is under general illumination by the radar. The combination of many shadowed or low-reflectivity weak cells together with many discrete-dominated strong cells causes a great deal of spread in the resultant low-angle amplitude distributions. As illumination angle increases, the low reflectivity areas between discrete vertical features become more strongly illuminated, resulting in less shadowing and a rapid decrease in the spread of the distributions. The upper tails of the clutter distributions, however, and the mean levels that are largely determined by the upper tails are still primarily caused by discrete sources and increase more slowly with increasing illumination angle.

Therefore, as a unifying mechanism, depression angle (i.e., the angle below the horizontal at which a clutter patch is observed at the radar) as it affects shadowing on a sea of discretes is the single most important parameter at work in low-angle ground clutter data, even at the very low angles of typically $<1°$ that usually occur for surface radar. This basic parametric dependence in ground clutter spatial amplitude distributions is such that strengths increase and spreads decrease with increasing depression angle. This parametric dependency with depression angle is strong enough to largely wash out many fine-scaled differences between similar terrain types. Past attempts to refine this basic dependency through use of grazing angle (i.e., the angle between the tangent to the local terrain surface at the terrain point and the direction of illumination) have met with little additional success because of the extreme complexity that exists in terrain surfaces, because of the lack of detailed information defining these surfaces such that slopes (i.e., rates of change of elevation) are accurate, and because of difficulties in formulating a quantitative definition of terrain slope uniformly applicable across the various physical scales (centimeters to kilometers) at which slopes exist in landscape. Over and above such considerations of scale and accuracy in terrain elevation data is the fact that the backscatter is frequently dominated by discrete elements of land cover rather than the underlying terrain itself.

This report presents general low-angle ground clutter modeling information for clutter amplitude statistics within a construct that requires relatively detailed specification of depression angle, but only

relatively coarse specification of terrain type. Terrain slope enters the model explicitly through two categories of relief. Modeling information is presented largely in terms of Weibull statistics, where $\overline{\sigma^\circ_w}$ is the Weibull mean strength and a_w is the Weibull spread parameter. Within this standard format, a_w may be observed to decrease, and $\overline{\sigma^\circ_w}$ may be observed to increase, as depression angle rises and percent shadowing falls. The important radar parameters are RF frequency as it affects $\overline{\sigma^\circ_w}$ and radar spatial resolution as it affects a_w.

One of the most important attributes of low-angle ground clutter is the extremely broad spread that exists in low-angle clutter amplitude distributions. Individual samples of clutter strength vary over orders of magnitude. Wide spreads occur at low angles because of the domination of low-angle ground clutter by discrete sources. As angle increases, this domination diminishes, and we gradually move from the low-angle heterogeneous regime of widespread spiky Weibull statistics applicable to surface radar to the high-angle, more homogeneous regime of Rayleigh statistics applicable to airborne radar.

Throughout this report, the emphasis has been on the importance of spatially localized or discrete sources in low-angle clutter statistics. The dominant role of discrete sources is not in itself a new idea in the clutter literature (e.g., "...dominant land clutter signals are from discrete isolated targets...[16]"). Clutter models, however, have traditionally been developed, first, on a basis of area-extensive scattering from the statistically rough surface itself, as opposed to localized scattering from just the high points of that surface or high objects on it. One of the more valuable results to us of the current extensive clutter measurements and analysis program is that we now imagine low-angle clutter as arising, first, from a sea of discrete vertical features or edges, separated by microshadow, and distributed over complex surfaces. The role of illumination angle in this construct is more as angle influences clutter strength through its effect on shadowing statistics between discrete features of vertical discontinuity, and less in its influence through grazing angle on area-extensive backscatter from tilted, statistically rough, terrain facets, although both sorts of illumination angle effects are at work in the real phenomenon.[5] Because of the primary role of discretes at low angles, effects in clutter statistics due to seasonal and weather-related changes in landscape are less than what otherwise might be the case.

The problem of making radar ground clutter understandable and predictable is as much one of statistics as of physics. Given enough time and effort, the physical backscattering processes within and contributions from any particular clutter patch can be understood, but the heterogeneity of terrain often prevents useful generalization of such particular results. The ambiguous state of the historical clutter literature fundamentally reflects this problem. Hence our approach is statistical in nature and involves measuring clutter data within many patches and across many sites. This approach bounds the problem of clutter strengths for various terrain types by presenting generalized data with considerable averaging across sites and patches and not data specific to some particular clutter scene that is nonrepresentative

[5]Recent research of the Phase One data at Defence Research Establishment Ottawa indicates that if strong, spatially isolated clutter cell returns (often occurring at approximately 20% incidence in the measured data) are analyzed separately, correlation of clutter strength versus grazing angle as defined by DTED can be shown to exist in the residual weaker cell returns.

of other scenes. In this report, such averaging and generalization has been performed both for site-specific use, where the actual terrain is deterministically represented through use of digitized terrain elevation data, and for non-site-specific use, where ground clutter is represented generically independent of how specific terrain features vary from site to site. The resultant empirical modeling information constitutes a reasonably accurate general predictive scheme for estimating and bounding low-angle ground clutter strengths at whatever level of fidelity of terrain representation is employed.

REFERENCES

1. J.B. Billingsley and J.F. Larrabee, "Multifrequency Measurements of Radar Ground Clutter at 42 Sites," Lexington, Mass.: MIT Lincoln Laboratory, Technical Report 916, Volumes 1, 2, 3 (15 November 1991). DTIC AD-A2467810.

2. J.B. Billingsley, "Radar ground clutter measurements and models, part 1: Spatial amplitude statistics," *AGARD Conference Proceedings on Target and Clutter Scattering and Their Effects on Military Radar Performance*, **AGARD-CP-501** (1991).

3. H.C. Chan, "Radar ground clutter measurements and models, part 2: Spectral characteristics and temporal statistics," *AGARD Conference Proceedings on Target and Clutter Scattering and Their Effects on Military Radar Performance*, **AGARD-CP-501** (1991).

4. G.C. Sarno, "A model of coherent radar land backscatter," *AGARD Conference Proceedings on Target and Clutter Scattering and Their Effects on Military Radar Performance*, **AGARD-CP-501** (1991).

5. S.P. Tonkin and M.A. Wood, "Stochastic model of terrain effects upon the performance of land-based radars," *AGARD Conference Proceedings on Target and Clutter Scattering and Their Effects on Military Radar Performance*, **AGARD-CP-501** (1991).

6. D.K. Barton, "Land clutter models for radar design and analysis," *Proc. IEEE* **73**, 198 (1985)

7. R.R. Boothe, "The Weibull Distribution Applied to the Ground Clutter Backscatter Coefficient," Report No. RE-TR-69-15, Redstone Arsenal, Ala.: U.S. Army Missile Command, (1969), DDC AD-691109.

8. E. Jakeman, "On the statistics of *K*-distributed noise," *J. Phys. A* **13**, 31 (1980).

9. C.J. Oliver, "A model for non-Rayleigh scattering statistics," *Opt. Acta* **31**, 701 (1984).

10. D.K. Barton, *Modern Radar System Analysis*, Norwood, Mass.: Artech House, Inc. (1988), pp. 124-128.

11. F.E. Nathanson, *Radar Design Principles*, 2nd ed., New York: McGraw-Hill (1991), pp. 329-332.

12. G.T. Ruck, D.E. Barrick, W.D. Stuart, and C.K. Krichbaum, *Radar Cross Section Handbook*, New York: Plenum Press (1970), p. 676.

13. M.I. Skolnik, *Introduction to Radar Systems*, 2nd ed., New York: McGraw-Hill (1980), p. 490.

14. J.B. Billingsley, "A Handbook of Multifrequency Land Clutter Coefficients for Surface Radar," Lexington, Mass.: MIT Lincoln Laboratory, Technical Report 958, to be published.

15. J.B. Billingsley and J.F. Larrabee, "Measured Spectral Extent of L- and X-Band Radar Reflections from Wind-Blown Trees," Lexington, Mass.: MIT Lincoln Laboratory, Project Report CMT-57 (6 February 1987). DTIC AD-A179942.

16. M.P. Warden and E.J. Dodsworth, "A Review of Clutter, 1974," Technical Note No. 783, Malvern, U.K.: Royal Radar Establishment (1974).

REPORT DOCUMENTATION PAGE

Form Approved
OMB No. 0704-0188

1. AGENCY USE ONLY (*Leave blank*)	2. REPORT DATE	3. REPORT TYPE AND DATES COVERED
	1 February 1993	Technical Report

4. TITLE AND SUBTITLE

Ground Clutter Measurements for Surface-Sited Radar

5. FUNDING NUMBERS

C — F19628-90-C-0002
PE — 62301E, 63003F
PR — 331

6. AUTHOR(S)

J. Barrie Billingsley

7. PERFORMING ORGANIZATION NAME(S) AND ADDRESS(ES)

Lincoln Laboratory, MIT
P.O. Box 73
Lexington, MA 02173-9108

8. PERFORMING ORGANIZATION REPORT NUMBER

TR-786, Revision 1

9. SPONSORING/MONITORING AGENCY NAME(S) AND ADDRESS(ES)

Department of the Air Force
SAF/AQL
The Pentagon
Washington, DC 20330

DARPA
3701 N. Fairfax Dr.
Arlington, VA 22203-1714

10. SPONSORING/MONITORING AGENCY REPORT NUMBER

ESC-TR-92-135

11. SUPPLEMENTARY NOTES

12a. DISTRIBUTION/AVAILABILITY STATEMENT

Approved for public release; distribution is unlimited.

12b. DISTRIBUTION CODE

13. ABSTRACT (*Maximum 200 words*)

A large volume of radar ground clutter measurement data has been collected from many sites that are widely dispersed over the North American continent. At each site backscatter was recorded from all the terrain within the field of view, typically to ranges extending to 25 or 50 km. As a result, in most of these measurements the angle of illumination of the earth's surface was usually very low, typically within a degree or so of grazing incidence, with much intermittent shadowing of low regions. This report examines the nature of low-angle radar ground clutter as it has come to be understood through analysis of this extensive new base of measurements. Depression angle, that is, the angle below the horizontal at which the backscattering terrain point is observed at the radar antenna, is shown to be the principal parametric influence on clutter amplitude statistics, even for the very low angles and small (i.e., typically fractional) variations in angle that occur in surface-sited radar. This principal role of depression angle is the result of its effect on shadowing in a sea of patchy visibility and discrete or localized scattering sources. Following this understanding, a general predictive model for ground clutter spatial amplitude statistics is developed based on very precise computation of depression angle but on only relatively gross specification of terrain type. The important radar parameters entering the model are rf frequency as it affects mean strength of clutter amplitude distributions and spatial resolution as it affects spread in these distributions.

14. SUBJECT TERMS

radar ground clutter; terrain reflectivity; land clutter; electromagnetic propagation; clutter measurements; low-angle; radar clutter; multipath; clutter models; multifrequency

15. NUMBER OF PAGES
96

16. PRICE CODE

17. SECURITY CLASSIFICATION OF REPORT	18. SECURITY CLASSIFICATION OF THIS PAGE	19. SECURITY CLASSIFICATION OF ABSTRACT	20. LIMITATION OF ABSTRACT
Unclassified	Unclassified	Unclassified	Same As Report